

Graphene-based materials for high-voltage and high-energy asymmetric supercapacitors

Shuanghao Zheng^{a,b,c,1}, Zhong-Shuai Wu^{a,*,1}, Sen Wang^{a,b}, Han Xiao^a, Feng Zhou^a,
Chenglin Sun^a, Xinhe Bao^{a,c}, Hui-Ming Cheng^{d,e}

^a Dalian National Laboratory for Clean Energy, Dalian Institute of Chemical Physics, Chinese Academy of Sciences, 457 Zhongshan Road, Dalian 116023, PR China

^b University of Chinese Academy of Sciences, 19 A Yuquan Rd, Shijingshan District, Beijing 100049, PR China

^c State Key Laboratory of Catalysis, Dalian Institute of Chemical Physics, Chinese Academy of Sciences, 457 Zhongshan Road, Dalian 116023, PR China

^d Shenyang National Laboratory for Materials Science, Institute of Metal Research, Chinese Academy of Sciences, 72 Wenhua Road, Shenyang 110016, PR China

^e Tsinghua-Berkeley Shenzhen Institute, Tsinghua University, 1001 Xueyuan Road, Shenzhen 518055, PR China

ARTICLE INFO

Keywords:

Graphene

2D materials

Asymmetric supercapacitors

High voltage

Hybrid supercapacitors

ABSTRACT

The ultrathin two-dimensional structure and unique properties of graphene make it highly attractive for high-performance asymmetric supercapacitors (ASCs), which are generally constructed by two different materials as positive electrode and negative electrode, respectively, in an asymmetric configuration. Here, a deep insight into the recent advances of graphene-based materials for high-voltage and high-energy asymmetric supercapacitors (ASCs) is presented. First, the critical aspects that directly affect the performance of ASCs and how they have been tackled in terms of the assembly principle of ASCs and standard methods of accurate performance evaluation are discussed. Second, the major categories and the state-of-the-art positive and negative electrode materials of ASCs are described. Third, the latest advances of different graphene-based nano-architectures, such as reduced graphene oxide, porous graphene, graphene quantum dots, graphene nanoribbons, graphene fibers, graphene films, graphene aerogels, graphene foams, and various hybrids of graphene/carbon nanotubes, graphene/metal oxides and graphene/conducting polymers, for ASCs are summarized. Fourth, major performance parameters, including high voltage, high capacitance, high power and high energy devices, as well as new device geometry of planar and all-solid-state devices, are described in details, highlighting the uniqueness and superiority of graphene for hybrid energy storage. Fifth, The elaborated screening of graphene-based materials with controllable morphologies, two-dimensional and three-dimensional well-defined nanostructures, and tailored compositions, architectures of the electrode, selection of electrolytes, and optimized integrity of different device components are overviewed. Finally, future perspectives and challenges of graphene-based ASCs are discussed.

1. Introduction

The continuously increasing concern on the world energy consumption and environmental pollution has promoted the rapid development of electrochemical energy storage devices, e.g., lithium ion batteries and supercapacitors, for various important uses, in particular, in electric vehicles, hybrid electric vehicles (HEV), plug-in HEV, and smart grids [1,2]. Although lithium ion batteries with high energy density of 100–250 W h kg⁻¹ are currently the best product for these zero-emission applications, but still suffer from low power density, limited cycle life, safety issue, high cost and limited availability of

lithium resources [3]. As a prime promising replacement or equivalent complement for lithium ion batteries, supercapacitors with high power density and long life span have been attracting more and more attention for next-generation, safe, clean energy storage systems, which can provide sufficient peak power and increase power efficiency when they work individually or together with high-energy batteries and fuel cells [4].

Supercapacitors or electrochemical capacitors have three categories, including electric double layer capacitors (EDLCs), pseudocapacitors and hybrid supercapacitors [5]. In principle, EDLCs electrostatically store charges on the interface of high surface area carbon

* Corresponding author.

E-mail address: wuzs@dicp.ac.cn (Z.-S. Wu).

¹ These authors have equally contributed.

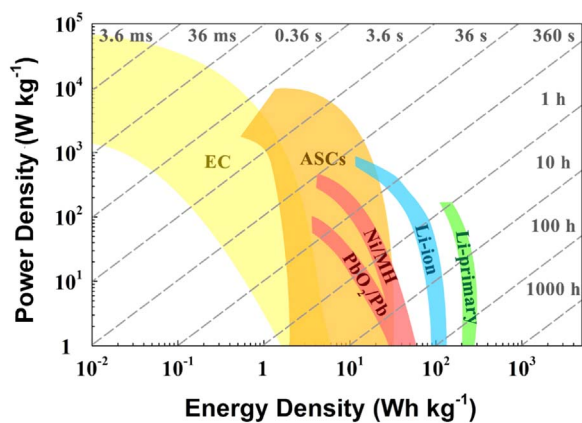


Fig. 1. Ragone plot of ASCs with various typical electrochemical energy storage devices. Times given in the plot are the time constants of the devices, obtained by dividing the energy density by the power.

electrodes, e.g., activated carbon (AC), carbon aerogel, porous carbon, carbon nanotube (CNT), and graphene, which characterizes the performance of rapid charge storage and limited specific capacitance [6]. Pseudocapacitors mainly store charges from reversible redox reactions of transition metal oxides/hydroxides, such as RuO_2 , MnO_2 , $\text{Ni}(\text{OH})_2$, and electrically conducting polymers (polyaniline (PANI), polypyrrole (PPy), etc) that could deliver high specific capacitance, but present poor cycle stability [7]. In efforts to enhance their energy density, hybrid supercapacitors combining the advantageous merits of EDLCs and pseudocapacitors have been developing since they can maintain high power feature. According to the disparity of two electrode materials used, hybrid supercapacitors could be generally divided into composite symmetric supercapacitors, battery-type supercapacitors, and asymmetric supercapacitors (ASCs) [8]. It is worthy to note that ASCs consisting of two different electrodes are becoming a more attractive class of supercapacitors, which can possibly achieve high energy density that approaches that of batteries and obtain high power density of supercapacitors, and fill up the gap between batteries and supercapacitors (Fig. 1) [9,10]. Besides this, ASCs possess excellent stable cyclability, wide range of operating temperatures with low maintenance cost, safe operation and environmental friendliness. Consequently, ASCs are acknowledged as one of the most advanced hybrid energy storage devices that not only are very attractive for various high power applications, but also properly overcome the intractable issues of energy density observed from traditional EDLCs [11].

In light of this, herein we review the latest advances of high-voltage and high-energy ASCs based on graphene-based materials. We will first

focus on the key aspects for the efficient assembly principle of ASCs with the full consideration of main device components, selection of electrolytes, and optimized integrity of different device components, and performance evaluation. Then we mainly concentrate on the prime negative electrodes and positive electrodes of graphene-based nano-architectures, such as reduced graphene oxide (rGO), porous graphene, graphene quantum dots (GQD), graphene films, graphene aerogels (GAs), graphene foams (GF), various hybrids of graphene/CNT, graphene/metal oxides and graphene/conducting polymers in term of the major performance parameters, including high voltage, high capacitance, high power and high energy devices as well as new-type device geometry of planar and all-solid-state devices, highlighting the uniqueness and superiority of graphene for ASCs. Finally, future perspectives and challenges of graphene-based ASCs are briefly highlighted.

2. Assembly principle and performance evaluation of ASCs

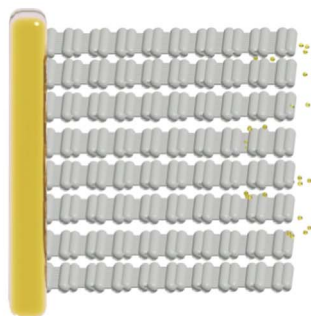
2.1. Main device components

The configuration of an ASC device is schematically shown in Fig. 2, composing of two different electrodes, a separator, two collectors, and an electrolyte as well as external electric circuit and sealed packaging. In principle, the entire device with a stacked geometry of collector/positive electrode/separator/negative electrode/collector is constructed [11]. Electrolyte (aqueous, organic electrolyte) is a conductive liquid mixture of an aqueous or organic solvent that is able to rapidly migrate into and out of positive and negative electrodes during charge and discharge. To prevent short circuiting, an ion-permeable insulating membrane acting as a separator is placed between these two electrodes. To accelerate the transport of electrons, metallic collectors as the input/output terminals of electricity to an outside circuit are applied to increase the electrical contact with the film electrodes. Nevertheless, the overall performance of ASCs is strongly dependent on the elaborated screening and integrity of all device components [12].

2.2. Design consideration

Elaborated screening and integrity of different main device components (e.g., electrodes, electrolyte, current collectors, and separator) for designing high-performance ASCs are greatly challenging. As we all have known, the improvement of the overall performance of ASCs is dependent not only on the intrinsic properties of positive and negative electrode materials, but also on the reasonable design, mass/kinetics match and compatible combination of each isolated device component in one single device [9]. As to graphene-based ASCs, the following three aspects need to be fully considered before assembly:

**Mostly electric double-layer
(non-faradic or electrostatic)
absorption/desorption**



**Redox (faradic) reactions
with or without non-faradic
reactions**

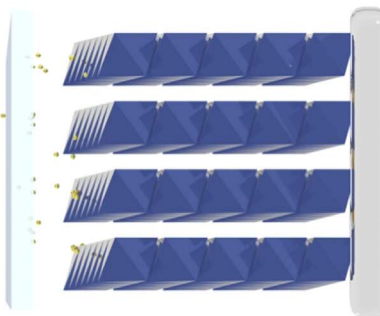


Fig. 2. Schematic of a ASC cell.

(1) Materials fabrication of high-quality graphene and unique nanostructural graphene hybrids is the key prerequisite to ensure good performance of ASCs [13]. It is well known that the performance of a device is directly dependent on the intrinsic properties of the electrode materials employed in asymmetric system. In particular, the advantageous properties of combining high specific surface area, excellent conductivity, rich hierarchical porous structure and robust electrochemically active sites into one single given electrode are the main target for the construction of high-performance graphene-based ASCs. Vice versa, the good performance of the ASCs can't be achieved [14].

(2) Rather than focusing on materials, the mass balance between positive and negative electrodes and the kinetics match of the two electrodes must be considered to fabricate a stable and efficient ASC system [11]. To realize this, making a balance of the charges stored between positive electrode (Q_P) and negative electrode (Q_N) in ASCs is highly required [15]. Otherwise, the assembled device can't ensure to work reversibly during the charge and discharge process. Usually, one can follow the relationship of charge balance, $Q_P = Q_N$, to calculate the ratio of positive and negative electrodes (m_+/m_-) with the equation below:

$$m_+/m_- = (C_- \times \Delta V_-)/(C_+ \times \Delta V_+)$$

The optimal mass ratio (m_+/m_-) between positive and negative electrodes should be perfect to be closed to 1 in a two-electrode cell if taking into consideration of volumetric and gravimetric capacitance. Regarding the match of the charge-storage kinetics of two electrodes, the fundamental understanding of two electrodes in ASCs is still in a very early stage. It is generally accepted that if working on a non-faradaic/non-faradaic process, e.g., carbon/carbon, the two matched electrodes always possess fast ionic diffusion and electron transport, and generate a high-power and very stable ASC [16]. However, faradaic/non-faradaic electrodes if combining a fast redox reaction kinetics with EDLC mechanism, e.g., intercalation metal oxide/carbon, and polymer/carbon, potentially produce a high-energy ASC without compromising the power density [17]. The third combination is an ASC with faradaic/faradaic reaction mechanism, e.g., oxide/oxide and polymer/polymer, which are promising to achieve high capacitance and energy density but the exploration is very limited [18].

(3) For any given electrode material and ASC system, a matching electrolyte must be carefully selected to maximize their electrochemical performance [19]. In principle, the nanopores of porous graphene-based materials and the interspace of electrochemically active species (e.g., CNT, RuO₂, MnO₂, Co₃O₄, Mn₃O₄) should be matched with the accessible electrolyte ions. Thereby the reasonable choice of a complemented electrolyte is important for the improvement of the performance of ASCs in addition to the match of both mass and charge-storage kinetics of two electrodes. Currently, the electrolytes used in ASCs are mainly categorized into aqueous electrolytes and nonaqueous electrolytes [20]. The latter using organic electrolytes with a large electrochemical window of up to 3 V or even more are widely used in commercial supercapacitors. However, some major issues associated with high flammability, low ionic conductivity, and easy short-circuiting of organic electrolytes eventually result in high safety risks and low capacitance and power density [20]. In fact, the practical energy density is not high, below 5 Wh kg⁻¹ for most available supercapacitors in organic electrolytes [21]. In comparison with organic electrolytes, aqueous electrolytes (Na₂SO₄, K₂SO₄) used in ASCs present the advantages of high ionic conductivity, low cost, non-flammability, good safety and convenient assembly in air. More importantly, aqueous based ASCs could offer much higher power density than organic based ASCs because of their high ionic conductivity and suitable size of ions, in addition to environmental friendliness particularly operating in neutral aqueous electrolytes

[15].

2.3. Performance evaluation

The capacitance values are usually calculated from discharge cyclic voltammetry (CV) and galvanostatic charge–discharge (GCD) curves according to the following Eqs. (1) and (2), respectively:

$$C = \frac{1}{v(V_f - V_i)} \int_{V_i}^{V_f} I(V) dV \quad (1)$$

$$C = \frac{I_{dis} \Delta t}{(V_0 - V_{IR-drop})} \quad (2)$$

where v is the scan rate (V/s), V_f and V_i are the integration potential limits of the voltammetric curve, and $I(V)$ is the voltammetric discharge current (A). I_{dis} is the constant discharge current (A), and Δt is the discharge time corresponding to the discharge change $V_0 - V_{IR-drop}$. V_0 is the cell voltage and $V_{IR-drop}$ is the voltage induced by the IR drop that is inevitable in GCD test. To calculate more accurately the capacitance, it is recommended to adjust the actual cell voltage after excluding the IR drop.

To evaluate the performance of a single electrode (positive electrode or negative electrode), specific capacitance is calculated based on the area ($A_{electrode}$) or the volume ($V_{electrode}$) or the mass ($m_{electrode}$) of the single electrode according to the following formula:

$$C_{electrode}^{areal} = C/A_{electrode} \quad (3)$$

$$C_{electrode}^{volumetric} = C/V_{electrode} \quad (4)$$

$$C_{electrode}^{gravimetric} = C/m_{electrode} \quad (5)$$

where $C_{electrode}^{areal}$ (F/cm²), $C_{electrode}^{volumetric}$ (F/cm³) and $C_{electrode}^{gravimetric}$ (F/g) refer to the areal capacitance, volumetric capacitance and gravimetric capacitance of the single electrode, respectively.

Specific emphasis is given to thin-film electrodes with thickness of submicrometer to micrometers for supercapacitors and micro-supercapacitors. A key consideration is that the mass of these thin film electrodes, often a small fraction of the total mass of a device, is almost negligible, making gravimetric capacitance and energy density inappropriate performance metrics [22]. In such cases, it is recommended that using areal capacitance, volumetric capacitance, volumetric energy density and volumetric power density, rather than the gravimetric ones, is more appropriate and reliable to evaluate their performance. In these systems, thin films are able to offer a very high gravimetric capacitance and power density, but those characteristics will not increase linearly with the thickness of the electrode [23].

Most recently, volumetric performance has becoming the focus over gravimetric performance, since future electric vehicles and electronics tend to require power sources delivering the maximum energy in a very limited space, in particular, which critically represents the intrinsic energy storage ability of the electrode materials stored in a unit volume of a packed cell. Among the volumetric parameters, it is considered that volumetric capacitance as a critical indicator can better understand the intrinsic properties of the electrode material and compare the performance of different materials.

Except the Eq. (4), another method for calculating the volumetric capacitance $C_{electrode}^{volumetric}$ (F/cm³) is:

$$C_{electrode}^{volumetric} = C_{electrode}^{gravimetric} \times \rho \quad (6)$$

where ρ (g/cm³) is the mass packing density of the film.

For an asymmetric two-electrode system, its cell capacitance Q_c ,

$$1/Q_c = 1/Q_P + 1/Q_N \quad (7)$$

where Q_c , Q_P and Q_N are the capacitive contribution from the cell, positive electrode and negative electrode, respectively. According to the relationship of $Q_c = C_{Sc} \times (m_+ + m_-)$, $Q_P = C_{Sp} \times m_+$ and $Q_N = C_{Sn} \times m_-$,

where C_{Sp} and m_+ , C_{Sn} and m_- are the specific capacitance and mass of positive electrode and negative electrode, respectively, the specific capacitance of the cell (C_{Sc}) by counting the mass for both electrodes is converted to the equation:

$$C_{Sc} = Q_c / (m_+ + m_-) = C_{Sp} \times m_+ \times C_{Sn} \times m_- / \{(m_+ + m_-)(C_{Sp} \times m_+ + C_{Sn} \times m_-)\} \quad (8)$$

Energy density (E) is the most important parameter for ASCs, and calculated by the following equation.

$$E = \frac{1}{2} \times C_{Sc} \times V^2 \quad (9)$$

where C_{Sc} and V are the gravimetric specific capacitance ($F g^{-1}$, mainly based on two electrodes) and the maximum working voltage of ASCs, respectively.

Power density (P) is another key parameter for evaluating the performance of ASCs, which can be calculated with the following two equations.

$$P = E/t \quad (10)$$

$$P_M = V^2 / (4 \times ESR \times m) \quad (11)$$

where P is the power density of an ASC device, which is inversely proportional to the energy density. P_M is the maximum power density of an ASC cell, and usually used to evaluate the maximum power output in relation to the maximum cell voltage (V) after eliminating the IR drop, the equivalent series resistance (ESR) and the average mass (m) of two electrodes without the involvement of current collectors.

3. Major categories and electrode materials of ASCs

3.1. Major categories

In 2001, Amatucci et al. reported the first construction of a nonaqueous ASC combining titanate negative electrode with an AC positive electrode, which could deliver an exceeded energy density of 20 Wh kg^{-1} in a bonded flat plate plastic cell configuration (Fig. 3) [24]. In light of two electrode materials and charge-storage mechanism, ASCs can be mainly classified into three categories. (i) The first prototype consists of a pseudocapacitive active material (e.g., metal oxide, conducting polymer) as positive electrode for energy source and an EDLC carbon material (e.g., AC, CNT, graphene) with strong electrostatically absorption/desorption as negative electrode for power source [25]. In this regard, the constructed ASC could significantly store charge by surface adsorption and desorption over the EDLC material and by redox reaction on the faradaic material, providing a wide electrochemical window to boost its energy density. (ii) The second type includes a faradic lithium-insertion compound (e.g., LiCoO_2 , LiMn_2O_4 , KMnO_2 , NaMnO_2) as positive electrode and a nonfaradaic carbon as negative electrode, generating a large voltage window [17]. (iii) The third combines two different pseudocapacitive

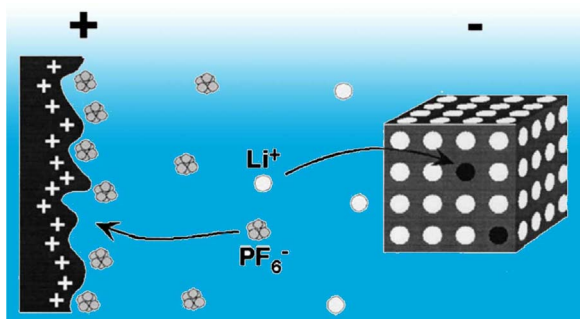


Fig. 3. Simplified schematic of electrode reactions of the earliest ASC based on activated carbon (AC) and nanostructured $\text{Li}_4\text{Ti}_5\text{O}_{12}$ in nonaqueous electrolyte [24].

(hybrid) materials as both positive and negative electrodes, in which one exhibits high overpotential towards hydrogen evolution and another has high overpotential for oxygen evolution, resulting in a wide voltage window of the cell [18]. Through efficient combination of the positive and negative electrodes, ASCs simultaneously promise high energy density which approaches that of batteries and high power density comparable to symmetric supercapacitors, accompanied with stable cyclability.

3.2. Major electrode materials

Regardless of device assembly, screening of new high-performance nanostructured electrode material is the core part in developing stable high-energy ASCs. So far, great progress has been made and many advanced energy materials have been applied as both positive and negative electrode materials for ASCs. For instance, the positive electrodes reported include nanocarbon materials (AC [26], graphite [16]), metal oxides (MnO_2 [18,27], PbO_2 [28], NiO [29], RuO_2 [30], V_2O_5 [31], NiCo_2O_4 [32], NiMoO_4 [33], Mn_3O_4 [34], Co_3O_4 [35], SnO_2 [36]), hydroxide (Ni(OH)_2 [37]), intercalation compounds (LiCoO_2 [38], LiMn_2O_4 [39,40], KMnO_2 [41], NaMnO_2 [42,43], $\text{Li[NiCoMn]}_{1/3}\text{O}_2$ [44]), conducting polymers (PANI [18], PPy [18], poly(3,4-ethylenedioxythiophene) (PEDOT) [18]) and their hybrids. In contrast, typical negative electrode materials basically cover all types of nanocarbons (AC [25], porous carbons [29], CNT [45], graphene [15]), oxides (e.g., $\text{Li}_4\text{Ti}_5\text{O}_{12}$ [46], In_2O_3 [47], $\text{Li}_2\text{Ti}_3\text{O}_7$ [48], MnO_2 [39], TiO_2 [49], $\text{LiTi}_2(\text{PO}_4)_3$ [50], Bi_2O_3 [51], MoO_3 [52], Fe_2O_3 [53], V_2O_5 [54], RuO_2 [55], Nb_2O_5 [56]), conducting polymers (PANI [18], PPy [18], PEDOT [18]), and their hybrids.

4. Graphene-based ASCs

Graphene is a perfect 2D form of single layer sp^2 -bond crystalline carbon with unique intriguing properties, and hold a wide range of potential applications [57,58]. Up to date, graphene has been demonstrated to be a robust and attractive electrode material for supercapacitors because of its excellent electrical conductivity, high surface-to-volume ratio, and outstanding theoretical capacitance (550 F g^{-1}) [59–64]. Significantly, the symmetric supercapacitors based on graphene-based materials, e.g., curved graphene [65], vertically oriented graphene [66], activated graphene [67], heteroatom-doped graphene [68,69], laser-scribed graphene films [70], graphene/metal oxide hybrids [71], graphene-based porous carbon nanosheets [72–74], and liquid electrolyte-mediated graphene compact films [75] as two same electrodes have shown impressive performance superior to other carbonaceous materials when processed into thin-films. In such architectures, the gravimetric energy of 70 Wh kg^{-1} and power density of 250 kW kg^{-1} (per weight of active material) can be reached. On the other hand, great efforts have also been devoted to developing new ASCs using graphene and graphene based hybrids as main active materials or components in one or two electrodes [15], exhibiting enhanced electrochemical performance, as shown in Table 1. The major unique roles of graphene for high-energy ASCs can be summarized: (i) a superior active material, (ii) an ultrathin 2D flexible support for uniformly loaded metal/metal oxide nanoparticles, and (iii) an inactive yet electrically conductive component. Apparently, it can be seen from Table 1 that a number of different graphene-based materials for ASCs have been reported so far. From the materials perspective, graphene-based materials for ASCs are usually divided into two categories: one is the positive electrode (cathode), including pure graphene, oxides/hydroxides of MnO_2 , Mn_3O_4 , Co_3O_4 , RuO_2 , Ni(OH)_2 , and conducting polymers of PANI and PPy. Another is the negative electrode (anode), which includes graphene, porous graphene, graphene fibers, graphene films, GAs, GF, GQD, and the composites of graphene/CNT and graphene/oxides (e.g., RuO_2 , V_2O_5 , MoO_3 , Nb_2O_5), for different ASCs targeting for high voltage, high capacitance, high

Table 1
Comparison of the performance of graphene-based ASCs.

Negative electrode (anode)	Positive electrode (cathode)	Electrolyte	Voltage (V)	Cell max. Cs (F g ⁻¹)	Max. E (W h kg ⁻¹)	Max. P (W kg ⁻¹)	Cycling stability (retention)	Ref.
G	PANI	1 M HCl	0–1.0	35	4.86	8750	–	[76]
G	MnO ₂ nanowires/G	1 M Na ₂ SO ₄	0–2.0	55.0	30.4	5000	1000 (79%)	[15]
AC nanofiber	G/MnO ₂	1 M Na ₂ SO ₄	0–1.8	113.5	51.1	198,000	1000 (97.3%)	[77]
rGO/RuO ₂	rGO/PANI	2 M H ₂ SO ₄	0–1.4	100 ^a	26.3	49,800	1000 (80%) 2500 (70%)	[55]
G film	RuO ₂ /G film	PVA/H ₂ SO ₄ gel	0–1.8	175	19.7	6800	2000 (95%)	[78]
CNT/G	Mn ₃ O ₄ /G	PAAC/KCl gel	0–1.8	72.6	32.7	9000	10,000 (86%)	[79]
G hydrogel	MnO ₂ nanoplates/ NF	0.5 M Na ₂ SO ₄	0–2.0	41.7	23.2	10,000	5000 (83.4%)	[80]
rGO	Co _{0.45} Ni _{0.55} O/rGO	1.0 M KOH	0–1.5	124 ^a	35.3	3614	1000 (96%)	[81]
Porous G	Ni(OH) ₂ /G	6 M KOH	0–1.6	218.4	77.8	15,200	3000 (94.3%)	[82]
FAC	MnO/rGO	1 M NaNO ₃	0–1.1	51.5	2.6	9024	15,000 (82%)	[83]
G	MnO ₂	1 M Na ₂ SO ₄	0–2.0	37	25.2	100	500 (96%)	[84]
G/MoO ₃	G/MnO ₂	1 M Na ₂ SO ₄	0–2.0	307	42.6	276	1000 (–)	[52]
G/CNT	G/CNT/PANI	EMI-TFSI	0–4.0	271	188	26,700	1000 (82%)	[85]
α-MnO ₂ /GO	CB/GO	1 M Li ₂ SO ₄	0–2.0	153	23.6	4500	1000 (56%)	[86]
α-MnO ₂ (SDS)/GO			0–1.8	280	35.0	7200	1000 (70%)	
CNT/PANI	CNT/MnO ₂ /GR	PVP/Na ₂ SO ₄ gel	0–1.6	70 ^a	24.8	584 ^a	1000	[87]
GO/CB	GO/CoTPyzPz	1 M Na ₂ SO ₄	0–1.4	160 ^a	44	31,000	1000 (99%)	[88]
QDs	PANI	0.5 M Na ₂ SO ₄	0–1.0	667.5 mF m ⁻²	0.029 mW h cm ⁻²	7.46 mW cm ⁻²	1500	[89]
rGO	NiO nanoflake	1.0 M KOH	0–1.7	50	39.9	–	3000 (95%)	[90]
G/Ag	G/MnO ₂	1 M Na ₂ SO ₄	0–1.8	112.8	50.8	90.3	–	[91]
aGNS	sGNS/cMWCNT/ PANI	1 M H ₂ SO ₄	0–1.6	107	20.5	25,000	5000 (91%)	[92]
RGO	RGO/MnO ₂	1 M Na ₂ SO ₄	0–1.5	113 mF m ⁻²	11.5 μW h cm ⁻²	3.8 mW cm ⁻²	3600 (84%)	[93]
Co ₃ O ₄ /GO	AC	6 M KOH	0–1.5	114.1	35.7	225	1000 (95%)	[94]
MnO ₂ /porous G gel/ NF	Porous G gel/NF	0.5 M Na ₂ SO ₄	0–1.8	0.89 F cm ⁻³	0.72 mW h cm ⁻³	–	10,000 (98.5%)	[95]
rGO/Co/Al LDHs	AC	6 M KOH	0–1.75	83.5	35.5	8.75	6000 (90%)	[96]
GNR	CoMn ₂ O ₄ /GNR	0.5 M Na ₂ SO ₄	0–1.9	169	84.69	22	1500 (96%)	[97]
MnOOH/rGO	AC	6 M KOH	0–1.6	115.6	41.1	400	5000 (98.3%)	[98]
GO	LiCoO ₂	1 M LiClO ₄	0–1.5	59	19.2 ^a	8.7	1500 (85%)	[38]
GO/PPy	AC	1 M Na ₂ SO ₄	0–1.6	60.2	21.4	453.9	5000 (85.7%)	[99]
MnO ₂ /rGO/ITO	PPy/rGO/ITO	PVA/LiCl gel	0–1.7	39	13	7.4	2000 (75%)	[100]
T-Nb ₂ O ₅ /G	Mesoporous carbon	1 M LiPF ₆	0.8–3	70	16	45	5000 (92%)	[56]
MnFe ₂ O ₄ /G	MnO ₂ /CNT	1 M Na ₂ SO ₄	1.8	57.6	25.9	225	4500 (90%)	[101]
Fe ₃ O ₄ /rGO	NiOOH/Ni ₃ S ₂ /3D G	1 M KOH.	0–1.6	233	82.5	930	1000 (111%)	[102]
rGO	Co/Al LDHs	6 M KOH	1.6	97.5	34.7	390	2000 (93%)	[103]
GF/CNT/PPy	G foam/CNT/MnO ₂	0.5 M Na ₂ SO ₄	1.6	64	22.8	860	10,000 (90.2– 83.5%)	[104]
GNR	GNR–MnO ₂	PAAC/KCl gel	0–2.0	212	29.4	12.1	5000 (88%)	[105]
rGO	rGO/V ₂ O ₅ nanosheets	1 M KCl	0–1.6	195	75.9	900	3000 (94%)	[106]
rGO/CNT/PPy/CB	Mn ₃ O ₄	0.5 M NaNO ₃	0–1.6	40.2	14.3	6.62	3250 (> 100%)	[107]
G nanoplatelets	MWCNT/NiS	6 M KOH	0–1.4	181	49	7000	1000 (92%)	[108]
NiO/G foam	N-doped CNT	1 M KOH	0–1.4	116	32	42,000	2000 (94%)	[109]
rGO	MnO ₂ /ZnO nanorod	PVA/LiCl gel	0–1.8	0.52 F cm ⁻³ ,	0.234 mW h cm ⁻³	0.133 W cm ⁻³	5000 (98.5%)	[110]
rGO hydrogel	rGO/MnO ₂	1 M Na ₂ SO ₄	1.6	59.6	21.2	6610	1000 (89.6%)	[111]
AC	rGO/Mn ₃ O ₄	1 M Na ₂ SO ₄	0–2	62	34.6	15,200	8000 (107%)	[112]
		6 M KOH	0–1.6	38	13.6	5100	8000 (150%)	
rGO/cMWCNT	carbon fiber paper/ PPy	PAAC/KCl gel	0–1.6	82.4	28.6	15,100	2000 (93%)	[113]
CNT/G foam	MnO ₂ /G foam	PAAC/KCl gel	0–1.8	69.4	31.8	9188.1	10,000 (84.4%)	[114]
G/CNT hybrid fibers	MnO ₂ /G fiber	PVA/LiCl gel	0–1.6	16.8 F cm ⁻³	6.7 mW h cm ⁻³	–	8000 (92.7%)	[115]
PEDOT/CNT	Activated G	2 M BMIBF ₄ /PC	0–4	81.6	176.6	233,000	5000 (92%)	[116]
rGO	rGO/CNF/MnCO ₃	1 M Na ₂ SO ₄	0–2	38	21	1070	1000 (97%)	[117]
AC	G foam/PVA-F	1 M Na ₂ SO ₄	0–1.8	31.5 ^a	14.2	174	2000 (98%)	[118]
rGO/CB	rGO/MnO ₂ /CB	0.5 M Na ₂ SO ₄	0–1.8	53.8	24.3	45,000	–	[119]
		PVA/LiClO ₄ gel	0–1.8	44.6	20	21,000	1000 (89%)	
CuO/rGO sponge	rGO sponge	1 M Na ₂ SO ₄	0–1.7	77.84	31.4	4232	2000 (83%)	[120]
3D porous G papers	NiCo ₂ O ₄ /carbon cloth	PVA/LiOH gel	0–1.8	71.32	60.9	11.36	5000 (96.8%)	[121]
Ni/rGO/Ni ₃ S ₂	Ni/rGO/Co ₃ S ₄	6 M KOH	0–1.3	940	55.16	13,000	3000 (96.2%)	[122]
rGO paper	Mn ₃ O ₄ /rGO nanohybrid paper	1 M Na ₂ SO ₄	0–2	54.6 F cm ⁻³	5.5 mW h cm ⁻³	6.86 W cm ⁻³	8000 (85%)	[34]
		1 M EMIMBF ₄	0–3	3.12 F cm ^{-3a}	3.9 mW h cm ⁻³	10.95 W cm ⁻³		
AC	NiO/G	2 M KOH	0–1.5	87.36 ^a	27.3	17,800	8000 (87.2%)	[123]
rGO	Co ₉ S ₈ /G	1 M KOH	0–1.8	70.2	31.6	910	1000 (60%)	[124]
Porous carbon	rGO/Ni/NiO	6 M KOH	0–1.6	183.8	65.3	8000	–	[125]
rGO	MnO ₂ /MnCO ₃ /rGO	1 M Na ₂ SO ₄	0–1.6	50.06	17.8	400	2000 (84.1%)	[126]
rGO	Ni(OH) ₂	2 M KOH	0–1.6	210.94 ^a	75	40,000	10,000 (89%)	[127]

(continued on next page)

Table 1 (continued)

Negative electrode (anode)	Positive electrode (cathode)	Electrolyte	Voltage (V)	Cell max. Cs (F g ⁻¹)	Max. E (W h kg ⁻¹)	Max. P (W kg ⁻¹)	Cycling stability (retention)	Ref.
rGO	Nanoparticles/G							
Activated G	h-BN/G	6 M KOH	0–1.4	145.7	39.6	4200	4000 (89%)	[128]
AC	SAC/G	6 M KOH	0.75–1.5	495 ^a	88.9	16,500	10,000 (88%)	[129]
MoS ₂ /rGO/MWCNT	CoS/G	2 M KOH	0–1.6	81.56 ^a	29	800	10,000 (70%)	[130]
IL/CNT/rGO	rGO/MWCNT	PVA/H ₂ SO ₄ gel	0–1.4	4.8 F cm ⁻³	1.307 W h cm ^{-3a}	–	–	[131]
G foam	MnO ₂ /G	1 M Na ₂ SO ₄	0–1.8	56.89 ^a	25.6	9070	10,000 (90%)	[132]
GNR	NiCo ₂ O ₄ /carbon fiber paper	2 M KOH	0–1.6	97.5	34.5	547	10,000 (92.2%)	[133]
rGO	Co ₃ O ₄ /G	1 M KOH	0–1.6	180.56 ^a	64.2	8300	2000 (94%)	[134]
G/Fe ₃ O ₄ /Carbon	CoMoO ₄	1 M NaOH	0–1.5	26.16	8.17	187.5	4000 (85%)	[135]
AC	Co(OH) ₂ nanosheets/G	1 M KOH	0–1.6	210	75	400	8000 (72%)	[136]
Fe ₂ O ₃ /G	a-MnO _x /rGO/CNT	0.25 M Na ₂ SO ₄	0–2.0	32.4 ^a	18	1000	–	[137]
NiCo ₂ S ₄ /G	MnO ₂ /G	1 M Na ₂ SO ₄	0–2.0	91.26 ^a	50.7	100	5000 (95%)	[138]
Porous N-doped G	AC	6 M KOH	0–1.7	170.6	68.5	850	5000 (95.8%)	[139]
Hierarchical porous carbon	CCH/N-doped G	PVA/KOH gel	0–1.9	153.5 mF cm ⁻²	0.77 W h m ⁻²	25.3 W m ⁻²	10,000 (94.2%)	[140]
rGO/MoO ₃ nanoparticle	3D Co ₃ O ₄ /rGO	6 M KOH	0–1.5	130	40.65	340	2000 (92.92%)	[35]
CCG	rGO/MnO ₂ nanospheres	1 M LiCl	0–2.0	62.7 F cm ⁻³	34.6 mW h cm ⁻³	100 mW cm ⁻³	3000 (94.2%)	[141]
Fe ₂ O ₃ /3D G	3D Al/Ni/MnO _x nanospikes	PVA/Na ₂ SO ₄ gel	0–1.8	58.78	23.02	947.11	10,000 (96.3%)	[142]
NG/Porous carbon	MnO ₂ /3D G	2 M LiCl	0–1.8	9.6 ^a	41.7	13,500	5000 (89%)	[143]
3D G network	LiMn ₂ O ₄	0.5 M Li ₂ SO ₄	0–1.8	98	44.3	595	2000(93%)	[144]
Pd/G aerogel	CNT/Ni(OH) ₂	KOH	0–1.6	124	19.6	16 000	8000 (83%)	[145]
AC	MnO ₂	0.1 M Na ₂ SO ₄	0–1.6	108.9	13.9	13,300	3000 (89.6%)	[146]
Ni/G foam/PPy	Ni(OH) ₂ /CFG	2 M NaOH	0–1.6	191.3	15	15,400	1000 (100%)	[147]
3D G hydrogels/ Copper wire	Ni/GF/MnO ₂	0.2 M NaClO ₄	0–1.8	175.2	1.23 mW h cm ⁻³	5.54 mW cm ⁻³	10,000 (90.2%)	[148]
3D porous carbon	MnO ₂ /G/Carbon fiber	PAAK/KCl gel	0–1.6	2.54 F cm ⁻³	0.9 mW h cm ⁻³	200 W cm ⁻³	10,000 (90%)	[149]
Activated GOs/MWCNTs	MnO ₂ /GO	1 M Na ₂ SO ₄	0–2.0	84	46.7	100	4000 (93%)	[150]
rGO	PANI/GOs/MWCNTs	1 M H ₂ SO ₄	0–1.6	194 ^a	69	6400	3000 (89%)	[151]
Carbon cloth	MnCO ₃ /rGO	1 M Na ₂ SO ₄	0–1.6	318	113	1600	10,000 (69%)	[152]
AC	Ni–Co binary hydroxide/G	6 M KOH	0–1.4	340	92	7000	10,000 (80%)	[153]
3D porous carbon	NG/MnO ₂	PVA/LiCl gel	0–1.8	71.9	3.5 mW h cm ⁻³	0.019 W cm ⁻³	1500 (90%)	[154]
G hydrogels	Ni-Co hydroxide/rGO	6 M KOH	0–1.6	162	56.1	76	17,000 (80%)	[155]
	NiOOH/G hydrogels	2 M KOH	0–1.6	188	66.8	800	800 (85.3%)	[156]

Cs: Specific capacitance; E: Energy density; P: Power density; G: graphene; GO: graphene oxide; IL: ionic liquid; NF: nickel foam; FAC: functionalised AC; CB: carbon black; GNR: graphene nanoribbon; CoTPyzPz: cobalt (II) tetrapyrzineporphyrazine composite; sGNS: sulfonated graphene nanosheet; cMWCNT: carboxylated multiwalled CNT; PPy: polypyrrole; PVP: polyvinylpyrrolidone; ITO: indium tin oxide; EMI-TFSI: 1-ethyl-3-methylimidazoliumbis(trifluoromethanesulfone)imide; PEDOT: poly(ethylenedioxythiophene); CCG: chemically converted graphene; Co/Al LDHs: CoAl layered double hydroxide; PAAK: potassium polyacrylate; PC: propylene carbonate; CNF: carbon nanofiber; aCNT: aligned CNT; PVA: polyvinyl alcohol; PVA-F: polyvinyl alcohol-formaldehyde; SAC: sulfanilic acid azocromotrop; CCH: cobalt carbonate hydroxide; FGA: functionalized GAS; CFG: cellulose-fiber covered with graphene.

^a Calculation values.

power density and energy density as well as planar and all-solid-state asymmetric devices (Table 1).

4.1. High-voltage aqueous ASCs

Recently, increasing efforts have been made to the improvement of the energy density of a ASC. From the Eq. (9) above, one can understand that energy density is proportional to the specific capacitance (C_s) and the square of the operating voltage (V). Therefore, the improvement of the energy density can be attained in two ways of (i) increasing the specific capacitance of the electrode materials and/or (ii) the voltage of the ASC cell by the elaborated selection of electrolytes. Taking into consideration of electrolytes, ASCs in aqueous electrolytes that could be assembled at atmospheric condition are more environment-friendly, and offer much higher power density than those in nonaqueous electrolytes due to their higher ionic conductivity. Although aqueous electrolytes are generally stable over a voltage window of 1.23 V, aqueous ASCs that can take advantage of high oxygen overpotentials of positive electrode and/or high hydrogen

overpotentials of negative electrode, could greatly widen the maximum operating voltage of aqueous electrolytes (1.4–2.2 V). To highlight this feature, high-voltage aqueous ASCs are referred to the ASCs that operate at a large working voltage of ≥ 1.8 V in aqueous electrolyte. In this section we mainly focus on the typical Mn-based oxides for high-voltage ASCs with a working voltage of ≥ 1.8 V [157].

4.1.1. Graphene/MnO₂ nanosheets

MnO₂ is one of the most promising positive electrode materials for low-cost and environment-friendly ASCs with high voltage [158]. Moreover, it can be used with high voltage of 1.8–2.2 V in neutral aqueous electrolytes of e.g., Li₂SO₄, Na₂SO₄, K₂SO₄, unlike RuO₂·xH₂O and NiOOH, both of which are usually working with a limited voltage window (1.4–1.6 V) in strong acidic or alkaline electrolytes, resulting in environmental issues [157]. For instance, a combination of a carbon capacitive electrode with a MnO₂ pseudo-capacitive electrode can readily result in a 2 V high-voltage cell in aqueous electrolytes due to the apparent water decomposition over-potential on MnO₂ and the high surface area of carbon [27,159]. Further, the use of nanostruc-

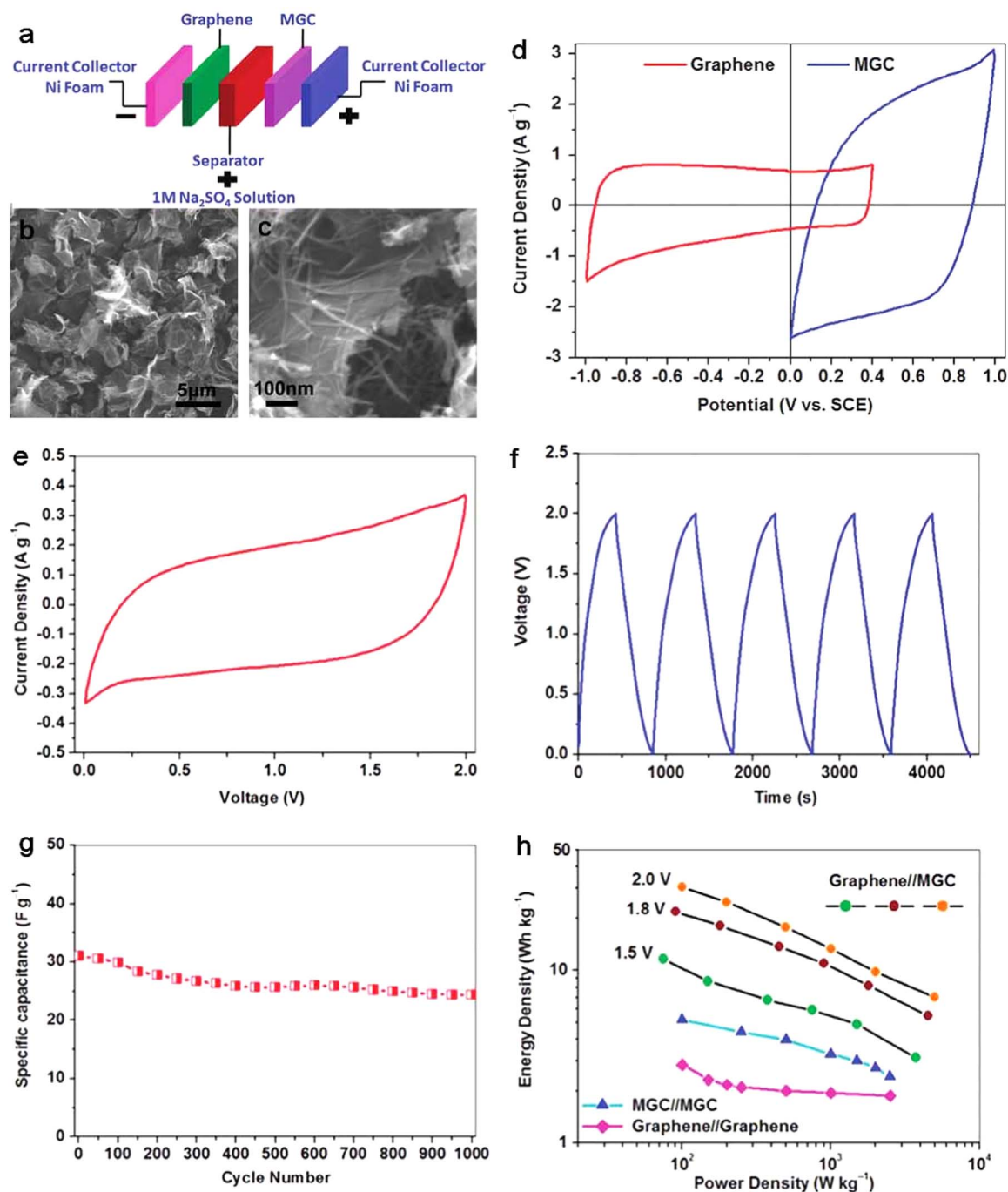


Fig. 4. (a) Schematic of the assembled structure of ASCs based on (b) graphene as negative electrode and (c) MGC as positive electrode. (d) CV curves of graphene and MGC electrodes performed in a three-electrode cell in 1 M Na₂SO₄ solution at 10 mV s⁻¹. (e) CV curve measured at 10 mV s⁻¹, (f) GCD profile tested at 200 mA g⁻¹ and (g) cycle performance of the graphene//MGC ASCs. (h) Ragone plot of graphene//MGC ASCs with various voltage windows, graphene//graphene and MGC//MGC symmetric supercapacitors [15].

tured MnO₂/carbon (e.g., graphene) composites as a faradic electrode can improve the electrical conductivity of the electrode and thus provides the potential for improvement in the cyclability of ECs. Typically, Wu et al. reported the pioneer demonstration of a high-voltage, high-energy ASC combined with a MnO₂ nanowire/graphene composite (MGC) as positive electrode in a neutral aqueous Na₂SO₄ solution as electrolyte (Fig. 4a–d) [15]. Such aqueous electrolyte-based ASCs can be cycled reversibly in the high-voltage region of 0–2.0 V, and exhibit a superior energy density of 30.4 W h kg⁻¹, much higher than those of symmetric supercapacitors based on graphene//graphene (2.8 W h kg⁻¹) and MGC//MGC (5.2 W h kg⁻¹). Moreover, they presented a high power density (5000 W kg⁻¹ at 7.0 W h kg⁻¹) and

acceptable cycling performance of ~79% retention after 1000 cycles (Fig. 4e–h) [15]. It should be noted that this work opens up the possibility of graphene-based composites for applications in safe aqueous electrolyte-based high-voltage ASCs with high energy and power densities. Special emphasis is given to graphene that is first considered as an advanced negative electrode material in this pioneer work because of its high specific surface area and high EDLC nature of graphene, and good stability with large resistance towards hydrogen evolution.

Later, Fan et al. developed high-energy ASCs using G/MnO₂ as positive electrode and AC nanofibers (ACN) as negative electrode in a neutral aqueous Na₂SO₄ electrolyte [77]. Interestingly, an optimized

ASCs could be cycled reversibly in the voltage range of 0–1.8 V, and exhibited maximum energy density of 51.1 W h kg^{-1} , and excellent cycling durability, with 97% capacitance retention after 1000 cycles due to the synergistic effects of high capacitance, excellent rate performance of G/MnO₂ and ACN electrodes. These encouraging achievements show great potential in developing G/MnO₂ hybrids for aqueous ASCs with high energy for practical applications. It should be pointed out that the pH of the electrolyte plays an important role in the discharging behavior of MnO₂, which can be illustrated by the Pourbaix's diagrams that display the relationship between potential and pH level [160]. For instance, MnO₂ shows relatively rectangular CVs in neutral electrolyte while a battery-like behaviour is observed in alkaline solution such as KOH due to the reduction of MnO₂ to Mn(OH)₂ at a higher pH of the electrolyte [9].

4.1.2. Graphene/MnO₂ films

Layer-structured graphene films possess high mechanical strength, high chemical stability, high electrical conductivity and remarkable capacitive performance, therefore it can be directly used as free-standing flexible electrodes [161]. However, serious stacking and aggregation of graphene layers in compact graphene films greatly reduce their electrochemical performance [162,163]. To fully utilize graphene, high electrochemically active nanopacers, such as CNT, metal, and metal oxide nanoparticles, are introduced to efficiently avoid or decrease the possibility of serious agglomeration and restacking of GS ensembles and consequently enable higher available electrochemically-active surface area for increasing EDLC energy storage [164,165].

Combining with a second component, e.g., highly-pseudocapacitive MnO₂ as nanopacers, electrically conductive graphene hybrid films with effective specific surface area and tunable porous structure could be achieved. For instance, Shao et al. used a filtration assembly approach for the preparation of flexible, free-standing hybrids of a graphene/MnO₂ nanorod film as positive electrode and a graphene/Ag film as negative electrode (Fig. 5) [91]. The as-fabricated ASC showed a maximum voltage of 1.8 V, resulting in high energy density of 50.8 W h kg^{-1} and power density of 90.3 kW kg^{-1} at an energy density of 7.53 W h kg^{-1} [91]. This exceptional performance is attributed to the synergistic effect produced between two components of graphene and MnO₂ (or Ag), which could accelerate ion and electron transport by providing low ion-transport resistance and short diffusion-distance, and eventually improve the electrochemical performance of the hybrid films for energy storage.

In another example, Sumboja et al. reported a template-free method for flexible rGO/MnO₂ paper electrode by vacuum filtration of GO/MnO₂ suspension and H₂N₄-modified vapor reduction of GO/MnO₂ paper, which aims to manufacture large areal mass, flexible, free-standing electrodes that combine high conductivity of flexible graphene and large specific capacitance of MnO₂. Remarkably, the areal capacitance achieved is as high as 897 mF cm^{-2} from the rGO/MnO₂ paper [93]. The assembled rGO/MnO₂//rGO ASCs working at 1.5 V, with total active mass of 15 mg and tested in bent condition, could yield a capacitance of 0.34 F, indicative of excellent mechanical robustness of the resultant device.

Furthermore, high conductive flexibility is another intriguing feature of graphene for assisting the manufacture of metal oxide flexible electrode for ASCs. Li's group assembled the multiscale active material/nanocarbon paper electrodes for flexible ASCs based on CNT/MnO₂/graphene paper as positive electrode and CNT/PANI paper as negative electrode separated by aqueous gel electrolyte, representing an operating voltage of 1.6 V and an energy density at 24.8 W h/kg [87]. It is worthy to note that nanocarbon paper of graphene and/or CNTs with 3D nanostructures not only are the robust scaffold loading MnO₂ nanospheres but also a conductive network for efficient ionic and electronic transport for flexible supercapacitors.

4.1.3. 3D Graphene/MnO₂ frameworks

3D graphene-based frameworks, e.g., GAs represent a new class of ultralight and porous carbon materials that are associated with high strength-to-weight and surface-area-to-volume ratios [69]. More importantly, monolithic GAs consisting of a 3D porous framework can provide multi-dimensional electron transport pathways, easy access to electrolyte, and minimized transport distance between bulk electrode and electrolyte [166,167]. Typically, three-dimensional (3D) GAs can be readily assembled using GO as precursors to form hydrogel via hydrothermal reaction and freeze-drying processes [168]. The resultant 3D GAs have been qualified for additive/binder-free electrodes in ASCs [69]. For instance, Duan's group constructed high-energy and high-power ASCs by using 3D porous interconnected graphene hydrogel (GH) as negative electrode and vertically aligned MnO₂ nanoplates on 3D nickel foam (MnO₂-NF) as positive electrode in a neutral aqueous Na₂SO₄ electrolyte (Fig. 6a) [80]. Benefiting for the desirable porous structure, high specific capacitance and rate capability of GH and MnO₂-NF (Fig. 6b–e), and complementary potential window of these two electrodes (Fig. 6f), the ASCs can be cycled reversibly in a wide potential window of 0–2.0 V (Fig. 6g) and exhibited higher energy density of 23.2 W h kg^{-1} and power density of 1.0 kW kg^{-1} , in comparison with those of symmetric supercapacitors based on GH (5.5 W h kg^{-1}) and MnO₂-NF (6.7 W h kg^{-1}). Even at a high power density of 10.0 kW kg^{-1} , the ASCs still provided a high energy density of 14.9 W h kg^{-1} . Further, the ASCs also presented stable cycling performance with 83.4% capacitance retention after 5000 cycles [80]. Zhai et al. synthesized MnO₂ on a porous graphene gel/Ni foam (MnO₂/G-gel/NF) as supercapacitor electrode, delivering a large areal capacitance of 3.18 F cm^{-2} at a high mass loading of 13.6 mg cm^{-2} of MnO₂. Moreover, an ASC based on MnO₂/G-gel/NF as positive electrode and G-gel/NF as negative electrode achieved a remarkable energy density of $0.72 \text{ mW h cm}^{-3}$, excellent cycling stability, with capacitance retention of 98.5% after 10000 cycles [95]. In addition, a surfactant-assisted hydrothermal strategy was also developed to fabricate 3D flower-like Ni₂S₃/GAs as cathode for ASCs [169]. The remarkable electrochemical properties of these ASCs are attributed to the enhanced conductivity and improved accessible surface area for electrolyte ions in the 3D interconnected porous framework, which offers new opportunities for assembling high-voltage ASCs with large mass loading, high areal capacitance and superior energy density.

4.1.4. Graphene/Mn₃O₄

As the potential alternative of MnO₂, Mn₃O₄, as a manganite, is considered as another most promising manganese oxide material for ASCs, in which can lead to a high cell voltage of up to 2 V with combination of nanocarbons for ASCs [34,112]. For example, Xiao et al. reported the composites of Mn₃O₄ nanoparticles anchored on graphene sheets (Mn₃O₄@GR) synthesized by a solvothermal approach [112]. Subsequently, an ASC was constructed with Mn₃O₄@GR as a positive electrode and AC as a negative electrode, displaying improved charge storage performance, high energy density of 34.6 W h kg^{-1} , maximum power density of 15.2 kW kg^{-1} with a wide voltage region of 0–2 V [112]. Also, it is challenging to process the Mn₃O₄ oxide into flexible electrodes without adding inactive supporting materials to address the limited power density of Mn₃O₄ in ASCs. To overcome this, Hu et al. fabricated Mn₃O₄ nanofibers loaded on rGO paper (MG) by hydrothermal method and electrochemical reduction, and used MG as cathode and rGO as anode to assemble the flexible ASCs, which possessed a large cell voltage of 2 V, high volumetric capacitance of 54.6 F cm^{-3} , remarkable volumetric energy density of $0.0055 \text{ W h cm}^{-3}$, and excellent cycling ability in aqueous Na₂SO₄ electrolyte. Very interestingly, such ASC tested in ionic liquid electrolyte showed the highest volumetric power density of 10.95 W cm^{-3} , which is the highest among the reported results for MnO_x-based flexible ASC devices. The impressive results is mainly assigned to the hybrid nanostructure, which can effectively accelerate the charge

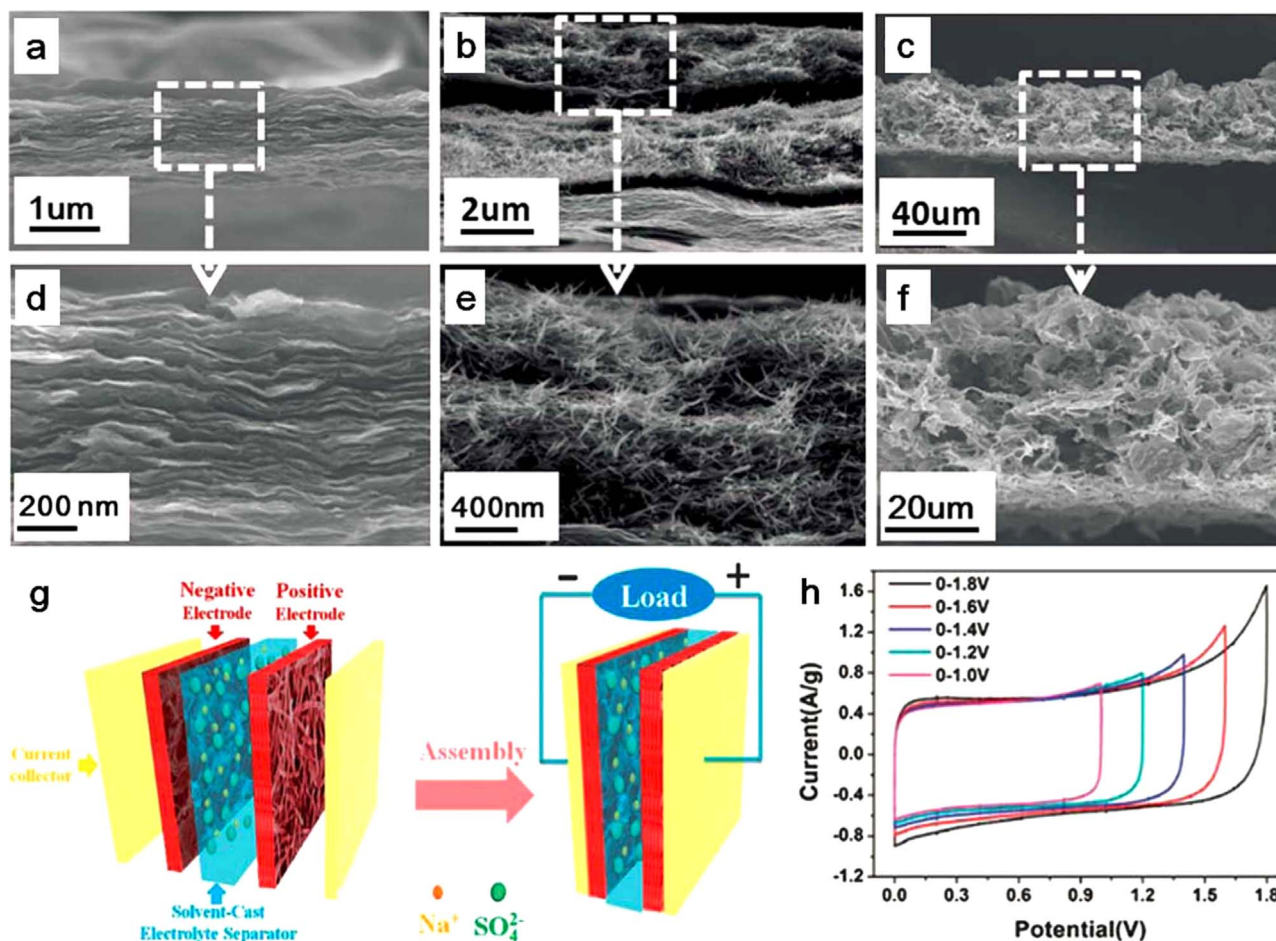


Fig. 5. (a–c) Side view and (d–f) high-magnification SEM images of (a, d) pure graphene, (b, e) graphene/MnO₂ and (c, f) graphene/Ag hybrid films, respectively. (g) Schematic of a fabricated ASC device, based on a graphene/MnO₂ film as positive electrode and a graphene/Ag film as negative electrode in Na₂SO₄ electrolyte. (h) CV curves of the ASC measured at different potential windows at 20 mV s⁻¹ [91].

transfer for a fast pseudoreaction even with high mass loading [34]. It is mentioned that, except the Mn-based oxides, other graphene-based hybrids of such as RuO₂/G [78], NiCo₂O₄/carbon cloth [121], Co₉S₈/G [124] for the aqueous ASCs with a high voltage of 1.8 V were also developed.

4.2. High-capacitance ASCs

As mentioned above, increasing the specific capacitance of electrode materials is acknowledged as one of two important approaches to the improvement of the energy density. Considering the fact that the low EDLC capacitance of nanocarbons, recent studies for ASCs are focused on graphene/oxide and graphene/polymer hybrids by introducing a synergistic effect between graphene and second pseudocapacitive species (oxide, polymer), which could serve as high-capacitance positive electrode and/or negative electrode, resulting in the enhancement of the energy density of an ASC cell. Considering the different requirements for positive electrode and negative electrode in an asymmetric configuration, in this section we mainly summarized the positive electrodes with a superior theoretical capacitance of > 1000 F/g and negative electrode with a larger capacitance than the typical nanocarbons, e.g., graphene powder, graphene films and GAs, respectively.

4.2.1. High-capacitance positive electrode

4.2.1.1. Graphene/Co₃O₄. Cobalt oxide (Co₃O₄) is one of the most attractive positive electrode materials owing to ultrahigh theoretical

specific capacitance up to 3560 F g⁻¹, good retention capability, and high redox reactivity [170]. However, as an electrode material, Co₃O₄ suffers from relatively low electrical conductivity (10⁻⁴–10⁻² S cm⁻¹) and a large volume change during charge/discharge, leading to sluggish electrode kinetics and low specific capacitance [171]. To overcome these issues, the general strategy is to reduce the size of the Co₃O₄ particles at a nanoscale and introduce these electrochemically active nanoparticles into carbon matrices acting as an efficient buffer for accommodating the volume change of nanoparticles and aggregation, and eventually improve the electronic conductivity of the electrode. For instance, Xie et al. prepared a 3D porous GA with embedded Co₃O₄ nanoparticles (3D Co₃O₄-RGO aerogel) by means of a solvothermal approach, followed by freeze-drying and thermal reduction process (Fig. 7a) [35]. The obtained 3D Co₃O₄-RGO aerogel showed a high specific capacitance of 660 F g⁻¹ at 0.5 A g⁻¹ and high rate capability of 65.1% retention at 50 A g⁻¹ in a three-electrode system. Moreover, an ASC device was assembled based on 3D Co₃O₄-RGO aerogel as cathode and hierarchical porous carbon (HPC) as anode in 6 M KOH aqueous electrolyte (Fig. 7b). Notably, the as-prepared device operated at an operating voltage of 1.5 V exhibited a maximum specific capacitance of 130 F g⁻¹, an excellent energy density of 40.65 W h kg⁻¹ at a power density of 340 W kg⁻¹, 23.7 W h kg⁻¹ retained at a power density of 17 kW kg⁻¹, and good cycling performance with 92.9% capacitance retention after 2000 cycles. It should be mentioned that three CR2032 coin-type ASCs connected in series could readily power up a red LED for 1 h after a 30 s charging, indicative of its huge application potential for commercial viability (Fig. 7c). In another example, Ujjain et al. successfully fabricated an aqueous high-voltage ASC, for which the

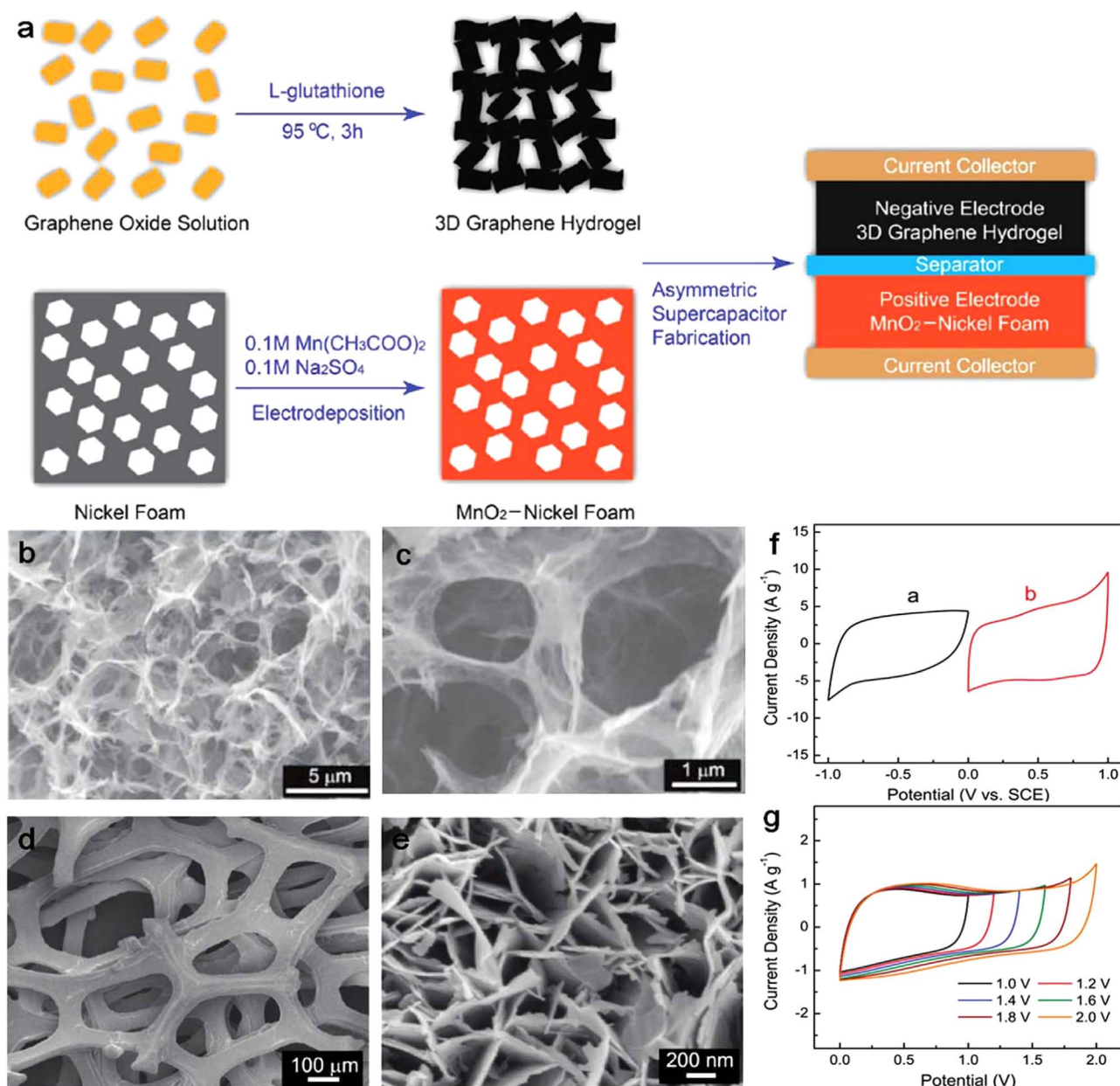


Fig. 6. Schematic of the ASC based on GH as negative electrode and MnO₂-NF as positive electrode. (b, c) SEM images of freeze-dried GH. (d) SEM image of a bare nickel foam, and (e) SEM image of MnO₂ nanoplates electrodeposited on the nickel foam. (f) Cyclic voltammograms of GH (a) and MnO₂-NF (b) electrodes in a three-electrode system at 20 mV s⁻¹. (g) CV curves of the ASC of GH//MnO₂-NF measured at different potential windows at 20 mV s⁻¹ [80].

Co₃O₄/graphene nanoribbons (GNR) hybrid with a noble specific capacitance of ~525 F g⁻¹ worked as positive electrode while GNR film served as negative electrode [134]. The resultant ASCs showed superior device performance with an energy density of 64.2 W h kg⁻¹, much higher than that of symmetric cell, and high power density of 8.3 kW kg⁻¹ due to optimized the mass ratio of the electrodes. In addition, long-term charge/discharge cycling stability was attained, with ~94% capacitance retention after 2000 cycles. Except Co₃O₄, Co(OH)₂ is also an important cobalt-based positive electrode material. For instance, Wang et al. successfully constructed a novel ASC using mesoporous Co(OH)₂ nanosheets arrays/GF with ultrahigh specific capacitance of 1160 F g⁻¹ (at 1 A g⁻¹) as cathode and graphene/Fe₃O₄@C with a maximum specific capacitance of 485 F g⁻¹ (1 A g⁻¹) as anode [136]. Remarkably, the as-assembled ASC device showed an extended cell voltage of 0.0–1.6 V, and acceptable cycle stability (72% capacitance retention after 8000 cycles). More importantly, high specific energy of 75 W h kg⁻¹ is achieved at a specific power of

400 kW kg⁻¹.

4.2.1.2. Graphene/Ni(OH)₂. Ni(OH)₂, as a non-noble metal hydroxide, has been regarded as one of the most attractive candidates of ASCs due to its low cost, simple synthesis process and extremely high theoretical capacitance of 2082 F g⁻¹ (within 0.5 V) [172]. To further boost ion transfer among components of electrode materials, Liu et al. has applied ultra-small Ni(OH)₂ nanoparticles decorated on rGO sheets (Fig. 8a) as cathode electrode and rGO as anode electrode to fabricate a novel Ni(OH)₂/rGO//rGO ASC [127]. Since the hybrid nanostructure can efficiently prevent the agglomeration of Ni(OH)₂ nanoparticles (Fig. 8b) and the stacking of RGO sheet, and achieve ultrahigh specific capacitance of 1717 F g⁻¹ at 0.5 A g⁻¹ due to a synergistic effect of Ni(OH)₂ nanoparticles and rGO. As a result, the assembled ASCs delivered a superior energy density of 75 W h kg⁻¹ and power density of 40 kW kg⁻¹ with a high voltage

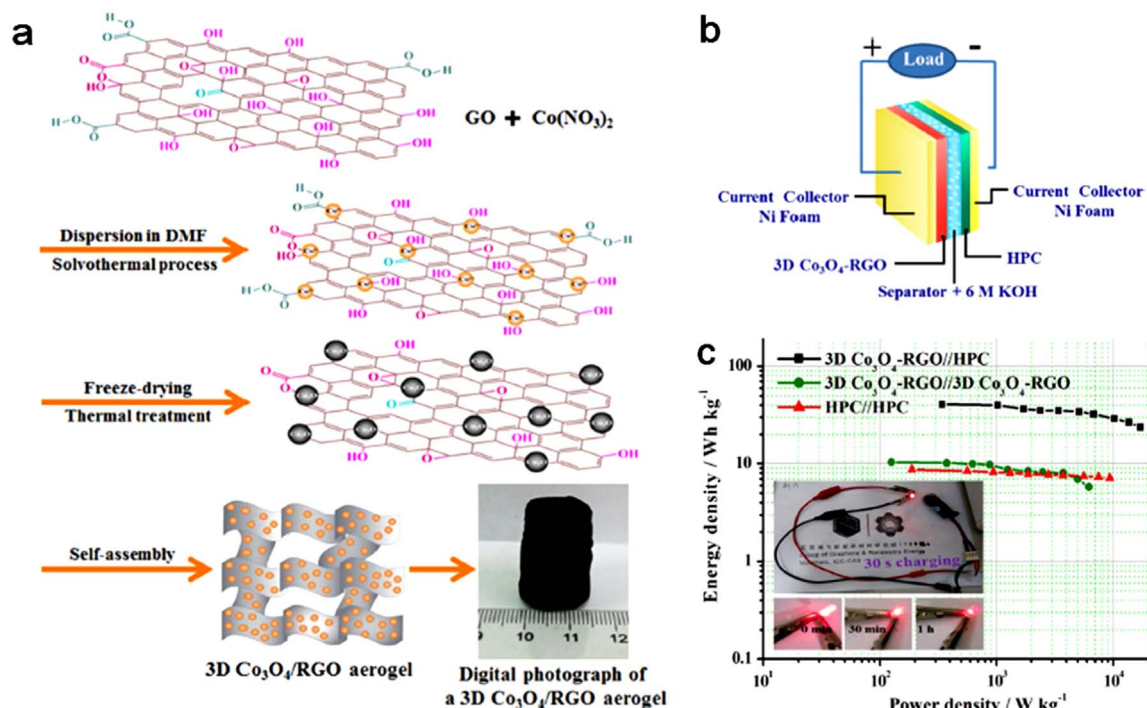


Fig. 7. (a) Fabrication illustration of the 3D Co₃O₄-RGO aerogel. (b) Schematic of the structure of an ASC consisting of 3D Co₃O₄-RGO aerogel and HPC electrodes, a separator, and two current collectors. (c) Ragone plot of the symmetric supercapacitors of 3D Co₃O₄-RGO//3D Co₃O₄-RGO, HPC//HPC and the ASCs of Co₃O₄-RGO//HPC [35]. The inset shows a red LED powered by three ASCs connected in series.

window of 0–1.6 V in 2 M KOH electrolyte (Fig. 8c) [127]. In another key example, Zhang et al. assembled a typical ASC with hierarchical flowerlike high-capacitance Ni(OH)₂ anchored on graphene (1735 F g⁻¹ obtained at 1 mV s⁻¹) as positive electrode (Fig. 8d and e) and porous graphene as negative electrode, respectively [82]. In light of its unique structure and efficient co-ordination of electrode materials, the fabricated ASCs possessed a high voltage region of 0–1.6 V in KOH aqueous electrolyte, and displayed high specific capacitance of 218.4 F g⁻¹, and maximum energy density and power density of 77.8 W h kg⁻¹ (at a power density of 174.7 W kg⁻¹) and 15.2 kW kg⁻¹ (at an energy density of 13.5 W h kg⁻¹), respectively. Moreover, the Ni(OH)₂/graphene/porous graphene ASC exhibited excellent cycling stability with capacitance retention of 94.3% after 3000 cycles [82]. More interestingly, Zhang et al. fabricated a hierarchical nanostructure Ni(OH)₂ with vertical and cross-linked network structure, which was grown on 3D carbon support of cellulose-fiber covered with graphene (CFG) (Fig. 8f–i). Notably, the Ni(OH)₂-CFG composite as a binder-free electrode revealed high mass capacitance of 2276 F g⁻¹, and good rate capability (Fig. 8j). And the assembled ASCs of Ni(OH)₂-CFG as positive electrode and AC as negative electrode exhibited a robust cycle life with almost no capacitance loss after 5000 cycles (Fig. 8k) [147]. The remarkable performance of Ni(OH)₂/graphene composite for hybrid energy storage demonstrates their promising potential in application.

4.2.1.3. Graphene/NiO. NiO is an attractive pseudocapacitive positive material for supercapacitors in aqueous alkaline solution because of its high theoretical capacitance of 2584 F g⁻¹ within 0.5 V, robust reversibility, low cost, excellent chemical and thermal stability [173]. In order to achieve the demand of high capacitance and address its poor conductivity, Liu et al. constructed a ternary system of RGO/Ni/NiO consisted of rGO, nickel and nickel oxide nanoparticles with the size of about 30 nm, strongly anchoring on graphene sheets [125], which achieved a high specific capacitance of 1410 F g⁻¹ at 1 A g⁻¹ and 1020 F g⁻¹ at a high current density of 15 A g⁻¹. Furthermore, the ASCs

composed of RGO/Ni/NiO as positive electrode and porous carbon as negative electrode exhibited an operation voltage of 1.6 V, large cell capacitance of 183.8 F g⁻¹, high energy density of 65.3 W h kg⁻¹, and high power density of 8000 W kg⁻¹ in aqueous KOH electrolyte. Note that this value of energy density was much higher than that of porous carbon-based symmetric supercapacitor, e.g., 9.2 W h kg⁻¹ at a power density of 500 W kg⁻¹. Moreover, the fabricated ASCs presented superior cycling stability without capacitance decay after 3000 cycles.

To achieve high areal capacitance, Luan et al. developed an ASC device with rGO electrochemically deposited on three-dimensional (3D) nickel foam as anode and nickel oxide nanoflake arrays on a flexible carbon cloth substrate as cathode in 1.0 M KOH electrolyte [90]. Notably, the nanostructured electrodes with 3D porous structures could offer large effective surface area for fast ion and electron transport, and the porous NiO nanoflake-arrayed electrode with a relatively high mass loading of 2.7 mg cm⁻² showed a remarkable areal capacitance of 1054 mF cm⁻² (specific capacitance of 392 F g⁻¹) at a current density of 0.5 mA cm⁻². The ASC device operates with a voltage of 1.7 V and achieved a remarkable areal capacitance of 248 mF cm⁻² and a maximum energy density of 39.9 W h kg⁻¹. The enhanced charge storage performance is assigned to the increased surface area of the porous NiO nanoflake and rGO sheets. Special emphasis is given to high mass loading of the active material in an ASC system that is desirable for practical application.

4.2.1.4. Graphene/Ni,Co-binary hydroxide (Oxide). Ni,Co-binary hydroxide (oxide) have been demonstrated enhanced electrochemical performance and significant advantages over single element material, in particular, with higher oxygen overpotential, lower resistance of the corresponding electrode, and rich multiple redox reactions [174,175]. To integrate the combined benefits of Ni,Co-binary hydroxide and graphene, Lee's group reported the facile synthesis of flower-like 3D framework of nickel-cobalt binary hydroxide (Ni-Co-BH) on rGO (Ni-Co-BH-G) sheets by a simple, cost-effective and additive-free ionic layer adsorption method [153]. Taking the advantage of 3D conductive

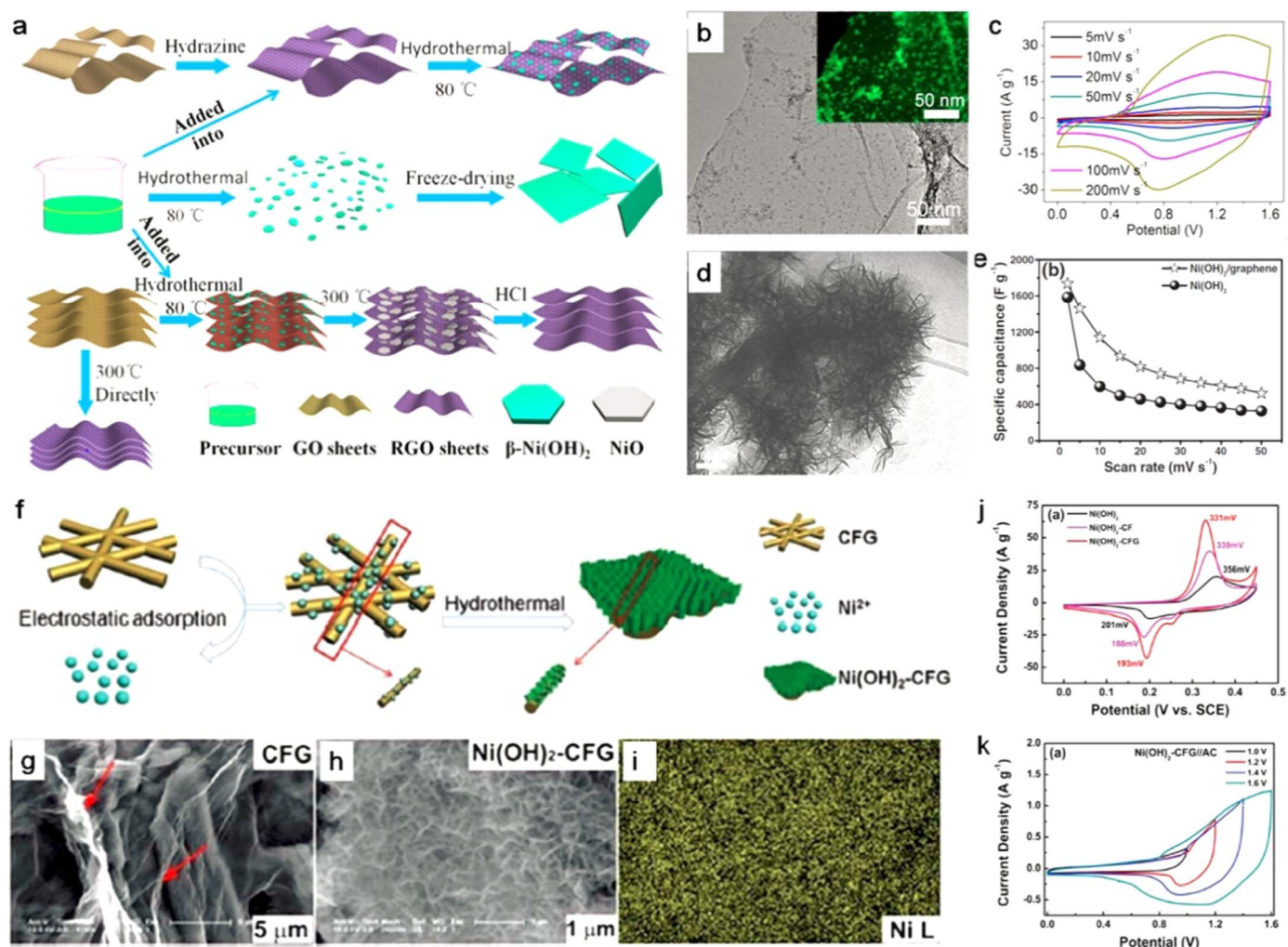


Fig. 8. (a) Schematic illustration of the synthesis process of the RGO-Ni(OH)₂ composite. (b) TEM image of the ultrasmall Ni(OH)₂ on rGO sheets. Inset: an annular dark field scanning TEM image. (c) CV curves at different scan rates. (d) TEM image of flower-like Ni(OH)₂/graphene composite. (e) Specific capacitance of pure Ni(OH)₂ and Ni(OH)₂/graphene composite as a function of the scan rates. (f) Schematic illustration of the fabricated process of the Ni(OH)₂-CFG. (g, h) SEM images of (g) CFG and (h) Ni(OH)₂-CFG. (i) Elemental mapping image of Ni in the Ni(OH)₂-CFG. (k) CV curves of the Ni(OH)₂-CFG//AC in different voltage windows at 10 mV s⁻¹.

mesoporous open framework, the obtained Ni-Co-BH-G offered a remarkable specific capacitance of 2130 F g⁻¹ at 2 A g⁻¹. Subsequently, the ASCs were constructed with the optimized Ni-Co-BH-G as cathode and concentrated nitric acid treated conducting carbon cloth (CCN) as anode, which obtained an ultrahigh energy density of ~92 W h kg⁻¹, and high power density of 7 kW kg⁻¹, and capacitance retention of ~80% after 10,000 charge-discharge cycles. The superior performance of this ASC was substantially ascribed to the porous nanostructure of Ni-Co-BH-G that can sufficiently facilitate ion diffusion and electron transport [153]. In addition, Xiao et al. developed a bio-inspired approach for synthesizing Co_{0.45}Ni_{0.55}O decorated on RGO sheets with a high capacitance of 823.0 F g⁻¹, and assembled Co_{0.45}Ni_{0.55}O/rGO//rGO ASCs at a cell voltage of 1.5 V (Fig. 9). The assembled ASCs displayed high energy density of 35.3 W h kg⁻¹, much higher than those of the symmetric cells (Co_{0.45}Ni_{0.55}O/RGO)/(Co_{0.45}Ni_{0.55}O/RGO) (20.2 W h kg⁻¹) and RGO//RGO (4.5 W h kg⁻¹) [81].

4.2.1.5. Graphene/V₂O₅. Vanadium pentoxide (V₂O₅) has a layered structure and possesses mixed valence state, which makes it a versatile electrode material for pseudocapacitors. Also, V₂O₅ has been studied as one promising positive electrodes for ASCs, due to its high capacitance, different redox peaks and high potential (~3.0 V vs. Li/Li⁺) [31]. To

enhance its electronic conductivity of V₂O₅, Nagaraju et al. reported the synthesis of 2D heterostructures of V₂O₅ nanosheets and rGO electrodes (G/V₂O₅) for ASCs (Fig. 10a). It is found that RGO/V₂O₅ showed a higher specific capacitance of 635 F g⁻¹ than that of pure V₂O₅ nanosheets (253 F g⁻¹, Fig. 10b) [106]. Correspondingly, the assembled G/V₂O₅//RGO ASCs exhibited a higher energy density of 79.5 W h kg⁻¹ compared with V₂O₅//RGO ASCs (39 W h kg⁻¹ at a power density of 900 W kg⁻¹) (Fig. 10c). Specific emphasis is placed on the achievement of high energy density of G/V₂O₅//RGO ASCs, which is much higher than any of those ASCs using V₂O₅ electrodes previously reported [31].

4.2.1.6. Graphene/polyaniline. The conductive polymers such as PANI and PPy have been considered as one class of the most promising positive electrode materials for supercapacitors including ASCs in terms of low-cost, ease of synthesis, good stability in air, excellent conductivity, and high specific capacitance [161,176–178]. The main drawback of conductive polymer as supercapacitor electrode is its poor electrochemical stability due to continuous swelling and shrinkage occurring during charging/discharging process. As a result, this will induce mechanical degradation of the electrode and weakening of its electrochemical performance. One possible way to overcome this issue is to fabricate the hybrid nanostructures of conductive polymer

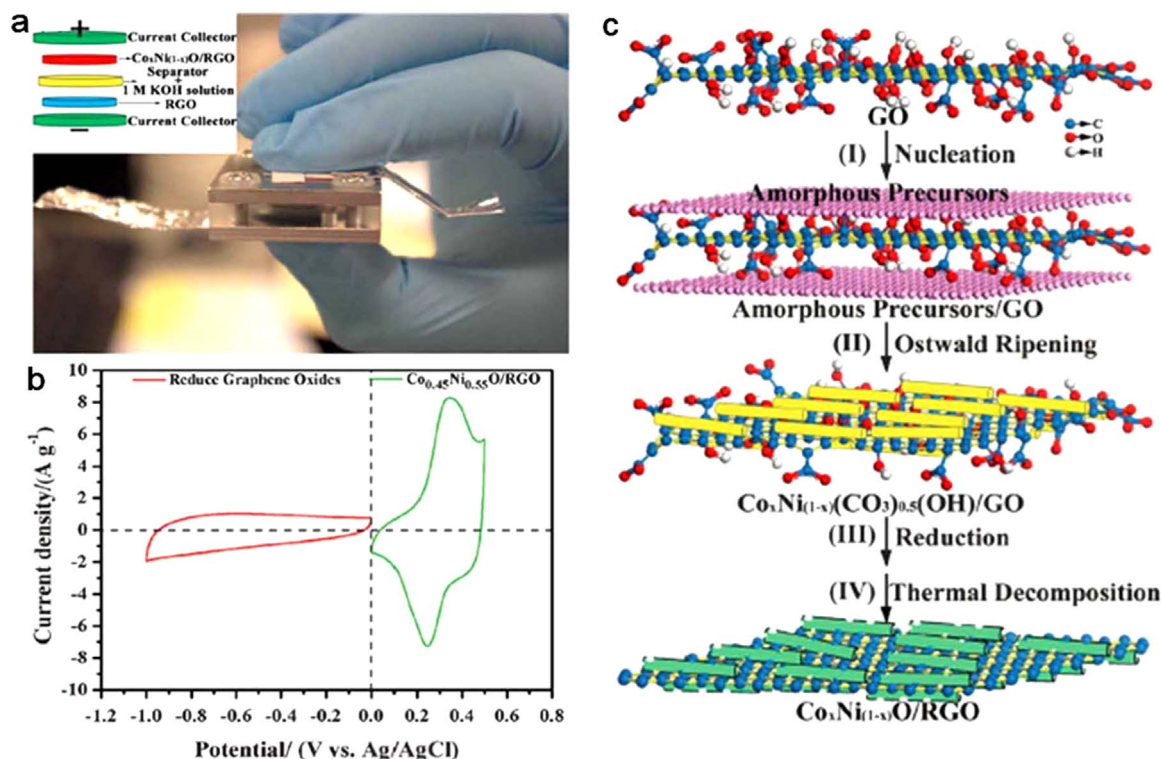


Fig. 9. (a) Photograph of an assembled ASC consisting of RGO as anode and Co_{0.45}Ni_{0.55}O/RGO as cathode, and inset is the schematic of the ASC. (b) CV curves of RGO and Co_{0.45}Ni_{0.55}O/RGO electrodes obtained at 5 mV s⁻¹ in 1 M KOH electrolyte. (c) Schematic illustrating the formation process of Co_xNi_{1-x}O/RGO composite [81].

with nanocarbon material such as graphene. In this regard, Zhang et al. assembled an ASC based on RGO sheets modified with PANI (RGO-PANi, ~400 F g⁻¹ at 0.3 A g⁻¹) as cathode and RGO-RuO₂ (340 F g⁻¹ at 0.3 A g⁻¹) as anode in an aqueous electrolyte, respectively [55], exhibiting an energy density of 26.3 W h kg⁻¹, and a power density of 49.8 kW kg⁻¹ (at 6.8 W h kg⁻¹). To improve the overall cell capacitance, Cheng et al. demonstrated graphene and single-walled CNT composites (graphene/CNT) as anode and graphene/CNT composite coating by PANI nano-cones (graphene/CNT-PANI) as cathode for safe aqueous high-energy ASCs [85], showing a superior energy density of 188 W h kg⁻¹ and maximum power density of 200 kW kg⁻¹ achieved (Fig. 10d–i). The excellent performance of the assembled ASCs is mainly attributed to the uniform and vertically aligned PANI coating on graphene, offering increased electrical conductivity and promoting the utilization of active material (Fig. 10d–i). To further enhance the conductivity with increased electron transfer rate and improved ion diffusion, Hao et al. reported a new ternary composite, in which PANI nano-dots were orderly grown on GO for the formation of the nano-ravines, and MWCNTs were surrounded by PANI connected all components for enhancing the conductivity, leading to outstanding specific capacitance up to 696 F g⁻¹ at 20 mV s⁻¹. Thus, the ASCs were assembled by PANI/GO/MWCNTs composite as positive electrode and GO/MWCNTs as negative electrode [151]. Notably, the ASC possessed an extended working potential of 1.6 V, good rate capability, excellent cycling stability (89% capacitance retention after 3000 cycles), and impressive energy and power density (69 W h kg⁻¹ and 6.4 kW kg⁻¹) [151]. It is suggested that strategy is also potentially useful for the preparation of other graphene-based composites to meet diverse application requirements ranging from supercapacitors to other energy storage devices.

4.2.2. High-capacitance negative electrode

4.2.2.1. Graphene/RuO₂.

Ruthenium oxide (RuO₂) is an important electrode material for oxide-based supercapacitors [179]. Especially hydrous and amorphous RuO₂ has a high capacitance, reversible charge-discharge feature and good electrical conductivity, making it the focus of research and development of supercapacitors with great potential for achieving higher energy and power densities than carbon-based EDLCs and polymer-based pseudocapacitors, even at the expense of its high cost [180]. However, RuO₂ particles often tend to form big agglomerates, resulting in the significant degradation of their electrochemical performance. In this case, graphene sheets, especially RGO possessing rich oxygen-containing functional groups, allow for the formation and uniform anchoring of fine oxide nanoparticles via strong chemical interactions between the functional groups of graphene and the nanoparticles. As an typical example, Wu et al. reported the synthesis of hydrous RuO₂/graphene sheet (GS) composites (ROGSCs) by combining sol-gel and low-temperature annealing processes (Fig. 11a) [71]. Benefiting from the positive synergistic effect of GSs and RuO₂ (5–20 nm) nanoparticles, the hybrid supercapacitors fabricated exhibited high specific capacitance (~570 F g⁻¹, Fig. 11b), enhanced rate capability, excellent electrochemical stability (~97.9% retention after 1000 cycles), high energy density (20.1 W h kg⁻¹), and high power density (10,000 W kg⁻¹, Fig. 11c) in comparison with the pure GSs and RuO₂ [71]. These findings demonstrate the importance and great potential of graphene/oxide composites in the development of high-performance energy storage systems. Later, Zhao's group developed a novel ASC using RGO modified with ruthenium oxide (RGO-RuO₂, Fig. 11d) or PANi (RGO-PANi) as the anode and cathode, respectively [55]. And the specific capacitance of symmetric supercapacitors of RGO-PANi//RGO-PANi and RGO-RuO₂//RGO-RuO₂ was calculated to be ~400 and ~340 F g⁻¹, respectively, at 0.3 A g⁻¹. The ASC exhibited a significantly improved capacitive performance in comparison with that of the symmetric supercapacitors fabricated with RGO-RuO₂ or

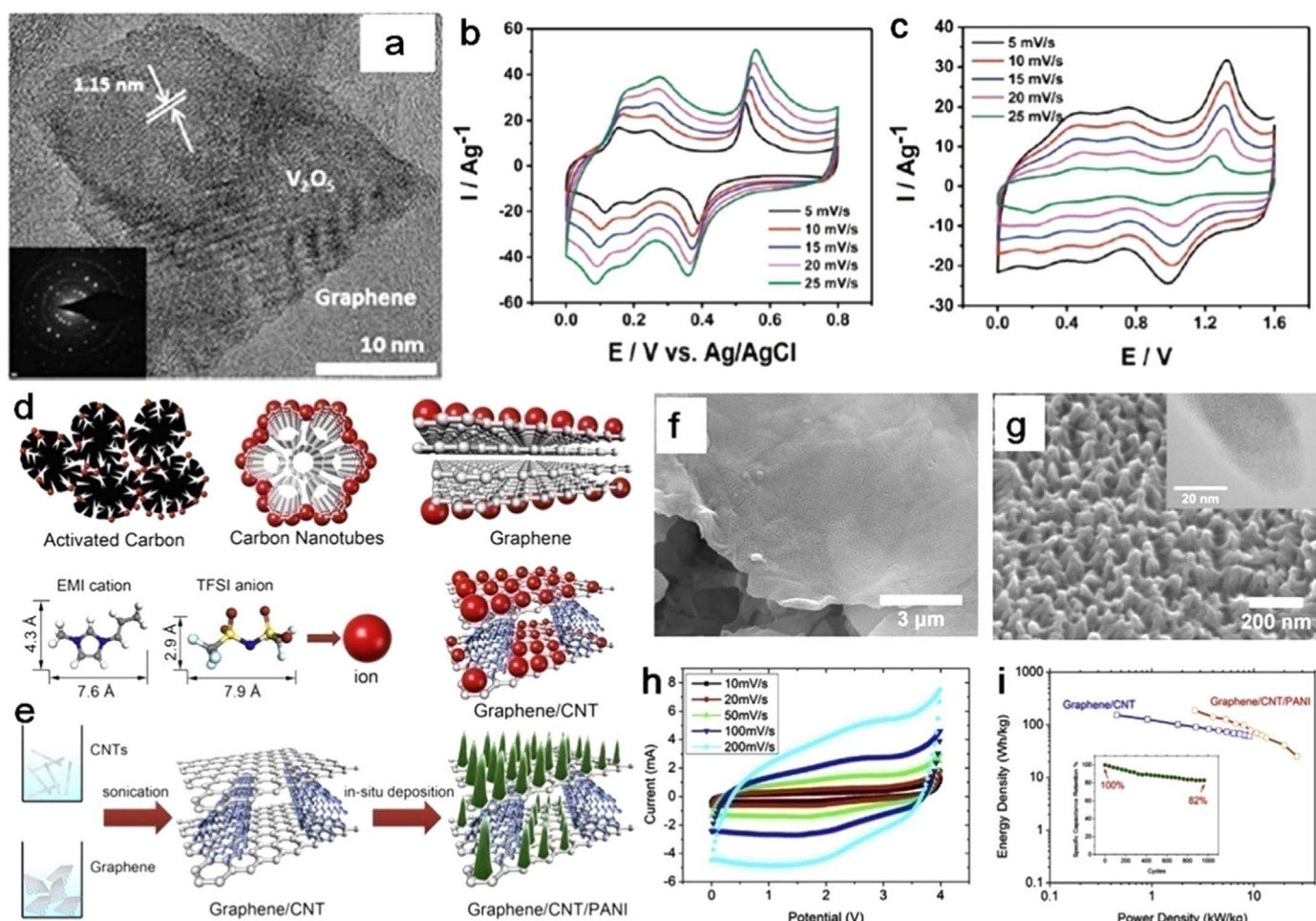


Fig. 10. (a) TEM image of rGO/V₂O₅ nanosheet. (b, c) CVs at different scan rates of (b) rGO/V₂O₅ electrode and (c) rGO/V₂O₅//RGO ASCs in aqueous 1 M KCl solution [106]. (d) Comparison of various carbon structures of AC, CNT, graphene and graphene/CNT as electrode material for supercapacitors and models of the structure of EMI and TFSI ions with a size correlation. (e) Illustration of fabrication of graphene/CNT and graphene/CNT-PANI composites. (f) Low-magnification and (g) high-magnification SEM images of graphene/CNT-PANI. Inset in (g) is TEM image of a PANI nano-cone. (h) CV curves of graphene/CNT composite at different scan rates from 10 to 200 mV s⁻¹ in 1-ethyl-3-methylimidazoliumbis(trifluoromethanesulfone)imide (EMI-TFSI) electrolyte. (i) Ragone plot of graphene/CNT and graphene/CNT-PANI composite electrodes [85]. Inset is the cycling performance of graphene/CNT-PANI at 2 A g⁻¹.

RGO-PANi as electrodes (Fig. 11e). The improvement was attributed to the broadened potential window in an aqueous electrolyte, leading to an energy density of 26.3 W h kg⁻¹, about two times higher than that of the symmetrical supercapacitors based on RGO-RuO₂ (12.4 W h kg⁻¹) and RGO-PANi (13.9 W h kg⁻¹) electrodes. In addition, a power density of 49.8 kW kg⁻¹ was obtained at an energy density of 6.8 W h kg⁻¹ (Fig. 11f) [55].

4.2.2.2. Graphene/MoO₃. MoO₃ is one of the limited important transition metal oxides with high capacitive performance for negative electrode of ASCs. To improve the electrical conductivity, the composites of nanocarbon and MoO₃ nanostructures such as nanoparticles, nanoplates and nanorods have been reported for ASCs [52]. In particular, layer-structured α-MoO₃ is proved to be a very suitable negative electrode with fast intercalation pseudocapacitance [181,182]. Combining the advantages of α-MoO₃ and graphene, Lee's group developed a facile self-assembly method for the fabrication of RGO-wrapped thin layered structure α-MoO₃ (GrMoO₃, 291 F g⁻¹ at 2 mV s⁻¹) for the negative electrode of ASCs, together with a self-assembled graphene/MnO₂ (GrMnO₂, ~350 F g⁻¹ at 200 mA g⁻¹) composite as a positive electrode in safe aqueous Na₂SO₄ electrolyte (Fig. 12) [52]. The fabricated ASCs has an operation voltage of 2.0 V, a maximum specific capacitance of 307 F g⁻¹, and a high energy density

of 42.6 W h kg⁻¹ at a power density of 276 W kg⁻¹. Therefore, this strategy through the reasonable choice of metal oxides supported on graphene offers a new direction for next-generation low-cost and environmental friendly ASCs with high energy and high power densities.

4.3. High-power ASCs

Regarding the true performance metrics for ASCs and other energy storage devices, power density and energy density are definitely recognized as the most important two parameters. It is well accepted that ASCs has a major merit of outstanding power performance, much higher than that of batteries. The maximum power of an ASC cell is widely calculated by the Eq. (11), which in principle can be realized by increasing the working voltage (V) and reducing the equivalent series resistance (ESR). It is worthy of note that, although the maximum power density is commonly used for comparison, it is unable to generally represent the actually deliverable power density of an ASC device [5]. In this case, we can use another calculation method from the Eq. (10) to compute the actual power capability. In addition, we should keep in mind that the boosted power density of ASCs is intrinsically originated from the optimal integration of all isolated device components, in particular, the combination of high conducting activated

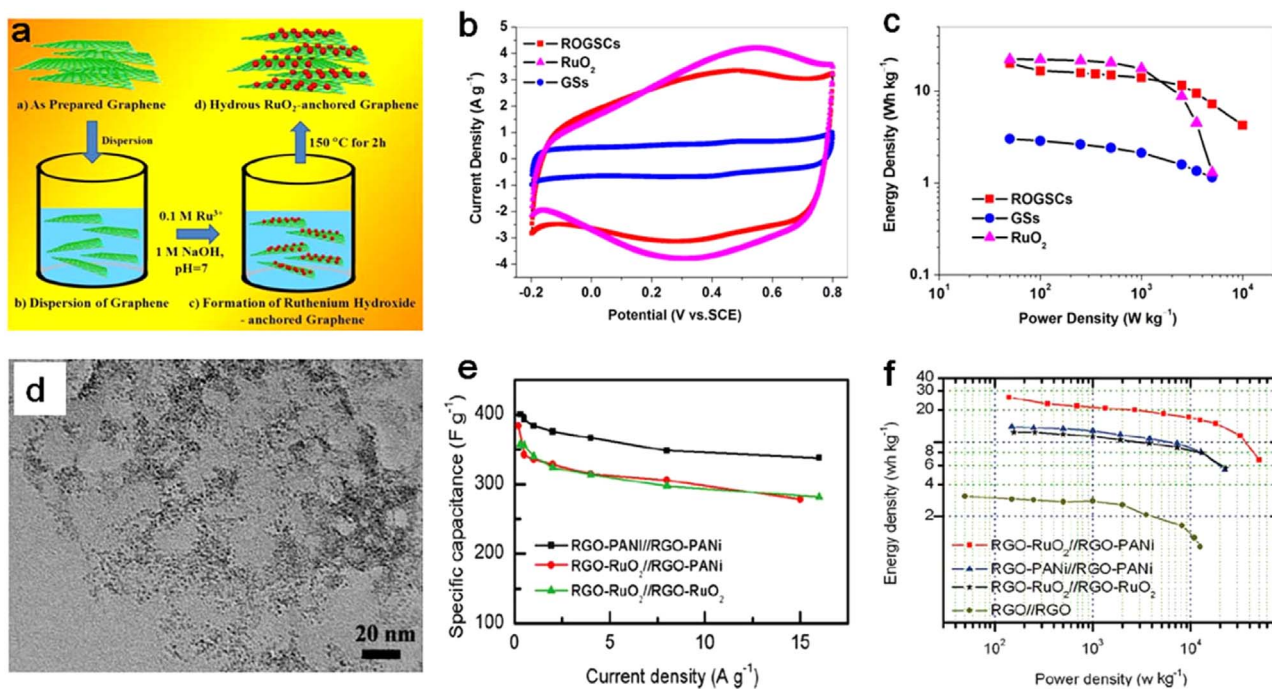


Fig. 11. (a) Preparation illustration of ROGSCs. (b) CV curves of GS, RuO₂, and ROGSC electrodes measured at 5 mV s⁻¹. (c) Ragone plot of GS, RuO₂, and ROGSC supercapacitors [71]. (d) TEM image of RGO-RuO₂. (e) Specific capacitance and (f) Ragone plot of RGO-RuO₂//RGO-PANI ASCs, RGO-RuO₂//RGO-RuO₂ and RGO-PANI//RGO-PANI symmetric cells [55].

materials and current collectors, e.g., porous graphene and 3D graphene framework.

4.3.1. Porous graphene

Porous graphene materials have spurred intensive interests because of combining the merits from both porous materials and graphene, such as large surface area, unique porous structure, tailored composition and excellent electronic conductivity. These fascinating character-

istics enable porous graphene materials to act as superior components in high-performance electrochemical energy storage and conversion devices such as supercapacitors [183]. The main synthesis methods include chemical activation [67], template, hydrothermal assembly, and chemical vapor deposition (CVD). For the use of ASCs, Shen et al. developed a combined chemical foaming, thermal reduction and KOH activation method to produce activated porous graphene (aGNS) with high specific surface area of 1383 m² g⁻¹ for negative electrode, and

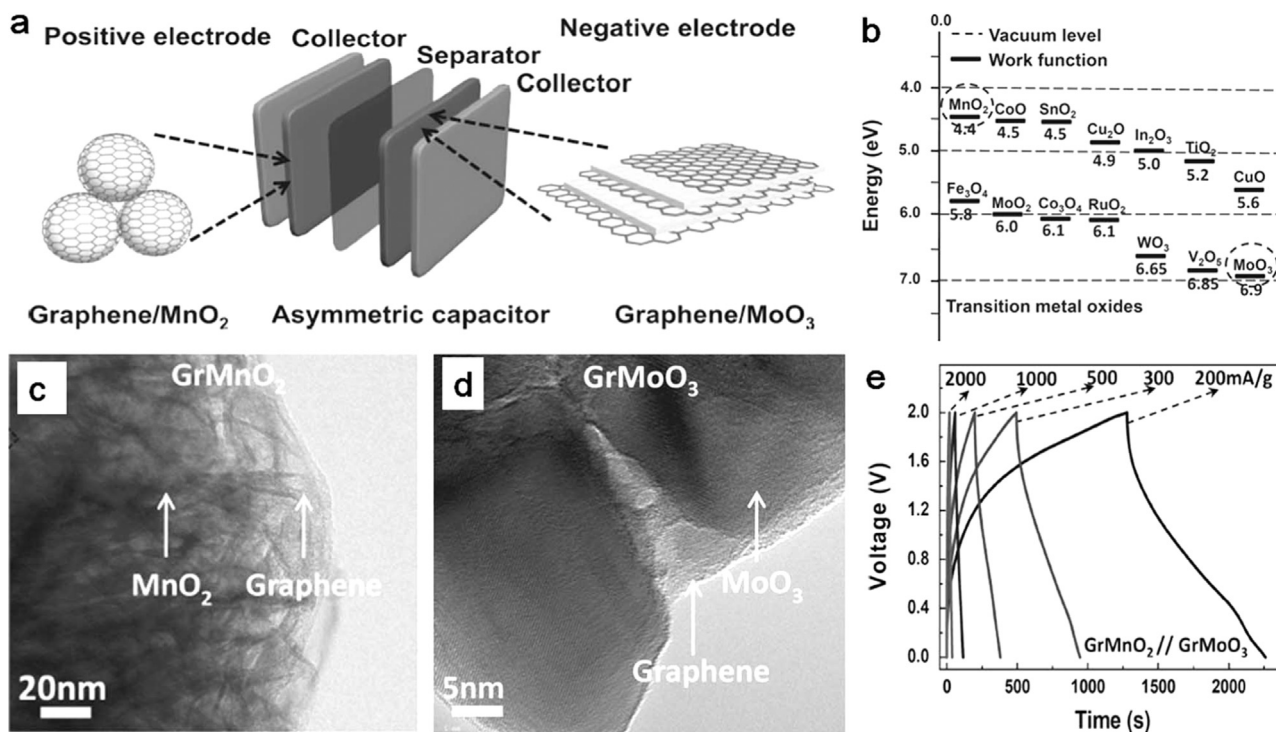


Fig. 12. (a) Schematic of an ASC of GrMoO₃//GrMnO₂ in neutral aqueous Na₂SO₄ electrolyte. (b) Schematic of work function of different metal oxides. (c, d) HRTEM images of (c) GrMnO₂ and (d) GrMoO₃ composite. (e) Galvanostatic charge/discharge curves of a GrMoO₃//GrMnO₂ ASC at different current densities [52].

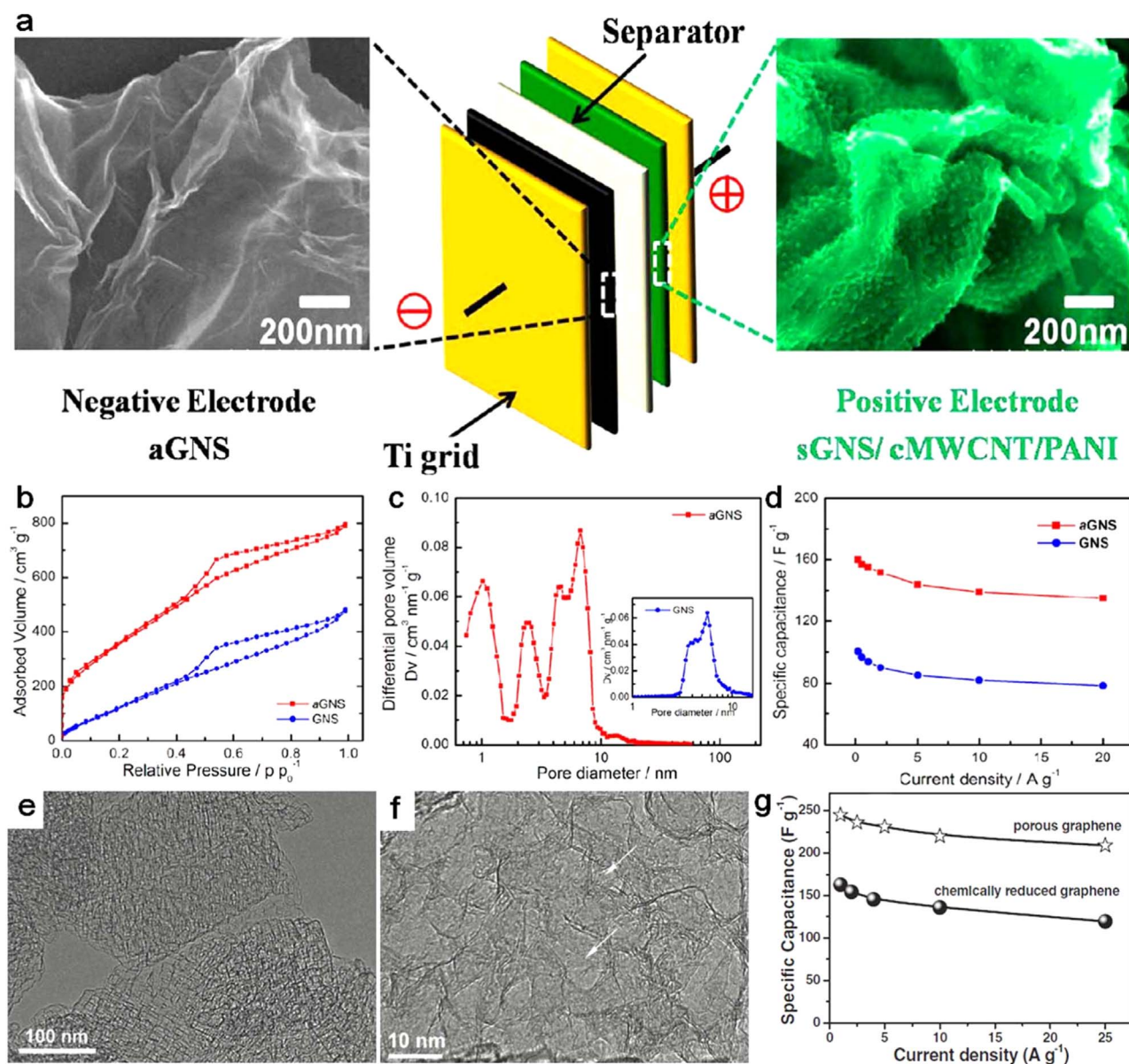


Fig. 13. (a) Schematic of an ASC based on a sGNS/cMWCNT/PANI composite as positive electrode and aGNS as negative electrode. (b) Nitrogen adsorption–desorption isotherms and (c) corresponding pore-size distributions of GNS and aGNS. (d) Specific capacitance as a function of current density of the GNS and aGNS. (e) TEM and (f) HRTEM images of porous graphene. (g) Specific capacitance of porous graphene and chemically reduced GO as a function of current density.

used an interfacial polymerization method to synthesize sulfonated graphene nanosheet (sGNS)/carboxylated multi-walled CNT/PANI (sGNS/cMWCNT/PANI) composite for positive electrode [92]. The fabricated ASCs could be cycled reversibly at a cell voltage of 1.6 V in 1 M H₂SO₄ aqueous electrolyte, and showed an energy density of 20.5 W h kg⁻¹ at a power density of 25 kW kg⁻¹ (Fig. 13a–d). Interestingly, Yan et al. reported that porous graphene as negative electrode was successfully grown on porous MgO sheets as a template by CVD, and accordingly synthesized hierarchical flower-like nickel hydroxide decorated on graphene as positive electrode for the assembly of a high-voltage ASC device [82]. It should be pointed out that, compared to rGO, porous graphene not only exhibits high specific capacitance but also maintains it at high current density, e.g., 245, 236, 231, 220, and 209 F g⁻¹ at different current densities of 1, 2.5, 5, 10, and 25 A g⁻¹, respectively (Fig. 13e–g), because of its narrow mesopore distribution and open flat layer with high surface area. More importantly, the ASCs could be cycled reversibly in the high-voltage region of 0–1.6 V, and showed excellent performance with high specific capacitance of 218.4 F g⁻¹ and energy density of 77.8 W h kg⁻¹ at a power

density of 174.7 W kg⁻¹, and still kept 13.5 W h kg⁻¹ at a power density of 15.2 kW kg⁻¹. Impressively, the ASCs maintained remarkable long-life stability of 94.3% capacitance retention after 3000 cycles [82]. These impressive performances demonstrate that porous graphene is a good candidate of high conducting activated material as negative electrode for ASCs.

4.3.2. Graphene foam

Monolithic GFs consisting of a 3D porous framework can provide multi-dimensional electron transport pathways, easy access to electrolyte, and minimized transport distance between bulk electrode and electrolyte [166,167]. Moreover, 3D interconnected porous GF grown by CVD possesses high electrical conductivity, low mass density, superior flexibility, high mechanical stiffness [184], which has been widely explored as a stable yet conductive substrate, a new 3D current collector, for the efficient deposition of active materials to facilitate fast electron and ion transportation, as a consequence, resulting in high power density [185]. For instance, Wang et al. used a pulsed laser deposition process for the growth of NiO nanoparticles on highly

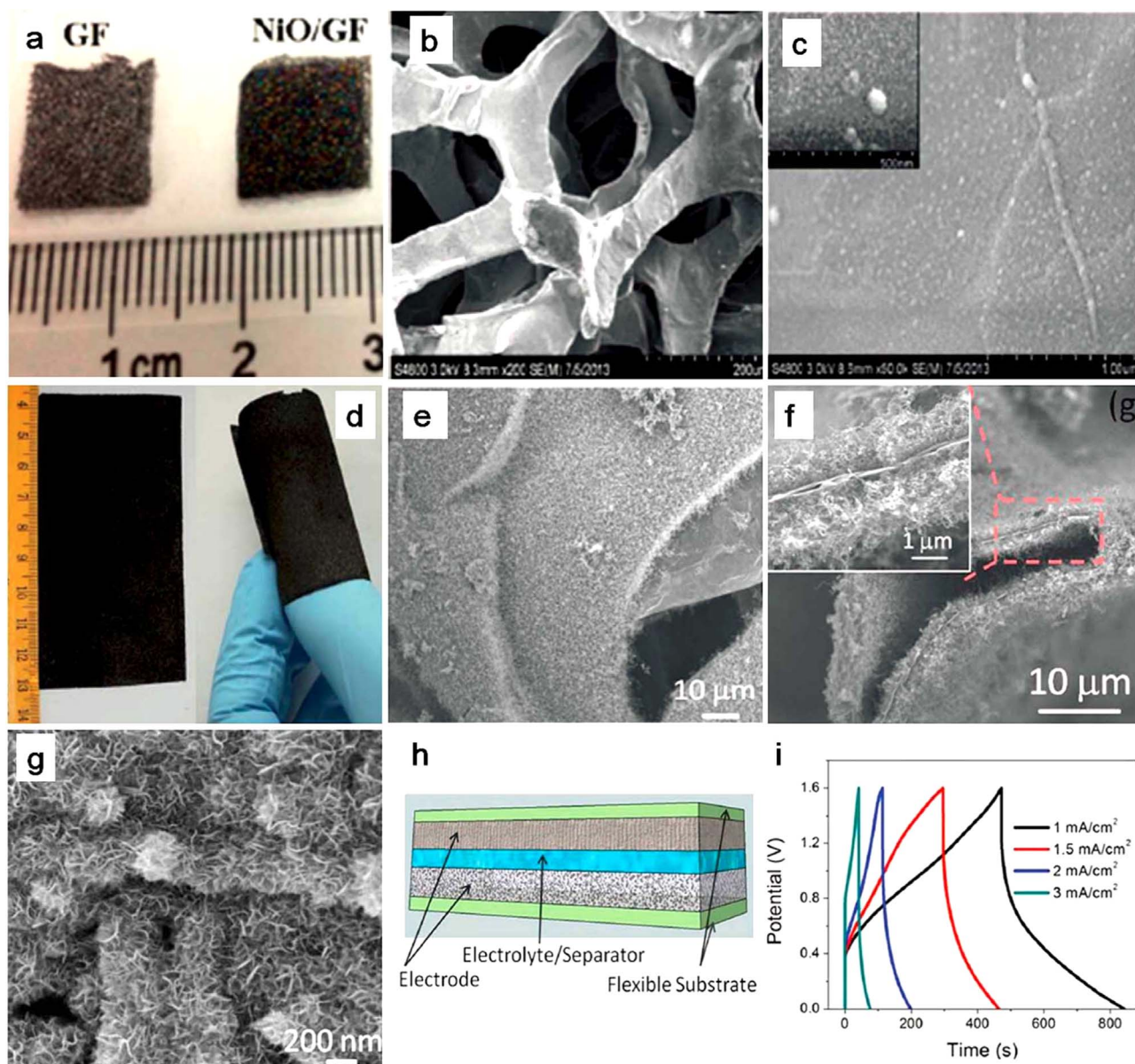


Fig. 14. (a) Optical images of a GF and NiO/GF. (b, c) SEM images of the (b) GF and (c) NiO/GF [109]. (d) Photograph showing the large size and flexibility of a GF/CNT film. (e, f) Typical SEM images of CNTs in a GF/CNT hybrid film. (g) SEM image of MnO₂ nanosheets on a GF/CNT/MnO₂ hybrid film. (h) Schematic of an ASC consisting of the GF/CNT/MnO₂ positive electrode, electrolyte-soaked separator and GF/CNT/Ppy negative electrode. (i) GCD curves of the ASC at different current densities [104].

conductive 3D GF (Fig. 14a–c), displaying a high specific capacitance of 1225 F g⁻¹. Using this NiO/GF as positive electrode and hierarchical porous nitrogen-doped CNTs as negative electrode, the assembled ASCs in aqueous KOH solution presented a working voltage of 0.0–1.4 V and energy density of 32 W h kg⁻¹ achieved at power density of 700 W kg⁻¹ [109]. Notably, ultrahigh power density of 42 kW kg⁻¹ was attained at an extremely short charge-discharge time of 2.8 s. In another example, Lou's group reported a 3D GF/CNT hybrid film with high flexibility and robustness as ideal support for deposition of a large amount of electrochemically active materials per unit area (Fig. 14d–f) [104]. To demonstrate the concept, MnO₂ (Fig. 14g) and polypyrrole (PPy) have been deposited on the GF/CNT film as positive and negative electrode for lightweight and flexible ASCs in an aqueous electrolyte. The ASCs could work with an output voltage of 1.6 V (Fig. 14h and i), and delivered high energy/power density (22.8 W h kg⁻¹ at 860 W kg⁻¹ and 2.7 kW kg⁻¹ at 6.2 W h kg⁻¹), and exhibited remarkable cycling stability (capacitance retention of 90.2–83.5% after 10000 cycles). Moreover, the ASCs could retain their electrochemical performance at different bending angles. Additionally, Ni(OH)₂ nanoflakes were also

electrodeposited on Ni foam-supported vertically oriented graphene sheets for ASCs [186]. These ASCs have great potential as power sources for flexible and lightweight electronic devices [104]. Moreover, the deposition of highly electrochemically active materials on 3D GFs is a practical strategy to overcome the challenge of low volumetric capacitance of GF.

4.4. High-energy ASCs

The energy density of the ASCs as discussed above can be enhanced by either increasing the device capacitance with novel graphene-based electrode materials or broadening the cell voltage, which can be significantly achieved by using nonaqueous electrolyte (e.g., ionic liquids, organic electrolyte) because they can offer a wider operating cell voltage, e.g., organic electrolytes (2.5–3.0 V) and ionic liquids (up to 4 V) compared with these of aqueous electrolytes (1.0–2.0 V) [187].

Recently, graphene-based nonaqueous ASCs, particularly lithium-ion ASCs (or hybrid supercapacitors) with a lithium-ion containing organic electrolyte, also attracted much attention due to the combina-

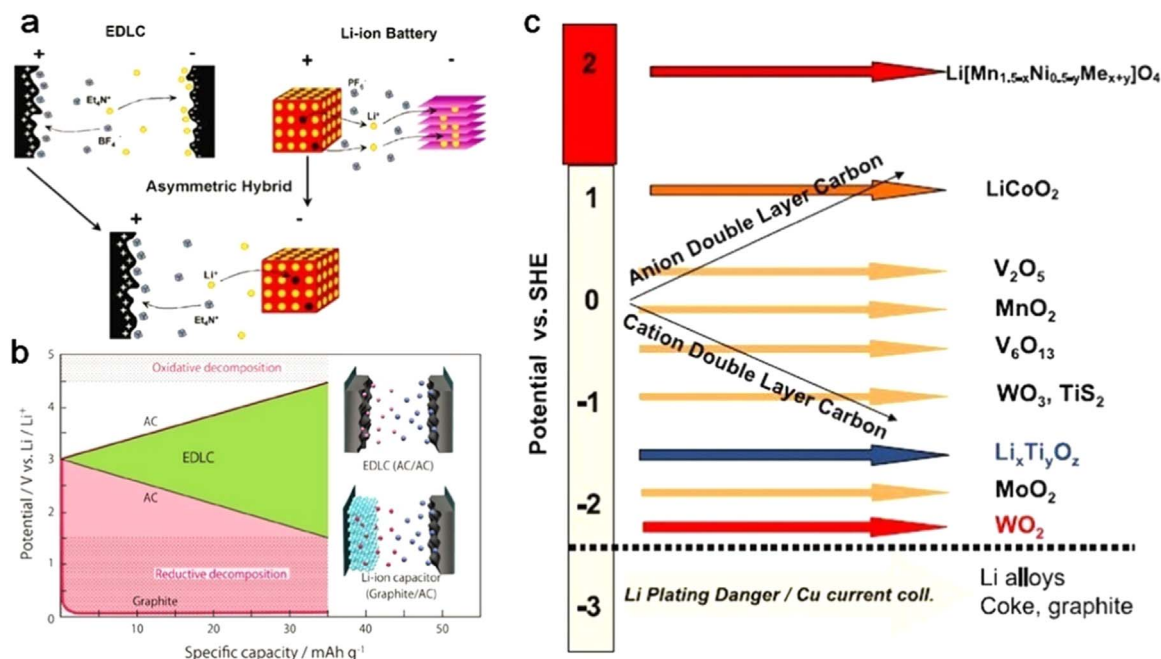


Fig. 15. (a) Scheme showing the configuration of a nonaqueous ASC cell composed of an AC positive electrode and an intercalation electrode traditionally used in nonaqueous EDLC and Li-ion battery, respectively [189]. (b) Typical voltage profiles for an EDLC cell (AC/AC) and a nonaqueous ASC cell (graphite/AC Li-ion capacitor) [187]. (c) Plot showing relative potentials of the positive and negative electrodes of an AC EDLC as a function of charge vs. general redox potential of various intercalation compounds [189].

tion of the rapid charge–discharge and long cycle life of supercapacitors and high energy-storage capacity of lithium-ion batteries, with the huge possibility to fill the gap between supercapacitors and lithium-ion batteries (Fig. 15a) [188]. This is the reason why the nonaqueous ASCs for hybrid energy storage systems can offer the considerably higher energy density than the aqueous ASCs (Fig. 15b) [187]. And the main redox potential of various intercalation compounds for nonaqueous ASCs based on AC as a function of charge have been summarized previously by Amatucci's group (Fig. 15c) [189]. Interestingly, Ren et al. reported the nonaqueous ASCs composed of pre-lithiated graphene negative electrode and AC positive electrode can provide higher energy and power density, for example, 222.2 W kg^{-1} at an energy density of 61.7 W h kg^{-1} when compared pre-lithiated graphene with graphite operated in the voltage range of 2.0–4.0 V [190]. It was found that pre-lithiated graphene could provide low potentials to negative electrodes and increased open circuit voltage for the enhancement of the energy density of the device [190]. In this section, we mainly discussed nonaqueous-based high-energy ASCs (or lithium-ion capacitors) working in a lithium-ion containing organic electrolyte.

4.4.1. Graphene/ $\text{Li}_4\text{Ti}_5\text{O}_{12}$

It should be mentioned that $\text{Li}_4\text{Ti}_5\text{O}_{12}$ anode with excellent rate capability and low-temperature performance down to 40°C for nonaqueous ASCs using AC positive electrode present a breakthrough material, in particular, ultrafast nanocrystalline $\text{Li}_4\text{Ti}_5\text{O}_{12}$ nucleated and grafted onto carbon nanofibers is regarded as an alternative for commercial supercapacitors [191]. As a typical example, Xu et al. reported a two-step method to synthesize graphene/ $\text{Li}_4\text{Ti}_5\text{O}_{12}$ (G/LTO) that delivered a high specific capacity of 194 mA h g^{-1} at 0.1 C, and 90 mA h g^{-1} at 28.6 C (Fig. 16) [192]. Using G/LTO as the anode material, the assembled AC/G/LTO Li-ion hybrid capacitors performed well between 1 and 2.5 V, and exhibited a reversible capacity of 80 mA h g^{-1} at 0.1 C. The energy density based on the total active material for these capacitors is 15 W h kg^{-1} at 4000 W kg^{-1} , and 22 W h kg^{-1} at 1000 W kg^{-1} after 10,000 cycles [192]. Ye and co-workers reported a 3D porous graphene macroform as positive electrode and $\text{Li}_4\text{Ti}_5\text{O}_{12}$ /C hybrid as the negative electrode for the construction of high-performance nonaqueous ASCs [193], delivering a

maximum energy density of 72 W h kg^{-1} at 650 W kg^{-1} in 1–3 V, and offering an energy density of 40 W h kg^{-1} with a power density of 8.3 kW kg^{-1} , and stable capacitance retention of 65% for 1000 cycles at an extremely high current density of 10 A g^{-1} . These results suggest that the LTO/C composite is a promising candidate anode material for Li-ion hybrid capacitors.

4.4.2. Graphene/ Fe_3O_4

Except $\text{Li}_4\text{Ti}_5\text{O}_{12}$ -based ASCs, most of nonaqueous systems usually suffer from poor rate capability and limited long-term cycling stability, due to the poor conductivity of AC and sluggish Li^+ diffusion of metal oxides. In this regard, graphene and graphene/metal oxides as new electrode materials with both high specific surface area and high conductivity possess numerous opportunities that are able to meet the requirements for high-performance hybrid energy storage systems in nonaqueous electrolyte [188]. As a typical example, Chen's group have designed and fabricated the pioneer work of graphene-based nonaqueous ASCs, using an Fe_3O_4 /graphene ($\text{Fe}_3\text{O}_4/\text{G}$) with high specific capacity of 1000 mA h g^{-1} at 90 mA g^{-1} as negative electrode, and 3D graphene-based porous carbon (3D Graphene) with high surface area ($3355 \text{ m}^2 \text{ g}^{-1}$), high capacitance of 187 F g^{-1} in 0–2.7 V, and excellent rate capability as positive electrode (Fig. 17a and b) [194]. With these two graphene-enhanced electrode materials, the fabricated hybrid supercapacitors offered an ultrahigh energy density of 147 W h kg^{-1} (at a power density of 150 W kg^{-1}), and kept 86 W h kg^{-1} even at high power density of 2587 W kg^{-1} (Fig. 17c) [194]. It is pointed out that the energy density of this hybrid supercapacitor is comparable to lithium ion batteries, and the power density also reaches that of symmetric supercapacitors, suggestive of a very competitive energy storage device for fast and efficient energy storage system.

4.4.3. Graphene/ Nb_2O_5

Orthorhombic Nb_2O_5 ($T\text{-Nb}_2\text{O}_5$) is one of the important intercalation pseudocapacitive electrodes with extraordinary charge storage ability, but suffers from poor electronic conductivity that greatly limits the electrochemical utilization and high rate performance especially for thick electrodes with high mass loading [195]. To this end, Kong et al.

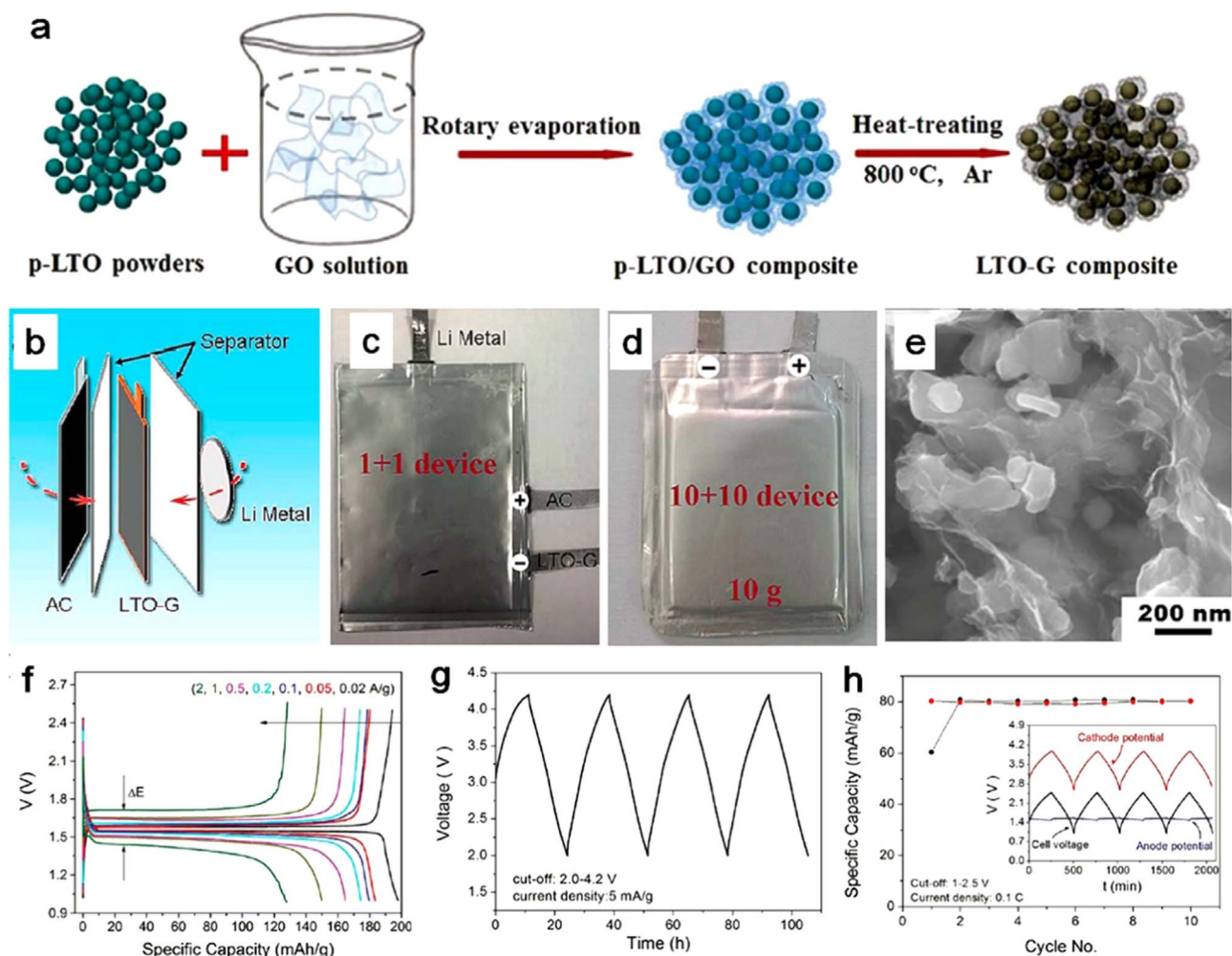


Fig. 16. (a) Schematic illustration of the fabrication of G/LTO composite. (b) Scheme of the three-electrode lithium-ion hybrid capacitors. (c,d) the make-up of the soft-packaged (c) 1+1 device and (d) 10+10 device. (e) SEM image and (f) Specific capacity–voltage profiles of G/LTO composite. (g) Potential profile of the AC electrode. (h) Cycling performance at 0.1 C (Inset: potential profile of first 4 cycles) of the AC//G/LTO Li-ion hybrid capacitors [192].

reported that a layer-by-layer integrated electrode of anchoring T-Nb₂O₅ nanocrystals on conductive graphene sheets had much shortened ion transport paths and excellent electrochemical properties of high capacitance, excellent rate capability and cycling stability (Fig. 18a–d). Furthermore, ASCs were constructed using T-Nb₂O₅/graphene and mesoporous carbon as the negative and positive electrode, respectively, which could offer an energy density of 16 W h kg⁻¹ at an unprecedented power density of 45 kW kg⁻¹ (Fig. 18e–g). The outstanding performance of the ASCs was attributed to the enhanced high-rate Li insertion/extraction capability of the T-Nb₂O₅/graphene electrode and appropriate electrode match of the mesoporous carbon [56]. It is believed that with the continuous development of both graphene and hybrid energy storage systems graphene-based nonaqueous ASCs will open up a new platform as one of the important power sources.

4.5. Planar ASCs

Recently, thin-film planar supercapacitors including micro-supercapacitors with desirable performance have been attracted much attention because they can take full advantage of the atomic layer thicknesses and flat morphology of graphene to maximize the charge storage [196,197]. In particular, planar supercapacitors are very favorable for electrolyte ions to interact with the whole surface of the graphene sheets in a short ion diffusion distance [198,199].

Combining the advantages of graphene and quantum dots, GQDs

present numerous outstanding features of abundant edge defects, large specific surface area, good electrical conductivity, chemical stability, and easy functionalization [200,201], which enable them good candidates for supercapacitors. For example, Yan's group demonstrated that GQD-based planar supercapacitors could be operated at ultrahigh scan rates up to 1000 V s⁻¹, and achieved fast frequency response with a relaxation time constant of 103.6 μs in aqueous electrolyte and 53.8 μs in ionic liquid electrolyte [202]. They also assembled aqueous planar ASCs using GQDs as negative electrode and MnO₂ nanoneedles as positive electrode in an aqueous electrolyte of 0.5 M Na₂SO₄ (Fig. 19) [202]. It was revealed that both specific capacitance (~1107.4 μF cm⁻²) and energy density (~0.154 μW h cm⁻²) of the GQD//MnO₂ ASCs are twice those of symmetric GQD supercapacitors (~468.1 μF cm⁻² & 0.074 μW h cm⁻²). Meanwhile, this group constructed all-solid-state planar ASCs with a PVA/H₃PO₄ gel electrolyte through the electrodeposition of GQDs as negative electrode and PANI nanofibers as positive electrode on each side of a Au microelectrode [89]. The GQD//PANI ASCs showed excellent rate capability of up to 700 V s⁻¹, a short relaxation time constant of 115.9 μs, and ~85.6% capacitance retention after 1500 cycles in a solid-state electrolyte. Recently, El-Kady et al. demonstrate 3D high-performance planar asymmetric micro-supercapacitors based on 3D laser-scribed graphene (LSG) as negative electrode and LSG-MnO₂ as positive electrode by rationally designing the electrode microstructure and combining active materials with in 1.0 M Na₂SO₄ electrolyte, exhibiting high areal capacitance approaching 400 mF/cm² and volumetric capacitance of 250 F/cm³ [203]. These

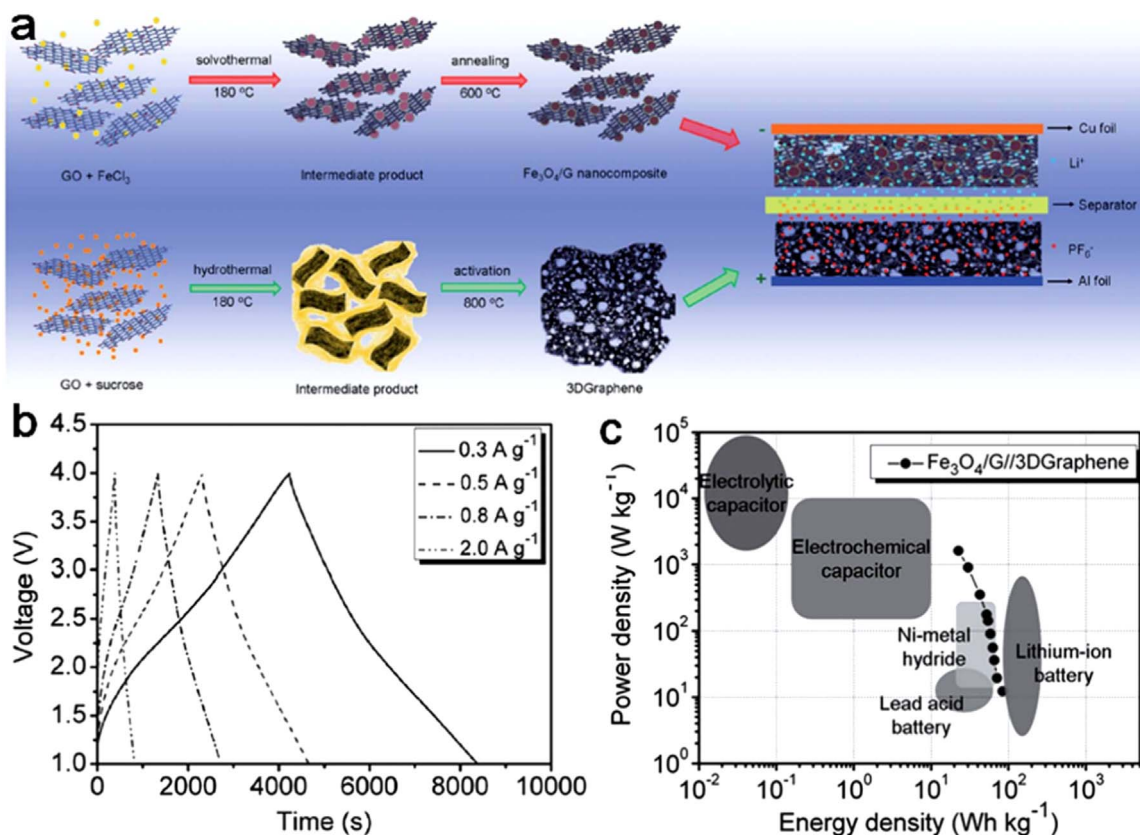


Fig. 17. (a) Schematic showing the synthesis of negative-electrode material $\text{Fe}_3\text{O}_4/\text{G}$ nanocomposite and positive-electrode material 3D graphene, together with the configuration of a Li-ion containing organic hybrid supercapacitor. (b) GCD curves at different current densities of $0.3\text{--}2.0 \text{ A g}^{-1}$. (c) Ragone plot of $\text{Fe}_3\text{O}_4/\text{G}/3\text{D graphene}$ ASCs compared with commercial energy storage devices [194].

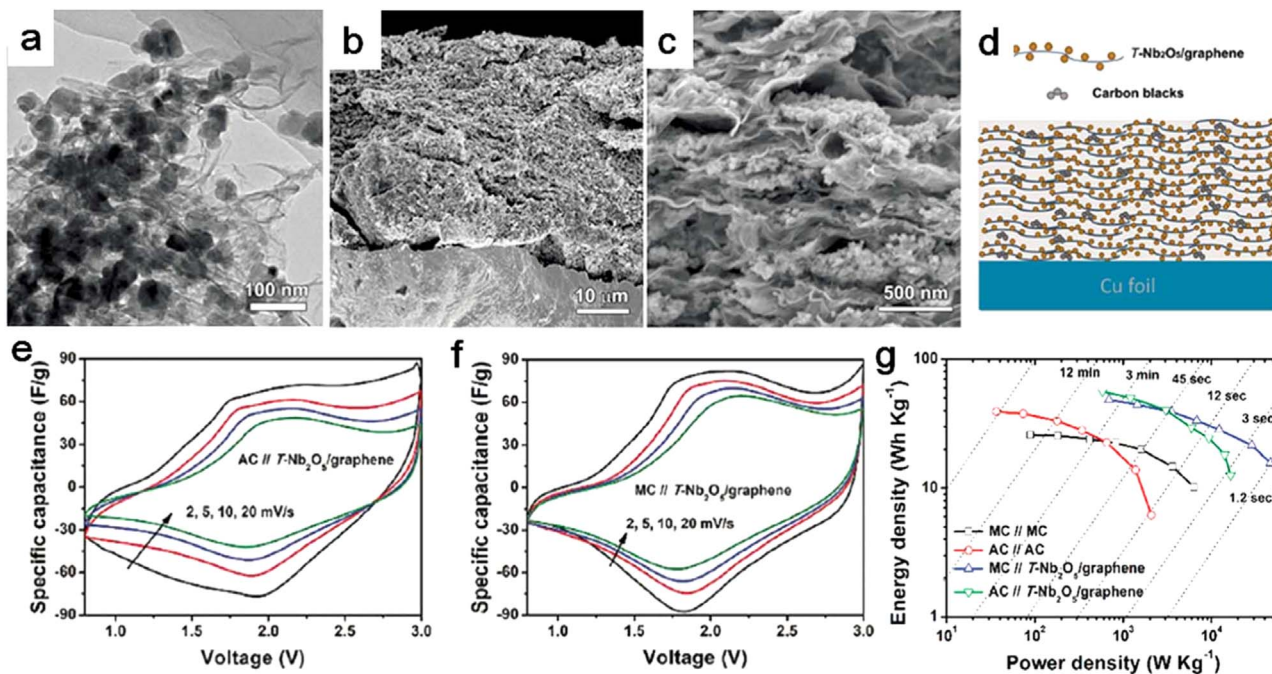


Fig. 18. (a) TEM image of T- $\text{Nb}_2\text{O}_5/\text{graphene}$. (b, c) SEM images of the cross-section of T- $\text{Nb}_2\text{O}_5/\text{graphene}$ electrode films. (d) Schematic of a T- $\text{Nb}_2\text{O}_5/\text{graphene}$ electrode. (e, f) CV curves of (e) AC//T- $\text{Nb}_2\text{O}_5/\text{graphene}$ and (f) MC//T- $\text{Nb}_2\text{O}_5/\text{graphene}$ ASCs. (g) Ragone plot of MC//T- $\text{Nb}_2\text{O}_5/\text{graphene}$ and AC//T- $\text{Nb}_2\text{O}_5/\text{graphene}$ ASCs [56].

results demonstrate that graphene-based asymmetric micro-supercapacitors with a planar geometry and high energy density are very promising micro-electrochemical energy-storage devices that can take full advantages of planar configuration and unique features of graphene

[196,199].

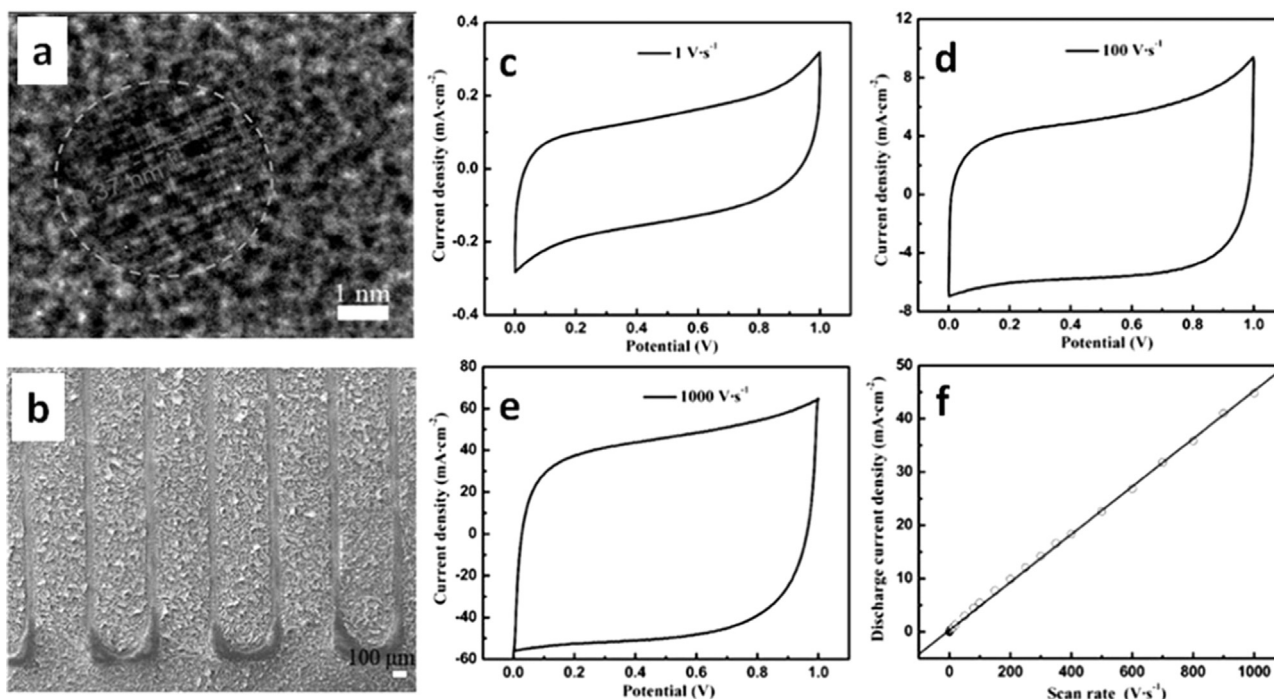


Fig. 19. (a) High-resolution TEM image of an individual GQD. (b) Top-view SEM image of the GQDs deposited on interdigital electrodes. (c–e) CV curves of GQD//MnO₂ planar ASCs in 0.5 M Na₂SO₄ at (c) 1, (d) 100, and (e) 1000 V s⁻¹, respectively. (f) Charge current density of GQD//MnO₂ ASCs as a function of scan rate [202].

4.6. All-solid-state ASCs

Currently, all-solid-state supercapacitors with unique promising advantages of such as flexibility, shape diversity, and light weight, have gained worldwide attention as an emerging candidate for smart energy storage devices due to the increasing demand for wearable and miniaturized electronics [69]. Therefore, considerable efforts have been made to fulfill the multiple requirements of future flexible energy storage devices [13]. Regarding this topic, it is emphasized that graphene is ideally suited for the use in flexible all-solid-state energy storage devices, including supercapacitors and ASCs [13].

4.6.1. Graphene-based films

The flexible and highly-conductive graphene open numerous opportunities for the preparation of binder-free film hybrid electrodes structurally integrated with transition metal oxides or conducting polymers for flexible all-solid-state ASCs. For instance, Duan's group reported all-solid-state ASCs based on free-standing CNT/graphene (CNTG) and Mn₃O₄ nanoparticles/graphene (MG) paper electrodes with a polymer gel electrolyte of potassium polyacrylate/KCl (Fig. 20a–e) [79]. The composite paper electrodes with CNTs or Mn₃O₄ nanoparticles uniformly intercalated between graphene sheets exhibited excellent mechanical stability, greatly improved active surface area, and enhanced ion transportation, in comparison with the pristine graphene paper. The CNTG//MG ASC endowed an increased cell voltage of 1.8 V (Fig. 20f–h), a stable cycling performance (86.0% capacitance retention after 10000 cycles), more than 2-fold increase of energy density (32.7 W h kg⁻¹) compared with the symmetric supercapacitors, and importantly a distinguished mechanical flexibility [79].

As discussed above, RuO₂ is also a very promising positive electrode material for ASCs. As a typical example, Choi et al. reported the fabrication of the hydrous RuO₂ coated on the ionic liquid functionalized chemically modified graphene nanosheets (RuO₂-IL-CMG) as positive electrode and IL-CMG as negative electrode for the assembly of all solid-state ASCs with polymer gel electrolyte as a separator (Fig. 21a–h). Importantly, the fabricated all solid-state ASCs exhibited a maximum voltage window of 0–1.8 V (Fig. 21i and j), and possessed

high energy density of 19.7 W h kg⁻¹ and high power density of 6.8 kW g⁻¹ at an energy density of 15.5 W h kg⁻¹, both of which are much higher than that of the corresponding symmetric supercapacitor, IL-CMG//IL-CMG [78]. Furthermore, the capacitance retention was attained as high as 95% after 2000 cycles even at the condition of harsh twist and bend states (Fig. 21k). This result is mainly attributed to the enhanced interfacial contact and good electrical conductivity of the IL-CMG films. Therefore, graphene based films show great promise for flexible energy devices in terms of electrochemical properties.

4.6.2. Graphene-based fibers

Recently, great efforts have been made to fabricate macroscopic graphene fibers from the direct self-assembly and chemical modification of graphene sheets by facile and scalable spinning processes. Very importantly, these graphene fibers as a novel class of one-dimensional porous interconnected monolith present high specific surface area, excellent electrical conductivity, high mechanical strength, outstanding flexibility and light weight, and remarkable electrochemical properties [204–207]. Therefore, graphene fibers were widely regarded as a promising electrode for fiber-based supercapacitors with flexibility and weavability [204–207]. As a typical example, Gao's group developed a facile wet-spinning assembly approach to process two different graphene-based fiber electrodes. One is a MnO₂-coated core-sheath graphene fibers (GMF, Fig. 22a–d), another is a graphene-CNT (GCF) hybrid [115]. Using the advantages of the pseudocapacitance of MnO₂ and the conductivity of graphene, GMFs can reach a high areal capacitance of 59.2 mF cm⁻², five times that of the neat graphene fiber. Accordingly, the GCFs delivered an improved areal capacitance of 32.6 mF cm⁻² due to the synergistic effect of graphene and CNTs. Furthermore, they assembled a novel flexible graphene fiber-based ASC using these two fibers as positive and negative electrodes in a PVA/LiCl gel electrolyte (Fig. 22e–i). Remarkably, the fiber-based ASCs had a wide potential window of 1.6 V (Fig. 22e and f), and achieved high areal energy density of 11.9 μW h cm⁻² and volume energy density of 11.9 mW h cm⁻³, which are among the highest values reported for fiber-based supercapacitors. Additionally, the resultant fiber-based ASCs exhibited good cycling stability with capacitance retention of

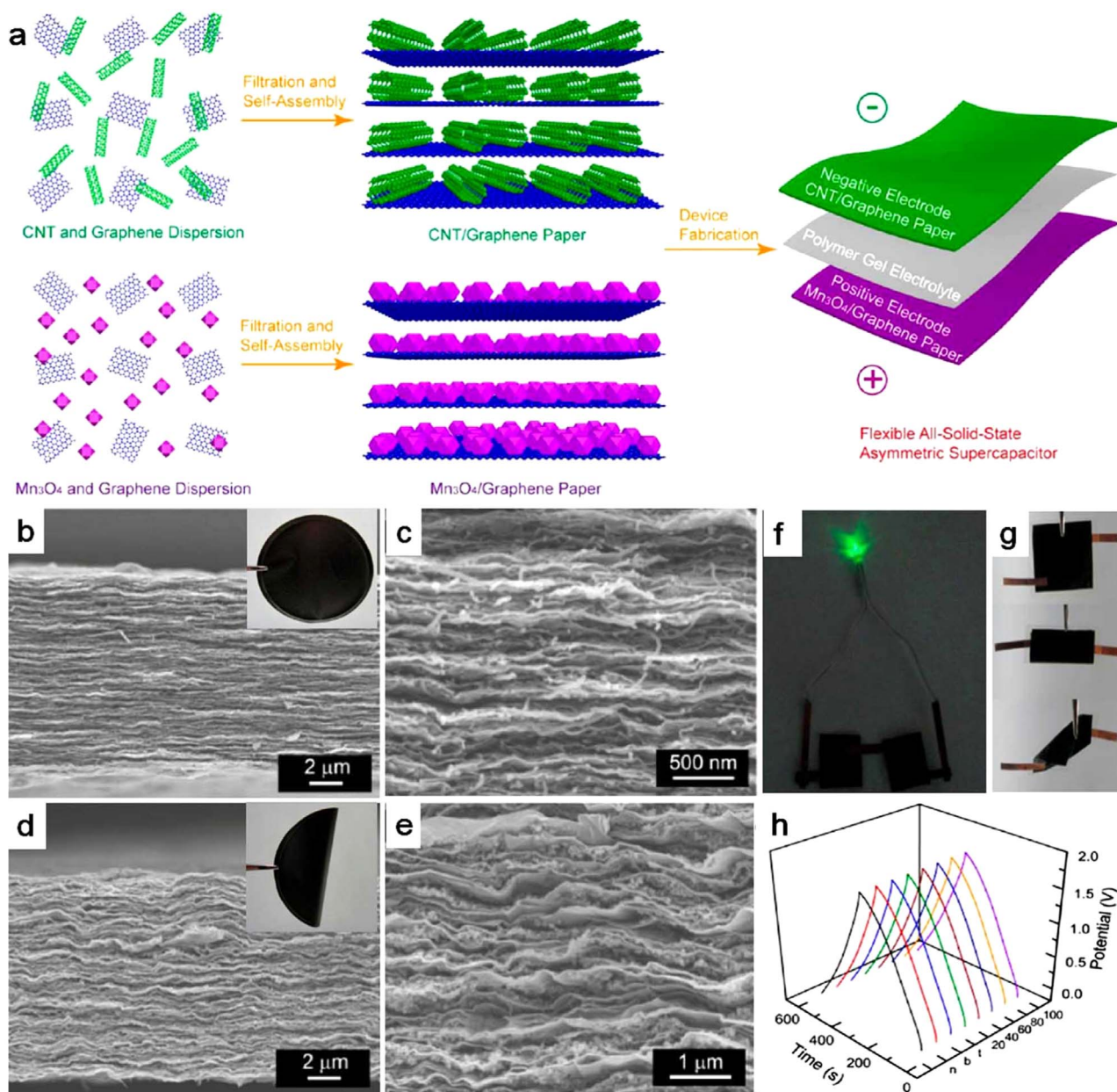


Fig. 20. (a) Fabrication illustration of a flexible all-solid-state ASC based on free-standing CNTG and MG paper electrodes. (b, c) Cross-section SEM images of CNTG paper. Inset in (b) is the photograph of CNTG paper. (d, e) Cross-section SEM images of MG paper. Inset in (d) is the photograph of MG paper. (f) A green LED lighted by two CNTG//MG ASCs in series. (g) Photographs of the ASC at normal, bending, and twisting states. (h) Galvanostatic charge/discharge profiles of the ASC at normal, bending, and twisting states and after being bent repeatedly [79].

92.7% after 8000 cycles (Fig. 22g), and could be readily integrated into a fiber-like device to realize the flexibility of fibers (Fig. 22h and i) [115]. To achieve high energy density without compromising their rate stability, Sun et al. reported that, by incorporating MoS_2 and rGO nanosheets into a well-aligned multi-walled CNT (MWCNT) sheet followed by twisting (Fig. 22j–l), MoS_2 -rGO/MWCNT fiber as cathode and rGO/MWCNT fiber as anode were fabricated for all-solid-state flexible ASCs [208]. These fiber-based ASCs can operate in a wide potential window of 1.4 V with high Coulombic efficiency, good rate and cycling stability, and improved energy density. This result is attributed to the wide potential window, electrochemical activity of MoS_2 , electrical conductivity of well aligned MWCNT fiber, and the incorporation of rGO. It is demonstrated that this fiber-based asymmetric device might have promising applications in flexible and wearable electronics.

5. Perspective and challenges

Recent advances in research and development of state-of-the-art graphene-based ASCs are reviewed, including the critical assembly principle (e.g., electrode, electrolyte, current collector, separator, and interfacial integrity), standard methods of performance evaluation, major categories of ASCs, positive and negative electrode materials, and the prime graphene-based materials for high-voltage, high-capacitance, high-power and high-energy asymmetric devices as well as new-type device geometry of planar and all-solid-state ASCs. It is emphasized that the combination of the elaborated screening of graphene-based materials with controllable structures, highly activated compositions, nanoarchitectures of electrode, selection of electrolytes, and the integration of different isolated device components are the key for the development of high-performance graphene-based ASCs with targeted performance metrics of high voltage, high capacitance, high

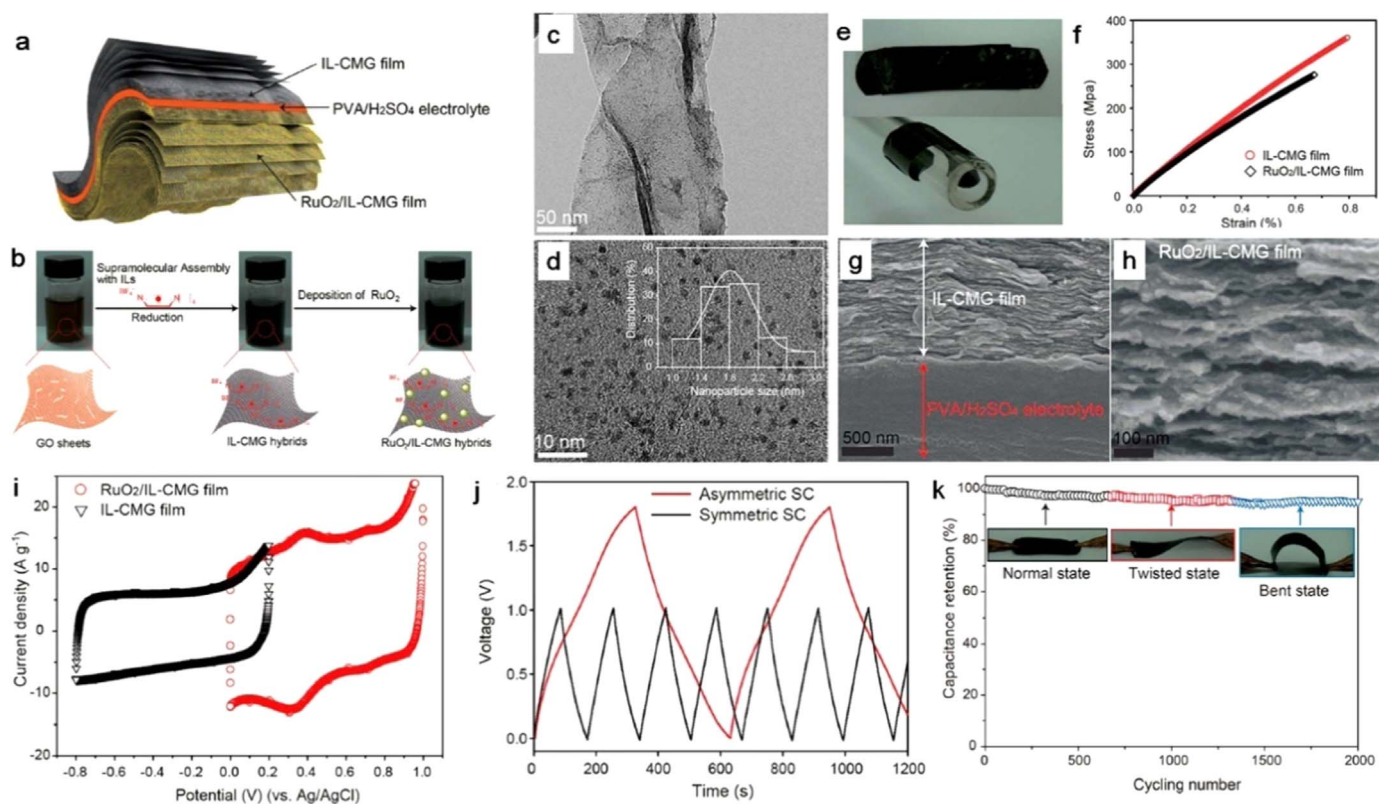


Fig. 21. (a) Schematic illustration of all-solid-state ASCs and (b) the synthesis of water-soluble IL-CMG and RuO₂-IL-CMG hybrids. (c) TEM and (d) HRTEM images of RuO₂-IL-CMG hybrid. Inset in (d) is histogram of the size distribution of RuO₂. (e) Photograph images of an ASC device (top) and a bent ASC device (bottom). (f) Stress and strain curves of IL-CMG and RuO₂-IL-CMG films. (g,h) Cross-sectional SEM images of (g) the interface between the IL-CMG film and PVA-H₂SO₄ electrolyte and (h) RuO₂-IL-CMG film in ASC device. (i) CV curves of IL-CMG and RuO₂-IL-CMG at 50 mV s⁻¹ in 1 M H₂SO₄. (j) GCD curves of ASC and IL-CMG-based symmetric supercapacitors at 1 A g⁻¹. (k) Cycling stability of the ASC devices under normal, twisted and bent states [78].

power density and energy density.

It is highlighted from material aspects that the tailored physical and chemical properties of graphene provides numerous opportunities in the designing and developing on a series of novel graphene-based nanoarchitectural electrodes, such as rGO, GQDs, graphene films, 3D graphene networks, various hybrids of graphene/CNT, graphene/metal oxide, and graphene/conducting polymer, which are widely considered as prime positive and negative electrodes for high-voltage, high-capacitance, high-power and high-energy asymmetric devices as well as new-type planar and all-solid-state ASCs.

Another key emphasis is given to the hybrid approach of graphene-based materials, which definitely allows for generating a positive synergic combination of the advantageous properties of different components of graphene and capacitive/pseudocapacitive materials [59]. It is well known that pseudocapacitive materials of transition metal oxides and conducting polymers are key electrode components to boost the capacitance and energy density of ASCs. To overcome the shortcomings of pseudocapacitive materials in ASCs, it is undoubtedly said that the presence of graphene with superior electrical conductivity and mechanical flexibility in these hybrids can not only increase their very low electrical conductivity, introduce more electrochemically active sites and shorten the transport path length for both electrons and ions, but also mechanically withstand the microscopic stress of electrodes during charging and discharging processes, leading to the performance improvement in long-life electrochemical stability. It is pointed out that, from graphene-based hybrid materials to hybrid energy storage devices, this hybrid approach could pave a feasible way to boost the electrochemical performance of ASCs.

Regarding the device aspect, the working cell voltage is the major issue of ASCs, which should be considered completely in order to address high energy storage capacity and power output capability. A

matching electrolyte from aqueous electrolytes, organic electrolytes or ionic liquids must be considered how to maximize the electrochemical working voltage with the possible combination of both positive electrode and negative electrode in an optimized ASC device. In order to reach the highest cell voltage, the charges stored in both electrodes must be balanced, even under high-rate charging and discharging process. Furthermore, considering the simultaneous improvement in thermodynamics and kinetics of a single ASC device, new-concept hybrid energy storage devices made with a graphene-like capacitor-type electrode and a battery-like hybrid electrode of graphene/metal oxide (polymer) could essentially help to improve the poor electrochemical reaction kinetics of ASC systems consisting of pure carbon capacitive electrode and pseudocapacitive electrode (e.g., metal oxide). Much attention is paid to the volumetric performance over gravimetric one especially for performance evaluation of thin-film planar ASCs and micro-supercapacitors [209].

Further research and development of graphene-based ASCs will undoubtedly extend the full coverage of all device components (e.g., graphene electrode materials, electrolytes, separators, current collectors, package), the integration of ASC devices with low cost for their perceived applications in the increasing civil and industrial filed for clean energy. To this end, some remarks on future perspectives and challenges of graphene-based ASCs should be considered:

- (1) Graphene-based ASCs are a very fundamental yet challenging topic. It may become a new, complementary or alternative technology that holds great potential to fill up the gap in the specific power and energy spectrum between supercapacitors and lithium ion batteries.
- (2) Deeper understanding of the electrochemical charge-storage mechanism of graphene-based ASCs is the core part to process the

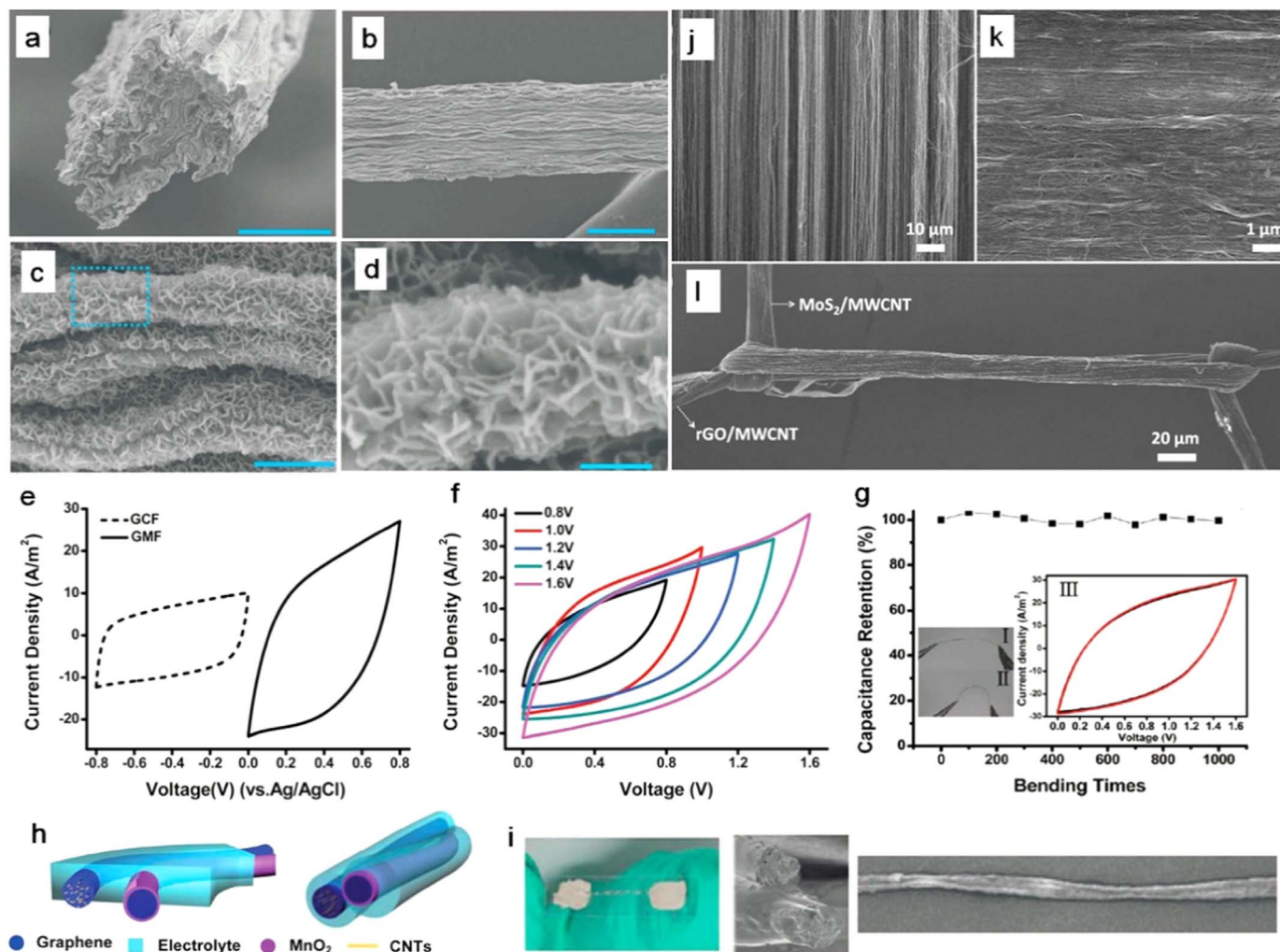


Fig. 22. (a) Cross section and (b) overview SEM images of GMF. (c) High-magnification SEM image of GMF, and (d) magnified picture of (c). (e) CV curves of GMF and GCF in a three-electrode system. (f) CV curves of parallel graphene fiber-based ASCs at different potential windows at 100 mV s^{-1} . (g) Capacitance retention at different bending times, inset: photograph of fiber-based ASC at flat (i) and bending (ii) states, and (iii) the related CV curves of at flat and bending states. (h) Schematic of parallel ASCs (left), and two-ply ASCs (right). (i) Photograph of a fiber-based ASC, cross section and surface SEM images of a two-ply fiber-based ASC (from left to right) [115]. (j–l) SEM images of (j) well-aligned MWCNT sheet, (k) MWCNT sheet incorporating with MoS_2 nanosheets, and (l) tightly knotted $\text{MoS}_2/\text{MWCNT}$ and rGO/MWCNT fibers [208].

optimized interfacial interactions of electrode and electrolyte, fabricate well-defined graphene-based nanostructures to enhance charge diffusion and electron transfer, and consequently obtain high cell voltage as well as high capacitance and rate capability in a single device. Proper evaluation of these new graphene materials and their charge storage mechanisms will promote progress in this important field of ASCs.

- (3) The prospect of developing novel devices, based on graphene-based materials, with energy density of batteries and power density of supercapacitors is an exciting research direction that has yet to be realized. Considering the fact that the great effect of both the composition and nanostructures of graphene-based electrodes on the electrochemical prosperities of ASCs, continuous research on graphene based nanoarchitectures with highly activated components and controlled nanostructures with open porous yet conductive networks should be further implemented [210,211]. Besides graphene, special attention should be paid to other novel classes of 2D nanomaterials. Particularly transition metal oxides, dichalcogenides, and carbides, are also the very important electrode materials for high-energy ASCs.
- (4) Considering final possible applications, it should be highlighted again that the overall performance of ASC devices will not only depend on graphene-based electrode materials, but also on their

efficient combination with other device components such as electrolytes, separators, current collectors, packages as well as other practical aspects that influence the overall cell performance. As a consequence, the integration of electrode design and device engineering will become intensively required in the near future.

It is believed that ASCs are a very emerging and environment friendly technology that may become a green and alternative solution to the existing energy storage devices of commercial supercapacitors and lithium ion batteries, offering the significant contribution to the ongoing energy crisis and environmental problems. Therefore, ASCs are considered as a novel competitive pure-electric power source or a complement alternative with batteries to power electric vehicles, HEV, plug-in HEV and other portable electronics in the future.

Acknowledgements

This work was financially supported by the Thousand Youth Talents Plan of China (Grant Y5061921T3), Ministry of Science and Technology of China (Grant 2016YBF0100100 and 2016YFA0200200), National Natural Science Foundation of China (Grant 51572259), Natural Science Foundation of Liaoning Province (Grant 201602737), DICP (Grant Y5610121T3).

References

- [1] C. Liu, F. Li, L.P. Ma, H.M. Cheng, Advanced materials for energy storage, *Adv. Mater.* 22 (2010) E28–E62.
- [2] J.B. Goodenough, Electrochemical energy storage in a sustainable modern society, *Energy Environ. Sci.* 7 (2014) 14–18.
- [3] J.B. Goodenough, Energy storage materials: a perspective, *Energy Storage Mater.* 1 (2015) 158–161.
- [4] J.R. Miller, P. Simon, Electrochemical capacitors for energy management, *Science* 321 (2008) 651–652.
- [5] S. Zhang, N. Pan, Supercapacitors performance evaluation, *Adv. Energy Mater.* 8 (2015) 1401401.
- [6] Y. Zhai, Y. Dou, D. Zhao, P.F. Fulvio, R.T. Mayes, S. Dai, Carbon materials for chemical capacitive energy storage, *Adv. Mater.* 23 (2011) 4828–4850.
- [7] V. Augustyn, P. Simon, B. Dunn, Pseudocapacitive oxide materials for high-rate electrochemical energy storage, *Energy Environ. Sci.* 7 (2014) 1597–1614.
- [8] D.P. Dubal, O. Ayyad, V. Ruiz, P. Gomez-Romero, Hybrid energy storage: the merging of battery and supercapacitor chemistries, *Chem. Soc. Rev.* 44 (2015) 1777–1790.
- [9] J.H. Chae, K.C. Ng, G.Z. Chen, Nanostructured materials for the construction of asymmetrical supercapacitors, *Proc. IMechE Part A: J. Power Energy* 224 (2010) 479–503.
- [10] P. Simon, Y. Gogotsi, Materials for electrochemical capacitors, *Nat. Mater.* 7 (2008) 845–854.
- [11] F. Wang, S. Xiao, Y. Hou, C. Hu, L. Liu, Y. Wu, Electrode materials for aqueous asymmetric supercapacitors, *RSC Adv.* 3 (2013) 13059–13084.
- [12] J.P. Zheng, The limitations of energy density of battery/double-layer capacitor asymmetric cells, *J. Electrochem. Soc.* 150 (2003) A484–A492.
- [13] L. Wen, F. Li, H.-M. Cheng, Carbon nanotubes and graphene for flexible electrochemical energy storage: from materials to devices, *Adv. Mater.* 28 (2016) 4306–4337.
- [14] R. Raccichini, A. Varzi, S. Passerini, B. Scrosati, The role of graphene for electrochemical energy storage, *Nat. Mater.* 14 (2015) 271–279.
- [15] Z.S. Wu, W.C. Ren, D.W. Wang, F. Li, B.L. Liu, H.M. Cheng, High-energy MnO₂ nanowire/graphene and graphene asymmetric electrochemical capacitors, *ACS Nano* 4 (2010) 5835–5842.
- [16] H.Y. Wang, M. Yoshio, A.K. Thapa, H. Nakamura, From symmetric AC/AC to asymmetric AC/graphite, a progress in electrochemical capacitors, *J. Power Sources* 169 (2007) 375–380.
- [17] Y.G. Wang, J.Y. Luo, C.X. Wang, Y.Y. Xia, Hybrid aqueous energy storage cells using activated carbon and lithium-ion intercalated compounds ii. Comparison of LiMn₂O₄, LiCo_{1/3}Ni_{1/3}Mn_{1/3}O₂, and LiCoO₂ positive electrodes, *J. Electrochem. Soc.* 153 (2006) A1425–A1431.
- [18] V. Khomenko, E. Raymundo-Pinero, E. Frackowiak, F. Beguin, High-voltage asymmetric supercapacitors operating in aqueous electrolyte, *Appl. Phys. A Mater.* 82 (2006) 567–573.
- [19] P. Simon, Y. Gogotsi, Capacitive energy storage in nanostructured carbon-electrolyte systems, *Acc. Chem. Res.* 46 (2013) 1094–1103.
- [20] Y. Wang, W.-H. Zhong, Development of electrolytes towards achieving safe and high-performance energy-storage devices: a review, *ChemElectroChem* 2 (2014) 22–36.
- [21] E. Frackowiak, F. Beguin, Carbon materials for the electrochemical storage of energy in capacitors, *Carbon* 39 (2001) 937–950.
- [22] M. Beidaghi, Y. Gogotsi, Capacitive energy storage in micro-scale devices: recent advances in design and fabrication of micro-supercapacitors, *Energy Environ. Sci.* 7 (2014) 867–884.
- [23] Y. Gogotsi, P. Simon, True performance metrics in electrochemical energy storage, *Science* 335 (2012) (167–167).
- [24] G.G. Amatucci, F. Badway, A. Du Pasquier, T. Zheng, An asymmetric hybrid nonaqueous energy storage cell, *J. Electrochem. Soc.* 148 (2001) A930–A939.
- [25] M.S. Hong, S.H. Lee, S.W. Kim, Use of KCl aqueous electrolyte for 2 V manganese oxide/activated carbon hybrid capacitor, *Electrochem. Solid State Lett.* 5 (2002) A227–A230.
- [26] W. Tang, L.L. Liu, S. Tian, L. Li, Y.B. Yue, Y.P. Wu, K. Zhu, Aqueous supercapacitors of high energy density based on MoO₃ nanoplates as anode material, *Chem. Commun.* 47 (2011) 10058–10060.
- [27] C.J. Xu, H.D. Du, B.H. Li, F.Y. Kang, Y.Q. Zeng, Asymmetric activated carbon-manganese dioxide capacitors in mild aqueous electrolytes containing alkaline-earth cations, *J. Electrochem. Soc.* 156 (2009) A435–A441.
- [28] N.F. Yu, L.J. Gao, S.H. Zhao, Z.D. Wang, Electrodeposited PbO₂ thin film as positive electrode in PbO₂/AC hybrid capacitor, *Electrochim. Acta* 54 (2009) 3835–3841.
- [29] D.W. Wang, F. Li, H.M. Cheng, Hierarchical porous nickel oxide and carbon as electrode materials for asymmetric supercapacitor, *J. Power Sources* 185 (2008) 1563–1568.
- [30] Z. Algharaibeh, X.R. Liu, P.G. Pickup, An asymmetric anthraquinone-modified carbon/ruthenium oxide supercapacitor, *J. Power Sources* 187 (2009) 640–643.
- [31] Q.T. Qu, Y. Shi, L.L. Li, W.L. Guo, Y.P. Wu, H.P. Zhang, S.Y. Guan, R. Holze, V₂O₅·0.6H₂O nanoribbons as cathode material for asymmetric supercapacitor in K₂SO₄ solution, *Electrochem. Commun.* 11 (2009) 1325–1328.
- [32] X.F. Lu, D.J. Wu, R.Z. Li, Q. Li, S.H. Ye, Y.X. Tong, G.R. Li, Hierarchical NiCo₂O₄ nanosheets/hollow microrod arrays for high-performance asymmetric supercapacitors, *J. Mater. Chem. A* 2 (2014) 4706–4713.
- [33] S. Peng, L. Li, H.B. Wu, S. Madhavi, X.W. Lou, Controlled growth of NiMoO₄ nanosheet and nanorod arrays on various conductive substrates as advanced electrodes for asymmetric supercapacitors, *Adv. Energy Mater.* 5 (2014) 1401172.
- [34] Y. Hu, C. Guan, G. Feng, Q. Ke, X. Huang, J. Wang, Flexible asymmetric supercapacitor based on structure-optimized Mn₃O₄/reduced graphene oxide nanohybrid paper with high energy and power density, *Adv. Funct. Mater.* 25 (2015) 7291–7299.
- [35] L. Xie, F. Su, L. Xie, X. Li, Z. Liu, Q. Kong, X. Guo, Y. Zhang, L. Wan, K. Li, C. Lv, C. Chen, Self-assembled 3D graphene-based aerogel with Co₃O₄ nanoparticles as high-performance asymmetric supercapacitor electrode, *ChemSusChem* 8 (2015) 2917–2926.
- [36] K.C. Ng, S.W. Zhang, C. Peng, G.Z. Chen, Individual and bipolarly stacked asymmetrical aqueous supercapacitors of CNTs/SnO₂ and CNTs/MnO₂ nanocomposites, *J. Electrochem. Soc.* 156 (2009) A846–A853.
- [37] S. Nohara, A.A. Toshihide, H. Wada, N. Furukawa, H. Inoue, N. Sugoh, H. Iwasaki, C. Iwakura, Hybrid capacitor with activated carbon electrode, Ni(OH)₂ electrode and polymer hydrogel electrolyte, *J. Power Sources* 157 (2006) 605–609.
- [38] A.B. Dighe, D.P. Dubal, R. Holze, Screen printed asymmetric supercapacitors based on LiCoO₂ and graphene oxide, *Z. Anorg. Allg. Chem.* 640 (2014) 2852–2857.
- [39] S.B. Ma, K.W. Nam, W.S. Yoon, X.Q. Yang, K.Y. Ahn, K.H. Oh, K.B. Kim, A novel concept of hybrid capacitor based on manganese oxide materials, *Electrochem. Commun.* 9 (2007) 2807–2811.
- [40] K. Machida, S. Suematsu, S. Ishimoto, K. Tamamitsu, High-voltage asymmetric electrochemical capacitor based on polyfluorene nanocomposite and activated carbon, *J. Electrochem. Soc.* 155 (2008) A970–A974.
- [41] Q.T. Qu, L. Li, S. Tian, W.L. Guo, Y.P. Wu, R. Holze, A cheap asymmetric supercapacitor with high energy at high power: activated carbon//K_{0.27}MnO₂·0.6H₂O, *J. Power Sources* 195 (2010) 2789–2794.
- [42] Q.T. Qu, Y. Shi, S. Tian, Y.H. Chen, Y.P. Wu, R. Holze, A new cheap asymmetric aqueous supercapacitor: activated carbon//NaMnO₂, *J. Power Sources* 194 (2009) 1222–1225.
- [43] J.-X. Feng, S.-H. Ye, X.-F. Lu, Y.-X. Tong, G.-R. Li, Asymmetric paper supercapacitor based on amorphous porous Mn₃O₄ negative electrode and Ni(OH)₂ positive electrode: a novel and high-performance flexible electrochemical energy storage device, *ACS Appl. Mater. Interfaces* 7 (2015) 11444–11451.
- [44] Y. Zhao, Y.Y. Wang, Q.Y. Lai, L.M. Chen, Y.J. Hao, X.Y. Ji, Pseudocapacitance properties of AC/LiNi_{1/3}Co_{1/3}Mn_{1/3}O₂ asymmetric supercapacitor in aqueous electrolyte, *Synth. Met.* 159 (2009) 331–337.
- [45] X. Xiao, T. Li, Z. Peng, H. Jin, Q. Zhong, Q. Hu, B. Yao, Q. Luo, C. Zhang, L. Gong, J. Chen, Y. Gogotsi, J. Zhou, Freestanding functionalized carbon nanotube-based electrode for solid-state asymmetric supercapacitors, *Nano Energy* 6 (2014) 1–9.
- [46] G. Zang, L.Y. Bao, Y.F. Su, F. Wu, S. Chen, Preparation of Li₄Ti₅O₁₂ with hydration titanium dioxide for electrochemical hybrid capacitor, *J. Inorg. Mater.* 24 (2009) 531–534.
- [47] P.C. Chen, G.Z. Shen, Y. Shi, H.T. Chen, C.W. Zhou, Preparation and characterization of flexible asymmetric supercapacitors based on transition-metal-oxide nanowire/single-walled carbon nanotube hybrid thin-film electrodes, *ACS Nano* 4 (2010) 4403–4411.
- [48] F. Chen, R.G. Li, M. Hou, L. Liu, R. Wang, Z.H. Deng, Preparation and characterization of ramsdellite Li₂Ti₃O₇ as an anode material for asymmetric supercapacitors, *Electrochim. Acta* 51 (2005) 61–65.
- [49] D.W. Wang, H.T. Fang, F. Li, Z.G. Chen, Q.S. Zhong, G.Q. Lu, H.M. Cheng, Aligned titania nanotubes as an intercalation anode material for hybrid electrochemical energy storage, *Adv. Funct. Mater.* 18 (2008) 3787–3793.
- [50] J.Y. Luo, Y.Y. Xia, Electrochemical profile of an asymmetric supercapacitor using carbon-coated LiTi₂(PO₄)₃ and active carbon electrodes, *J. Power Sources* 186 (2009) 224–227.
- [51] H. Xu, X. Hu, H. Yang, Y. Sun, C. Hu, Y. Huang, Flexible asymmetric micro-supercapacitors based on Bi₂O₃ and MnO₂ nanoflowers: larger areal mass promises higher energy density, *Adv. Energy Mater.* 5 (2014) 1401882.
- [52] J. Chang, M. Jin, F. Yao, T.H. Kim, L. Viet Thong, H. Yue, F. Gunes, B. Li, A. Ghosh, S. Xie, Y.H. Lee, Asymmetric supercapacitors based on graphene/MnO₂ nanospheres and graphene/MoO₃ nanosheets with high energy density, *Adv. Funct. Mater.* 23 (2013) 5074–5083.
- [53] P.H. Yang, Y. Ding, Z.Y. Lin, Z.W. Chen, Y.Z. Li, P.F. Qiang, M. Ebrahimi, W.J. Mai, C.P. Wong, Z.L. Wang, Low-cost high-performance solid-state asymmetric supercapacitors based on MnO₂ nanowires and Fe₂O₃ nanotubes, *Nano Lett.* 14 (2014) 731–736.
- [54] Q.T. Qu, Y.S. Zhu, X.W. Gao, Y.P. Wu, Core-shell structure of polypyrrole grown on V₂O₅ nanoribbon as high performance anode material for supercapacitors, *Adv. Energy Mater.* 2 (2012) 950–955.
- [55] J. Zhang, J. Jiang, H. Li, X.S. Zhao, A high-performance asymmetric supercapacitor fabricated with graphene-based electrodes, *Energy Environ. Sci.* 4 (2011) 4009–4015.
- [56] L. Kong, C. Zhang, S. Zhang, J. Wang, R. Cai, C. Lv, W. Qiao, L. Ling, D. Long, High-power and high-energy asymmetric supercapacitors based on Li⁺-intercalation into a T-Nb₂O₅/graphene pseudocapacitive electrode, *J. Mater. Chem. A* 2 (2014) 17962–17970.
- [57] K.S. Novoselov, A.K. Geim, S.V. Morozov, D. Jiang, Y. Zhang, S.V. Dubonos, I.V. Grigorieva, A.A. Firsov, Electric field effect in atomically thin carbon films, *Science* 306 (2004) 666–669.
- [58] A.K. Geim, Graphene: status and prospects, *Science* 324 (2009) 1530–1534.
- [59] Z.-S. Wu, G.M. Zhou, L.C. Yin, W.C. Ren, F. Li, H.M. Cheng, Graphene/metal oxide composite electrode materials for energy storage, *Nano Energy* 1 (2012) 107–131.
- [60] Y. Shao, M.F. El-Kady, L.J. Wang, Q. Zhang, Y. Li, H. Wang, M.F. Mousavi,

- R.B. Kaner, Graphene-based materials for flexible supercapacitors, *Chem. Soc. Rev.* 44 (2015) 3639–3665.
- [61] Z. Lei, J. Zhang, L.L. Zhang, N.A. Kumar, X.S. Zhao, Functionalization of chemically derived graphene for improving its electrocapacitive energy storage properties, *Energy Environ. Sci.* 9 (2016) 1891–1930.
- [62] Q. Huang, D. Wang, Z. Zheng, Textile-based electrochemical energy storage devices, *Adv. Energy Mater.* (2016) 1600783.
- [63] L. Liu, Z. Niu, J. Chen, Unconventional supercapacitors from nanocarbon-based electrode materials to device configurations, *Chem. Soc. Rev.* 45 (2016) 4340–4363.
- [64] S. Wan, J. Peng, L. Jiang, Q. Cheng, Bioinspired graphene-based nanocomposites and their application in flexible energy devices, *Adv. Mater.* (2016). <http://dx.doi.org/10.1002/adma.201601934>.
- [65] C.G. Liu, Z.N. Yu, D. Neff, A. Zhamu, B.Z. Jang, Graphene-based supercapacitor with an ultrahigh energy density, *Nano Lett.* 10 (2010) 4863–4868.
- [66] J.R. Miller, R.A. Outlaw, B.C. Holloway, Graphene double-layer capacitor with AC line-filtering performance, *Science* 329 (2010) 1637–1639.
- [67] Y.W. Zhu, S. Murali, M.D. Stoller, K.J. Ganesh, W.W. Cai, P.J. Ferreira, A. Pirkle, R.M. Wallace, K.A. Cychoz, M. Thommes, D. Su, E.A. Stach, R.S. Ruoff, Carbon-based supercapacitors produced by activation of graphene, *Science* 332 (2011) 1537–1541.
- [68] Z.-S. Wu, K. Parvez, A. Winter, H. Viekler, X. Liu, S. Han, A. Turchanin, X. Feng, K. Müllen, Layer-by-layer assembled heteroatom-doped graphene films with ultrahigh volumetric capacitance and rate capability for micro-supercapacitors, *Adv. Mater.* 26 (2014) 4552–4558.
- [69] Z.-S. Wu, A. Winter, L. Chen, Y. Sun, A. Turchanin, X.L. Feng, K. Müllen, Three-dimensional nitrogen and boron co-doped graphene for high-performance all-solid-state supercapacitors, *Adv. Mater.* 24 (2012) 5130–5135.
- [70] M.F. El-Kady, V. Strong, S. Dubin, R.B. Kaner, Laser scribing of high-performance and flexible graphene-based electrochemical capacitors, *Science* 335 (2012) 1326–1330.
- [71] Z.-S. Wu, D.W. Wang, W. Ren, J. Zhao, G. Zhou, F. Li, H.M. Cheng, Anchoring hydrous RuO₂ on graphene sheets for high-performance electrochemical capacitors, *Adv. Funct. Mater.* 20 (2010) 3595–3602.
- [72] X.D. Zhuang, F. Zhang, D.Q. Wu, N. Forler, H.W. Liang, M. Wagner, D. Gehrig, M.R. Hansen, F. Laquai, X.L. Feng, Two-dimensional sandwich-type, graphene-based conjugated microporous polymers, *Angew. Chem. Int. Ed.* 52 (2013) 9668–9672.
- [73] X.D. Zhuang, F. Zhang, D.Q. Wu, X.L. Feng, Graphene coupled schiff-base porous polymers: towards nitrogen-enriched porous carbon nanosheets with ultrahigh electrochemical capacity, *Adv. Mater.* 26 (2014) 3081–3086.
- [74] K. Yuan, X.D. Zhuang, H.Y. Fu, G. Brunklau, M. Forster, Y.W. Chen, X.L. Feng, U. Scherf, Two-dimensional core-shelled porous hybrids as highly efficient catalysts for the oxygen reduction reaction, *Angew. Chem. Int. Ed.* 55 (2016) 6858–6863.
- [75] X.W. Yang, C. Cheng, Y.F. Wang, L. Qiu, D. Li, Liquid-mediated dense integration of graphene materials for compact capacitive energy storage, *Science* 341 (2013) 534–537.
- [76] P.-J. Hung, K.-H. Chang, Y.-F. Lee, C.-C. Hu, K.-M. Lin, Ideal asymmetric supercapacitors consisting of polyaniline nanofibers and graphene nanosheets with proper complementary potential windows, *Electrochim. Acta* 55 (2010) 6015–6021.
- [77] Z. Fan, J. Yan, T. Wei, L. Zhi, G. Ning, T. Li, F. Wei, Asymmetric supercapacitors based on graphene/MnO₂ and activated carbon nanofiber electrodes with high power and energy density, *Adv. Funct. Mater.* 21 (2011) 2366–2375.
- [78] B.G. Choi, S.-J. Chang, H.-W. Kang, C.P. Park, H.J. Kim, W.H. Hong, S. Lee, Y.S. Huh, High performance of a solid-state flexible asymmetric supercapacitor based on graphene films, *Nanoscale* 4 (2012) 4983–4988.
- [79] H. Gao, F. Xiao, C.B. Ching, H. Duan, Flexible all-solid-state asymmetric supercapacitors based on free-standing carbon nanotube/graphene and Mn₃O₄ nanoparticle/graphene paper electrodes, *ACS Appl. Mater. Interfaces* 4 (2012) 7020–7026.
- [80] H. Gao, F. Xiao, C.B. Ching, H. Duan, High-performance asymmetric supercapacitor based on graphene hydrogel and nanostructured MnO₂, *ACS Appl. Mater. Interfaces* 4 (2012) 2801–2810.
- [81] J. Xiao, S. Yang, Bio-inspired synthesis of nacl-type Co_xNi_{1-x}O (0 ≤ x < 1) nanorods on reduced graphene oxide sheets and screening for asymmetric electrochemical capacitors, *J. Mater. Chem.* 22 (2012) 12253–12262.
- [82] J. Yan, Z. Fan, W. Sun, G. Ning, T. Wei, Q. Zhang, R. Zhang, L. Zhi, F. Wei, Advanced asymmetric supercapacitors based on Ni(OH)₂/graphene and porous graphene electrodes with high energy density, *Adv. Funct. Mater.* 22 (2012) 2632–2641.
- [83] D. Antiohos, K. Pingmuang, M.S. Romano, S. Beirne, T. Romeo, P. Aitchison, A. Minett, G. Wallace, S. Phanichphant, J. Chen, Manganosite-microwave exfoliated graphene oxide composites for asymmetric supercapacitor device applications, *Electrochim. Acta* 101 (2013) 99–108.
- [84] J. Cao, Y. Wang, Y. Zhou, J.-H. Ouyang, D. Jia, L. Guo, High voltage asymmetric supercapacitor based on MnO₂ and graphene electrodes, *J. Electroanal. Chem.* 689 (2013) 201–206.
- [85] Q. Cheng, J. Tang, N. Shinya, L.-C. Qin, Polyaniline modified graphene and carbon nanotube composite electrode for asymmetric supercapacitors of high energy density, *J. Power Sources* 241 (2013) 423–428.
- [86] C.J. Jafta, F. Nkosi, L. le Roux, M.K. Mathe, M. Kebede, K. Makgopa, Y. Song, D. Tong, M. Oyama, N. Manyala, S. Chen, K.I. Ozoemena, Manganese oxide/graphene oxide composites for high-energy aqueous asymmetric electrochemical capacitors, *Electrochim. Acta* 110 (2013) 228–233.
- [87] Y. Jin, H. Chen, M. Chen, N. Liu, Q. Li, Graphene-patched CNT/MnO₂ nanocomposite papers for the electrode of high-performance flexible asymmetric supercapacitors, *ACS Appl. Mater. Interfaces* 5 (2013) 3408–3416.
- [88] J.N. Lektima, K.I. Ozoemena, C.J. Jafta, N. Kobayashi, Y. Song, D. Tong, S. Chen, M. Oyama, High-performance aqueous asymmetric electrochemical capacitors based on graphene oxide/cobalt(II)-tetrapyrrolineporphyrazine hybrids, *J. Mater. Chem. A* 1 (2013) 2821–2826.
- [89] W. Liu, X. Yan, J. Chen, Y. Feng, Q. Xue, Novel and high-performance asymmetric micro-supercapacitors based on graphene quantum dots and polyaniline nanofibers, *Nanoscale* 5 (2013) 6053–6062.
- [90] F. Luan, G. Wang, Y. Ling, X. Lu, H. Wang, Y. Tong, X.-X. Liu, Y. Li, High energy density asymmetric supercapacitors with a nickel oxide nanoflake cathode and a 3D reduced graphene oxide anode, *Nanoscale* 5 (2013) 7984–7990.
- [91] Y. Shao, H. Wang, Q. Zhang, Y. Li, High-performance flexible asymmetric supercapacitors based on 3D porous graphene/MnO₂ nanorod and graphene/Ag hybrid thin-film electrodes, *J. Mater. Chem. C* 1 (2013) 1245–1251.
- [92] J. Shen, C. Yang, X. Li, G. Wang, High-performance asymmetric supercapacitor based on nanoarchitected polyaniline/graphene/carbon nanotube and activated graphene electrodes, *ACS Appl. Mater. Interfaces* 5 (2013) 8467–8476.
- [93] A. Sumboja, C.Y. Foo, X. Wang, P.S. Lee, Large areal mass, flexible and free-standing reduced graphene oxide/manganese dioxide paper for asymmetric supercapacitor device, *Adv. Mater.* 25 (2013) 2809–2815.
- [94] L.-J. Xie, J.-F. Wu, C.-M. Chen, C.-M. Zhang, L. Wan, J.-L. Wang, Q.-Q. Kong, C.-X. Lv, K.-X. Li, G.-H. Sun, A novel asymmetric supercapacitor with an activated carbon cathode and a reduced graphene oxide-cobalt oxide nanocomposite anode, *J. Power Sources* 242 (2013) 148–156.
- [95] T. Zhai, F. Wang, M. Yu, S. Xie, C. Liang, C. Li, F. Xiao, R. Tang, Q. Wu, X. Lu, Y. Tong, 3D MnO₂-graphene composites with large areal capacitance for high-performance asymmetric supercapacitors, *Nanoscale* 5 (2013) 6790–6796.
- [96] W. Zhang, C. Ma, J. Fang, J. Cheng, X. Zhang, S. Dong, L. Zhang, Asymmetric electrochemical capacitors with high energy and power density based on graphene/CoAl-LDH and activated carbon electrodes, *RSC Adv.* 3 (2013) 2483–2490.
- [97] P. Ahuja, V. Sahu, S.K. Ujjain, R.K. Sharma, G. Singh, Performance evaluation of asymmetric supercapacitor based on cobalt manganite modified graphene nanoribbons, *Electrochim. Acta* 146 (2014) 429–436.
- [98] Y. Cao, Y. Xiao, Y. Gong, C. Wang, F. Li, One-pot synthesis of mnooh nanorods on graphene for asymmetric supercapacitors, *Electrochim. Acta* 127 (2014) 200–207.
- [99] L.-Q. Fan, G.-J. Liu, J.-H. Wu, L. Liu, J.-M. Lin, Y.-L. Wei, Asymmetric supercapacitor based on graphene oxide/poly pyrrole composite and activated carbon electrodes, *Electrochim. Acta* 137 (2014) 26–33.
- [100] W.-H. Khoh, J.-D. Hong, Solid-state asymmetric supercapacitor based on manganese dioxide/reduced-graphene oxide and polypyrrole/reduced-graphene oxide in a gel electrolyte, *Colloid Surf. A Physicochem. Eng. Asp.* 456 (2014) 26–34.
- [101] B. Li, Y. Fu, H. Xia, X. Wang, High-performance asymmetric supercapacitors based on MnFe₂O₄/graphene nanocomposite as anode material, *Mater. Lett.* 122 (2014) 193–196.
- [102] T.-W. Lin, C.-S. Dai, K.-C. Hung, High energy density asymmetric supercapacitor based on NiOOH/Ni₃S₂/3D graphene and Fe₃O₄/graphene composite electrodes, *Sci. Rep.* 4 (2014) 7274.
- [103] W. Lin, W. Yu, Z. Hu, W. Ouyang, X. Shao, R. Li, D.S. Yuan, Superior performance asymmetric supercapacitors based on flake-like Co/Al hydroxalite and graphene, *Electrochim. Acta* 143 (2014) 331–339.
- [104] J. Liu, L. Zhang, H.B. Wu, J. Lin, Z. Shen, X.W. Lou, High-performance flexible asymmetric supercapacitors based on a new graphene foam/carbon nanotube hybrid film, *Energy Environ. Sci.* 7 (2014) 3709–3719.
- [105] M. Liu, W.W. Tjui, J. Pan, C. Zhang, W. Gao, T. Liu, One-step synthesis of graphene nanoribbon-MnO₂ hybrids and their all-solid-state asymmetric supercapacitors, *Nanoscale* 6 (2014) 4233–4242.
- [106] D.H. Nagaraju, Q. Wang, P. Beaujuge, H.N. Alshareef, Two-dimensional heterostructures of V₂O₅ and reduced graphene oxide as electrodes for high energy density asymmetric supercapacitors, *J. Mater. Chem. A* 2 (2014) 17146–17152.
- [107] Y.-J. Peng, T.-H. Wu, C.-T. Hsu, S.-M. Li, M.-G. Chen, C.-C. Hu, Electrochemical characteristics of the reduced graphene oxide/carbon nanotube/polypyrrole composites for aqueous asymmetric supercapacitors, *J. Power Sources* 272 (2014) 970–978.
- [108] A. Singh, A.J. Roberts, R.C.T. Slade, A. Chandra, High electrochemical performance in asymmetric supercapacitors using MWCNT/nickel sulfide composite and graphene nanoplatelets as electrodes, *J. Mater. Chem. A* 2 (2014) 16723–16730.
- [109] H. Wang, H. Yi, X. Chen, X. Wang, Asymmetric supercapacitors based on nano-architected nickel oxide/graphene foam and hierarchical porous nitrogen-doped carbon nanotubes with ultrahigh-rate performance, *J. Mater. Chem. A* 2 (2014) 3223–3230.
- [110] Z. Wang, Z. Zhu, J. Qiu, S. Yang, High performance flexible solid-state asymmetric supercapacitors from MnO₂/ZnO core shell nanorods/specially reduced graphene oxide, *J. Mater. Chem. C* 2 (2014) 1331–1336.
- [111] S. Wu, W. Chen, L. Yan, Fabrication of a 3D MnO₂/graphene hydrogel for high-performance asymmetric supercapacitors, *J. Mater. Chem. A* 2 (2014) 2765–2772.
- [112] Y. Xiao, Y. Cao, Y. Gong, A. Zhang, J. Zhao, S. Fang, D. Jia, F. Li, Electrolyte and composition effects on the performances of asymmetric supercapacitors constructed with Mn₃O₄ nanoparticles-graphene nanocomposites, *J. Power Sources* 246 (2014) 926–933.
- [113] C. Yang, J. Shen, C. Wang, H. Fei, H. Bao, G. Wang, All-solid-state asymmetric

- supercapacitor based on reduced graphene oxide/carbon nanotube and carbon fiber paper/polypyrrole electrodes, *J. Mater. Chem. A* 2 (2014) 1458–1464.
- [114] Z. Zhang, F. Xiao, L. Qian, J. Xiao, S. Wang, Y. Liu, Facile synthesis of 3d MnO₂-graphene and carbon nanotube-graphene composite networks for high-performance, flexible, all-solid-state asymmetric supercapacitors, *Adv. Energy Mater.* 4 (2014) 1400064.
- [115] B. Zheng, T. Huang, L. Kou, X. Zhao, K. Gopalsamy, C. Gao, Graphene fiber-based asymmetric micro-supercapacitors, *J. Mater. Chem. A* 2 (2014) 9736–9743.
- [116] Y. Zhou, N. Lachman, M. Ghaffari, H. Xu, D. Bhattacharya, P. Fattahi, M.R. Abidian, S. Wu, K.K. Gleason, B.L. Wardle, Q.M. Zhang, A high performance hybrid asymmetric supercapacitor via nano-scale morphology control of graphene, conducting polymer, and carbon nanotube electrodes, *J. Mater. Chem. A* 2 (2014) 9964–9969.
- [117] B. Amutha, M. Sathish, A 2 V asymmetric supercapacitor based on reduced graphene oxide-carbon nanofiber-manganese carbonate nanocomposite and reduced graphene oxide in aqueous solution, *J. Solid State Electrochem.* 19 (2015) 2311–2320.
- [118] A. Bello, F. Barzegar, D. Momodu, J. Dangbegnon, F. Taghizadeh, M. Fabiane, N. Manyala, Asymmetric supercapacitor based on nanostructured graphene foam/polyvinyl alcohol/formaldehyde and activated carbon electrodes, *J. Power Sources* 273 (2015) 305–311.
- [119] J. Chen, Y. Wang, J. Cao, Y. Liu, J.-H. Ouyang, D. Jia, Y. Zhou, Flexible and solid-state asymmetric supercapacitor based on ternary graphene/MnO₂/carbon black hybrid film with high power performance, *Electrochim. Acta* 182 (2015) 861–870.
- [120] D.P. Dubal, N.R. Chodankar, G.S. Gund, R. Holze, C.D. Lokhande, P. Gomez-Romero, Asymmetric supercapacitors based on hybrid CuO@reduced graphene oxide@sponge versus reduced graphene oxide@sponge electrodes, *Energy Technol.* 3 (2015) 168–176.
- [121] Z. Gao, W. Yang, J. Wang, N. Song, X. Li, Flexible all-solid-state hierarchical NiCo₂O₄/porous graphene paper asymmetric supercapacitors with an exceptional combination of electrochemical properties, *Nano Energy* 13 (2015) 306–317.
- [122] D. Ghosh, C.K. Das, Hydrothermal growth of hierarchical Ni₃S₂ and Co₃S₄ on a reduced graphene oxide hydrogel@ni foam: a high-energy-density aqueous asymmetric supercapacitor, *ACS Appl. Mater. Interfaces* 7 (2015) 1122–1131.
- [123] M. Jing, C. Wang, H. Hou, Z. Wu, Y. Zhu, Y. Yang, X. Jia, Y. Zhang, X. Ji, Ultrafine nickel oxide quantum dots embedded with few-layer exfoliated graphene for an asymmetric supercapacitor: enhanced capacitances by alternating voltage, *J. Power Sources* 298 (2015) 241–248.
- [124] T.-W. Lin, C.-S. Dai, T.-T. Tasi, S.-W. Chou, J.-Y. Lin, H.-H. Shen, High-performance asymmetric supercapacitor based on Co₉S₈/3D graphene composite and graphene hydrogel, *Chem. Eng. J.* 279 (2015) 241–249.
- [125] M. Liu, J. Chang, Y. Bai, J. Sun, An advanced asymmetric supercapacitor based on a novel ternary graphene/nickel/nickel oxide and porous carbon electrode with superior electrochemical performance, *RSC Adv.* 5 (2015) 91389–91397.
- [126] Y. Liu, D. He, H. Wu, J. Duan, Y. Zhang, Hydrothermal self-assembly of manganese dioxide/manganese carbonate/reduced graphene oxide aerogel for asymmetric supercapacitors, *Electrochim. Acta* 164 (2015) 154–162.
- [127] Y. Liu, R. Wang, X. Yan, Synergistic effect between ultra-small nickel hydroxide nanoparticles and reduced graphene oxide sheets for the application in high-performance asymmetric supercapacitor, *Sci. Rep.* 5 (2015) 11095.
- [128] S. Saha, M. Jana, P. Khanra, P. Samanta, H. Koo, N.C. Murmu, T. Kuila, Band gap engineering of boron nitride by graphene and its application as positive electrode material in asymmetric supercapacitor device, *ACS Appl. Mater. Interfaces* 7 (2015) 14211–14222.
- [129] S. Saha, M. Jana, P. Samanta, N.C. Murmu, T. Kuila, In situ preparation of a SAC-rGO@ni electrode by electrochemical functionalization of reduced graphene oxide using sulfanic acid azocomotrop and its application in asymmetric supercapacitors, *J. Mater. Chem. A* 3 (2015) 19461–19468.
- [130] J. Shi, X. Li, G. He, L. Zhang, M. Li, Electrodeposition of high-capacitance 3D CoS/graphene nanosheets on nickel foam for high-performance aqueous asymmetric supercapacitors, *J. Mater. Chem. A* 3 (2015) 20619–20626.
- [131] G. Sun, X. Zhang, R. Lin, J. Yang, H. Zhang, P. Chen, Hybrid fibers made of molybdenum disulfide, reduced graphene oxide, and multi-walled carbon nanotubes for solid-state, flexible, asymmetric supercapacitors, *Angew. Chem. Int. Ed.* 54 (2015) 4651–4656.
- [132] Y. Sun, Y. Cheng, K. He, A. Zhou, H. Duan, One-step synthesis of three-dimensional porous ionic liquid-carbon nanotube-graphene gel and MnO₂-graphene gel as freestanding electrodes for asymmetric supercapacitors, *RSC Adv.* 5 (2015) 10178–10186.
- [133] Q. Tang, M. Chen, L. Wang, G. Wang, A novel asymmetric supercapacitors based on binder-free carbon fiber paper@ nickel cobaltite nanowires and graphene foam electrodes, *J. Power Sources* 273 (2015) 654–662.
- [134] S.K. Ujjain, G. Singh, R.K. Sharma, Co₉O₄@reduced graphene oxide nanoribbon for high performance asymmetric supercapacitor, *Electrochim. Acta* 171 (2015) (189–189).
- [135] G.K. Veerasubramani, K. Krishnamoorthy, S.J. Kim, Electrochemical performance of an asymmetric supercapacitor based on graphene and cobalt molybdate electrodes, *RSC Adv.* 5 (2015) 16319–16327.
- [136] H. Wang, H.T. Tan, H. Yi, Y. Zhang, G. Guo, X. Wang, S. Madhavi, Q. Yan, Integrating three-dimensional graphene/Fe₃O₄@C composite and mesoporous Co(OH)₂ nanosheets arrays/graphene foam into a superior asymmetric electrochemical capacitor, *RSC Adv.* 5 (2015) 88191–88201.
- [137] Y.-S. Wang, S.-M. Li, S.-T. Hsiao, W.-H. Liao, S.-Y. Yang, C.-C.M. Ma, C.-C. Hu, Electrochemical composite deposition of porous cactus-like manganese oxide/reduced graphene oxide-carbon nanotube hybrids for high-power asymmetric supercapacitors, *J. Mater. Chem. C* 3 (2015) 4987–4996.
- [138] H. Xia, C. Hong, B. Li, B. Zhao, Z. Lin, M. Zheng, S.V. Savilov, S.M. Aldoshin, Facile synthesis of hematite quantum-dot/functionalized graphene-sheet composites as advanced anode materials for asymmetric supercapacitors, *Adv. Funct. Mater.* 25 (2015) 627–635.
- [139] Y. Xiao, D. Su, X. Wang, L. Zhou, S. Wu, F. Li, S. Fang, In situ growth of ultradispersed NiCo₂S₄ nanoparticles on graphene for asymmetric supercapacitors, *Electrochim. Acta* 176 (2015) 44–50.
- [140] H. Xie, S. Tang, J. Zhu, S. Vongehr, X. Meng, A high energy density asymmetric all-solid-state supercapacitor based on cobalt carbonate hydroxide nanowire covered n-doped graphene and porous graphene electrodes, *J. Mater. Chem. A* 3 (2015) 18505–18513.
- [141] C. Yang, Y. Shi, N. Liu, J. Tao, S. Wang, W. Liu, Y. Wang, J. Su, L. Li, C. Yang, Y. Gao, Freestanding and flexible graphene wrapped MnO₂/MoO₃ nanoparticle based asymmetric supercapacitors for high energy density and output voltage, *RSC Adv.* 5 (2015) 45129–45135.
- [142] J. Yang, G. Li, Z. Pan, M. Liu, Y. Hou, Y. Xu, H. Deng, L. Sheng, X. Zhao, Y. Qiu, Y. Zhang, All-solid-state high-energy asymmetric supercapacitors enabled by three-dimensional mixed-valent MnO_x nanospike and graphene electrodes, *ACS Appl. Mater. Interfaces* 7 (2015) 22172–22180.
- [143] M. Yang, K.G. Lee, S.J. Lee, S.B. Lee, Y.-K. Han, B.G. Choi, Three-dimensional expanded graphene-metal oxide film via solid-state microwave irradiation for aqueous asymmetric supercapacitors, *ACS Appl. Mater. Interfaces* 7 (2015) 22364–22371.
- [144] X. Yang, F. Qu, H. Niu, Q. Wang, J. Yan, Z. Fan, High-performance aqueous asymmetric supercapacitor based on spinel LiMn₂O₄ and nitrogen-doped graphene/porous carbon composite, *Electrochim. Acta* 180 (2015) 287–294.
- [145] H. Yi, H. Wang, Y. Jing, T. Peng, Y. Wang, J. Guo, Q. He, Z. Guo, X. Wang, Advanced asymmetric supercapacitors based on CNT@Ni(OH)₂ core-shell composites and 3D graphene networks, *J. Mater. Chem. A* 3 (2015) 19545–19555.
- [146] Z. Yu, M. McInnis, J. Calderon, S. Seal, L. Zhai, J. Thomas, Functionalized graphene aerogel composites for high-performance asymmetric supercapacitors, *Nano Energy* 11 (2015) 611–620.
- [147] L.-L. Zhang, H.-H. Li, C.-Y. Fan, K. Wang, X.-L. Wu, H.-Z. Sun, J.-P. Zhang, A vertical and cross-linked Ni(OH)₂ network on cellulose-fiber covered with graphene as a binder-free electrode for advanced asymmetric supercapacitors, *J. Mater. Chem. A* 3 (2015) 19077–19084.
- [148] Z. Zhang, K. Chi, F. Xiao, S. Wang, Advanced solid-state asymmetric supercapacitors based on 3D graphene/MnO₂ and graphene/polypyrrole hybrid architectures, *J. Mater. Chem. A* 3 (2015) 12828–12835.
- [149] Z. Zhang, F. Xiao, S. Wang, Hierarchically structured MnO₂/graphene/carbon fiber and porous graphene hydrogel wrapped copper wire for fiber-based flexible all-solid-state asymmetric supercapacitors, *J. Mater. Chem. A* 3 (2015) 11215–11223.
- [150] Y. Zhao, W. Ran, J. He, Y. Huang, Z. Liu, W. Liu, Y. Tang, L. Zhang, D. Gao, F. Gao, High-performance asymmetric supercapacitors based on multilayer MnO₂/graphene oxide nanoflakes and hierarchical porous carbon with enhanced cycling stability, *Small* 11 (2015) 1310–1319.
- [151] M. Hao, Y. Chen, W. Xiong, L. Zhang, L. Wu, Y. Fu, T. Mei, J. Wang, J. Li, X. Wang, Coherent polyaniline/graphene oxides/multi-walled carbon nanotubes ternary composites for asymmetric supercapacitors, *Electrochim. Acta* 191 (2016) 165–172.
- [152] M. Jana, J.S. Kumar, P. Khanra, P. Samanta, H. Koo, N.C. Murmu, T. Kuila, Superior performance of asymmetric supercapacitor based on reduced graphene oxide-manganese carbonate as positive and sono-chemically reduced graphene oxide as negative electrode materials, *J. Power Sources* 303 (2016) 222–233.
- [153] M. Jana, S. Saha, P. Samanta, N.C. Murmu, N.H. Kim, T. Kuila, J.H. Lee, Growth of Ni-Co binary hydroxide on a reduced graphene oxide surface by a successive ionic layer adsorption and reaction (SILAR) method for high performance asymmetric supercapacitor electrodes, *J. Mater. Chem. A* 4 (2016) 2188–2197.
- [154] Y. Liu, X. Miao, J. Fang, X. Zhang, S. Chen, W. Li, W. Feng, Y. Chen, W. Wang, Y. Zhang, Layered-MnO₂ nanosheet grown on nitrogen-doped graphene template as a composite cathode for flexible solid-state asymmetric supercapacitor, *ACS Appl. Mater. Interfaces* 8 (2016) 5251–5260.
- [155] H. Ma, J. He, D.-B. Xiong, J. Wu, Q. Li, V. Dravid, Y. Zhao, Nickel cobalt hydroxide @reduced graphene oxide hybrid nanolayers for high performance asymmetric supercapacitors with remarkable cycling stability, *ACS Appl. Mater. Interfaces* 8 (2016) 1992–2000.
- [156] R. Wang, C. Xu, J.-M. Lee, High performance asymmetric supercapacitors: new NiOOH nanosheet/graphene hydrogels and pure graphene hydrogels, *Nano Energy* 19 (2016) 210–221.
- [157] Q.T. Qu, P. Zhang, B. Wang, Y.H. Chen, S. Tian, Y.P. Wu, R. Holze, Electrochemical performance of MnO₂ nanorods in neutral aqueous electrolytes as a cathode for asymmetric supercapacitors, *J. Phys. Chem. C* 113 (2009) 14020–14027.
- [158] P. Xu, B. Wei, Z. Cao, J. Zheng, K. Gong, F. Li, J. Yu, Q. Li, W. Lu, J.-H. Byun, B.-S. Kim, Y. Yan, T.-W. Chou, Stretchable wire-shaped asymmetric supercapacitors based on pristine and MnO₂ coated carbon nanotube fibers, *ACS Nano* 9 (2015) 6088–6096.
- [159] V. Khomenko, E. Raymundo-Pinero, F. Beguin, Optimisation of an asymmetric manganese oxide/activated carbon capacitor working at 2 V in aqueous medium, *J. Power Sources* 153 (2006) 183–190.
- [160] B. Messaoudi, S. Joiret, M. Keddah, H. Takenouti, Anodic behaviour of manganese in alkaline medium, *Electrochim. Acta* 46 (2001) 2487–2498.
- [161] D.W. Wang, F. Li, J.P. Zhao, W.C. Ren, Z.G. Chen, J. Tan, Z.-S. Wu, I. Gentle, G.Q. Lu, H.M. Cheng, Fabrication of graphene/polyaniline composite paper via in situ anodic electropolymerization for high-performance flexible electrode, *ACS*

- Nano 3 (2009) 1745–1752.
- [162] Z.-S. Wu, W. Ren, L. Gao, B. Liu, C. Jiang, H.M. Cheng, Synthesis of high-quality graphene with a pre-determined number of layers, *Carbon* 47 (2009) 493–499.
- [163] Z.-S. Wu, W.C. Ren, L.B. Gao, J.P. Zhao, Z.P. Chen, B.L. Liu, D.M. Tang, B. Yu, C.B. Jiang, H.M. Cheng, Synthesis of graphene sheets with high electrical conductivity and good thermal stability by hydrogen arc discharge exfoliation, *ACS Nano* 3 (2009) 411–417.
- [164] Z.-S. Wu, W. Ren, L. Wen, L. Gao, J. Zhao, Z. Chen, G. Zhou, F. Li, H.M. Cheng, Graphene anchored with Co_3O_4 nanoparticles as anode of lithium ion batteries with enhanced reversible capacity and cyclic performance, *ACS Nano* 4 (2010) 3187–3194.
- [165] Z.-S. Wu, L.L. Xue, W.C. Ren, F. Li, L. Wen, H.M. Cheng, A LiF , nanoparticle-modified graphene electrode for high-power and high-energy lithium ion batteries, *Adv. Funct. Mater.* 22 (2012) 3290–3297.
- [166] Z.-S. Wu, Y. Sun, Y.Z. Tan, S.B. Yang, X.L. Feng, K. Müllen, Three-dimensional graphene-based macro- and mesoporous frameworks for high-performance electrochemical capacitive energy storage, *J. Am. Chem. Soc.* 134 (2012) 19532–19535.
- [167] Z.-S. Wu, S.B. Yang, Y. Sun, K. Parvez, X.L. Feng, K. Müllen, 3d nitrogen-doped graphene aerogel-supported Fe_3O_4 nanoparticles as efficient electrocatalysts for the oxygen reduction reaction, *J. Am. Chem. Soc.* 134 (2012) 9082–9085.
- [168] Y.X. Xu, K.X. Sheng, C. Li, G.Q. Shi, Self-assembled graphene hydrogel via a one-step hydrothermal process, *ACS Nano* 4 (2010) 4324–4330.
- [169] H. Lin, F. Liu, X. Wang, Y. Ai, Z. Yao, L. Chu, S. Han, X. Zhuang, Graphene-coupled flower-like Ni_3S_2 for a free-standing 3D aerogel with an ultra-high electrochemical capacity, *Electrochim. Acta* 191 (2016) 705–715.
- [170] X.H. Xia, J.P. Tu, X.L. Wang, C.D. Gu, X.B. Zhao, Mesoporous Co_3O_4 monolayer hollow-sphere array as electrochemical pseudocapacitor material, *Chem. Commun.* 47 (2011) 5786–5788.
- [171] M.J. Zhi, C.C. Xiang, J.T. Li, M. Li, N.Q. Wu, Nanostructured carbon-metal oxide composite electrodes for supercapacitors: a review, *Nanoscale* 5 (2013) 72–88.
- [172] J.F. Xie, X. Sun, N. Zhang, K. Xu, M. Zhou, Y. Xie, Layer-by-layer $\beta\text{-Ni}(\text{OH})_2$ /graphene nanohybrids for ultraflexible all-solid-state thin-film supercapacitors with high electrochemical performance, *Nano Energy* 2 (2013) 65–74.
- [173] S.Q. Ci, Z.H. Wen, Y.Y. Qian, S. Mao, S.M. Cui, J.H. Chen, NiO -microflower formed by nanowire-weaving nanosheets with interconnected ni-network decoration as supercapacitor electrode, *Sci. Rep.* 5 (2015) 11919.
- [174] C.C. Hu, J.C. Chen, K.H. Chang, Cathodic deposition of $\text{Ni}(\text{OH})_2$ and $\text{Co}(\text{OH})_2$ for asymmetric supercapacitors: importance of the electrochemical reversibility of redox couples, *J. Power Sources* 221 (2013) 128–133.
- [175] L. Yu, B.Y. Guan, W. Xiao, X.W. Lou, Formation of yolk-shelled Ni-Co mixed oxide nanoprisms with enhanced electrochemical performance for hybrid supercapacitors and lithium ion batteries, *Adv. Energy Mater.* 5 (2015) 1500981.
- [176] Z.-S. Wu, K. Parvez, S. Li, S. Yang, Z.Y. Liu, S.H. Liu, X.L. Feng, K. Müllen, Alternating stacked graphene-conducting polymer compact films with ultrahigh areal and volumetric capacitances for high-energy micro-supercapacitors, *Adv. Mater.* 27 (2015) 4054–4061.
- [177] Y.F. Xu, M.G. Schwab, A.J. Strudwick, J. Hennig, X.L. Feng, Z.-S. Wu, K. Müllen, Screen-printable thin film supercapacitor device utilizing graphene/polyaniline inks, *Adv. Energy Mater.* 3 (2013) 1035–1040.
- [178] S. Liu, P. Gordiichuk, Z.-S. Wu, Z. Liu, W. Wei, M. Wagner, N. Mohamed-Noriega, D. Wu, Y. Mai, A. Herrmann, K. Müllen, X. Feng, Patterning two-dimensional free-standing surfaces with mesoporous conducting polymers, *Nat. Commun.* 6 (2015) 8817.
- [179] A. Ferris, S. Garbarino, D. Guay, D. Pech, 3D RuO_2 microsupercapacitors with remarkable areal energy, *Adv. Mater.* 27 (2015) 6625–6629.
- [180] L.Y. Chen, Y. Hou, J.L. Kang, A. Hirata, T. Fujita, M.W. Chen, Toward the theoretical capacitance of RuO_2 reinforced by highly conductive nanoporous gold, *Adv. Energy Mater.* 3 (2013) 851–856.
- [181] T. Brezesinski, J. Wang, S.H. Tolbert, B. Dunn, Ordered mesoporous $\alpha\text{-MoO}_3$ with iso-oriented nanocrystalline walls for thin-film pseudocapacitors, *Nat. Mater.* 9 (2010) 146–151.
- [182] X. Xiao, C. Zhang, S. Lin, L. Huang, Z. Hu, Y. Cheng, T. Li, W. Qiao, D. Long, Y. Huang, L. Mai, Y. Gogotsi, J. Zhou, Intercalation of cations into partially reduced molybdenum oxide for high-rate pseudocapacitors, *Energy Storage Mater.* 1 (2015) 1–8.
- [183] Z.-S. Wu, S. Yang, L. Zhang, J.B. Wagner, X. Feng, K. Müllen, Binder-free activated graphene compact films for all-solid-state micro-supercapacitors with high areal and volumetric capacitances, *Energy Storage Mater.* 1 (2015) 119–126.
- [184] Z.P. Chen, W.C. Ren, L.B. Gao, B.L. Liu, S.F. Pei, H.M. Cheng, Three-dimensional flexible and conductive interconnected graphene networks grown by chemical vapour deposition, *Nat. Mater.* 10 (2011) 424–428.
- [185] N. Li, Z.P. Chen, W.C. Ren, F. Li, H.M. Cheng, Flexible graphene-based lithium ion batteries with ultrafast charge and discharge rates, *Proc. Natl. Acad. Sci. USA* 109 (2012) 17360–17365.
- [186] X. Wang, J. Liu, Y. Wang, C. Zhao, W. Zheng, $\text{Ni}(\text{OH})_2$ nanoflakes electrodeposited on Ni foam-supported vertically oriented graphene nanosheets for application in asymmetric supercapacitors, *Mater. Res. Bull.* 52 (2014) 89–95.
- [187] K. Naoi, S. Ishimoto, J. Miyamoto, W. Naoi, Second generation ‘nanohybrid supercapacitor’: evolution of capacitive energy storage devices, *Energy Environ. Sci.* 5 (2012) 9363–9373.
- [188] Y. Ma, H. Chang, M. Zhang, Y. Chen, Graphene-based materials for lithium-ion hybrid supercapacitors, *Adv. Mater.* 27 (2015) 5296–5308.
- [189] I. Plitz, A. DuPasquier, F. Badway, J. Gural, N. Pereira, A. Gmitter, G.G. Amatucci, The design of alternative nonaqueous high power chemistries, *Appl. Phys. A: Mater. Sci. Process.* 82 (2006) 615–626.
- [190] J.J. Ren, L.W. Su, X. Qin, M. Yang, J.P. Wei, Z. Zhou, P.W. Shen, Pre-lithiated graphene nanosheets as negative electrode materials for Li-ion capacitors with high power and energy density, *J. Power Sources* 264 (2014) 108–113.
- [191] K. Naoi, ‘Nanohybrid capacitor’: the next generation electrochemical capacitors, *Fuel Cells* 10 (2010) 825–833.
- [192] N.S. Xu, X.Z. Sun, X. Zhang, K. Wang, Y.W. Ma, A two-step method for preparing $\text{Li}_4\text{Ti}_5\text{O}_{12}$ -graphene as an anode material for lithium-ion hybrid capacitors, *RSC Adv.* 5 (2015) 94361–94368.
- [193] L. Ye, Q.H. Liang, Y. Lei, X.L. Yu, C.P. Han, W.C. Shen, Z.H. Huang, F.Y. Kang, Q.H. Yang, A high performance Li-ion capacitor constructed with $\text{Li}_4\text{Ti}_5\text{O}_{12}/\text{C}$ hybrid and porous graphene macroform, *J. Power Sources* 282 (2015) 174–178.
- [194] F. Zhang, T.F. Zhang, X. Yang, L. Zhang, K. Leng, Y. Huang, Y.S. Chen, A high-performance supercapacitor-battery hybrid energy storage device based on graphene-enhanced electrode materials with ultrahigh energy density, *Energy Environ. Sci.* 6 (2013) 1623–1632.
- [195] H. Nakazawa, K. Sano, T. Abe, M. Baba, N. Kumagai, Charge-discharge characteristics of all-solid-state thin-film lithium-ion batteries using amorphous Nb_2O_5 negative electrodes, *J. Power Sources* 174 (2007) 838–842.
- [196] Z.-S. Wu, X. Feng, H.-M. Cheng, Recent advances in graphene-based planar micro-supercapacitors for on-chip energy storage, *Natl. Sci. Rev.* 1 (2014) 277–292.
- [197] Z.-S. Wu, K. Parvez, X.L. Feng, K. Müllen, Photolithographic fabrication of high-performance all-solid-state graphene-based planar micro-supercapacitors with different interdigital fingers, *J. Mater. Chem. A* 2 (2014) 8288–8293.
- [198] S. Wang, S.H. Zheng, Z.-S. Wu, C.L. Sun, Recent advances in graphene-based planar micro-supercapacitors, *Sci. Sin. Chim.* 46 (2016) 1–13.
- [199] Z.-S. Wu, K. Parvez, X.L. Feng, K. Müllen, Graphene-based in-plane micro-supercapacitors with high power and energy densities, *Nat. Commun.* 4 (2013) 2487.
- [200] Y. Li, Y. Hu, Y. Zhao, G.Q. Shi, L.E. Deng, Y.B. Hou, L.T. Qu, An electrochemical avenue to green-luminescent graphene quantum dots as potential electron-acceptors for photovoltaics, *Adv. Mater.* 23 (2011) 776–780.
- [201] Y. Li, Y. Zhao, H.H. Cheng, Y. Hu, G.Q. Shi, L.M. Dai, L.T. Qu, Nitrogen-doped graphene quantum dots with oxygen-rich functional groups, *J. Am. Chem. Soc.* 134 (2012) 15–18.
- [202] W.W. Liu, Y.Q. Feng, X.B. Yan, J.T. Chen, Q.J. Xue, Superior micro-supercapacitors based on graphene quantum dots, *Adv. Funct. Mater.* 23 (2013) 4111–4122.
- [203] M.F. El-Kady, M. Ihms, M.P. Li, J.Y. Hwang, M.F. Mousavi, L. Chaney, A.T. Lech, R.B. Kaner, Engineering three-dimensional hybrid supercapacitors and micro-supercapacitors for high-performance integrated energy storage, *Proc. Natl. Acad. Sci. USA* 112 (2015) 4233–4238.
- [204] T. Huang, B. Zheng, L. Kou, K. Gopalsamy, Z. Xu, C. Gao, Y. Meng, Z. Wei, Flexible high performance wet-spun graphene fiber supercapacitors, *RSC Adv.* 3 (2013) 23957–23962.
- [205] X. Li, T. Zhao, Q. Chen, P. Li, K. Wang, M. Zhong, J. Wei, D. Wu, B. Wei, H. Zhu, Flexible all solid-state supercapacitors based on chemical vapor deposition derived graphene fibers, *Phys. Chem. Chem. Phys.* 15 (2013) 17752–17757.
- [206] K. Gopalsamy, Z. Xu, B. Zheng, T. Huang, L. Kou, X. Zhao, C. Gao, Bismuth oxide nanotubes-graphene fiber-based flexible supercapacitors, *Nanoscale* 6 (2014) 8595–8600.
- [207] X. Chen, H. Lin, J. Deng, Y. Zhang, X. Sun, P. Chen, X. Fang, Z. Zhang, G. Guan, H. Peng, Electrochromic fiber-shaped supercapacitors, *Adv. Mater.* 26 (2014) 8126–8132.
- [208] G.Z. Sun, X. Zhang, R.Z. Lin, J. Yang, H. Zhang, P. Chen, Hybrid fibers made of molybdenum disulfide, reduced graphene oxide, and multi-walled carbon nanotubes for solid-state, flexible, asymmetric supercapacitors, *Angew. Chem. Int. Ed.* 54 (2015) 4651–4656.
- [209] C. Zhang, W. Lv, Y. Tao, Q.-H. Yang, Towards superior volumetric performance: design and preparation of novel carbon materials for energy storage, *Energy Environ. Sci.* 8 (2015) 1390–1403.
- [210] H. Wu, Y. Zhang, L. Cheng, L. Zheng, Y. Li, W. Yuan, X. Yuan, Graphene based architectures for electrochemical capacitors, *Energy Storage Mater.* 5 (2016) 8–32.
- [211] X.-Y. Liu, K.-X. Wang, J.-S. Chen, Template-directed metal oxides for electrochemical energy storage, *Energy Storage Mater.* 3 (2016) 1–17.